UNIVERSITY OF PARDUBICE

FACULTY OF TRANSPORT ENGINEERING

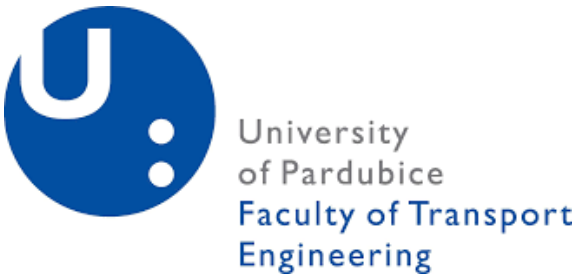

ACCURACY IMPROVEMENT OF MEASUREMENTS BY ANALYZING DYNAMIC RESPONSE OF A TRAM WHEEL ROLLER-RIG

Ing. Bekir Tuna KAYAALP

DISSERTATION THESIS

2019

Program of Study:

Technique and Technology in Transport and Communications

Branch of study:

Transport Means and Infrastructure

Dissertation Title:

Accuracy improvement of measurements by analysing dynamic response of a tram wheel roller rig

Author:

Ing. Bekir Tuna KAYAALP

Supervisor:

Doc. Ing. Michael Lata, Ph.D.

Specialist supervisor:

The dissertation has arisen at the supervising:

Department of Transport Means and Infrastructure

AUTHOR'S DECLARATION

I hereby declare:

This thesis was prepared individually. All the literary sources and the information I used in the thesis are listed in the bibliography.

I was familiar with the fact that rights and obligations arising from the Act No. 121/2000 Coll., the Copyright Act, apply to my thesis, especially with the fact that the University of Pardubice has the right to enter into a license agreement for use of this thesis as a school work pursuant to § 60, Section 1 of the Copyright Act, and the fact that should this thesis be used by me or should a license be granted for the use to another entity, the University of Pardubice is authorized to claim from me a reasonable contribution to cover the costs incurred during the making of the thesis, according to the circumstances up to the actual amount thereof.

I agree with the reference-only disclosure of my thesis in the University Library.

In Pardubice on …../…./….. Bekir Tuna KAYAALP

ABSTRACT

Railway transport is becoming popular due to efficiency in long distances also being an environment-friendly solution when it is compared to other transportation methods. Thus, more innovative solutions to existing problems are essential. Roller-rigs are very efficient testing tools which are widely prevalent around the world for researchers studying on the railway industry directly or indirectly. They are being used for validating, testing, improving the railway vehicles or related components from many years. Hence, demanding to the roller-rigs are also increasing parallel to the development of the railway industry. In this study, a full-scale vertical plane tram wheel roller-rig has been investigated from several aspects in order to provide improvement of its measurement capabilities and dynamic behaviour. Firstly, the issues related to the measurements and behaviour have been determined. Followingly, the possible hypothesis of the reasons for the issues proposed and these hypotheses have been tested in a systematically order to verify or falsify. From the general aspect the system divided into two components; Mechanical parts, Electric parts. From the mechanical aspect, the whole system considered as two sub-systems which are steady parts and moving parts. In order to define their behaviour and influence on the measurement quality, several numerical and experimental studies have been performed in order. Steady parts of the system (Frame) has been investigated by an FE solution, and the obtained values have been verified via experimental study. Moving parts (Wheel, Rotating Rail and Motors) have been modelled on MATLAB environment and results of the simulation has been verified by experimental studies. After verification of the simulation, several parametric studies have been performed, and two main solutions have been generated in order to eliminate the issues regarding the measurement quality and dynamic behaviour. From the data acquisition aspect, a smoothing filter has been generated in order to provide better measurement results. Two main solutions have been provided and simulated on verified models. Also, the generated filter has been tried for a variety of speeds. With the generated solutions, the measurement issues have been eliminated, and dynamic behaviour has been improved.

TABLE OF CONTENTS

LIST OF FIGURES

LIST OF TABLES

LIST OF ABBREVIATIONS AND SYMBOLS

List of Abbreviations

FEM	Finite Element Method
BEM	Boundary Element Method
e.g.	in Latin *exempli gratia* (in English For Example)
ICE	InterCity-Express train
DPP	Dopravní Podnik Hlavního Města Prahy (Prague Public Transport Company)
VUKV	Výzkumný Ústav Kolejových Vozidel (Rail Vehicle Research Institute)
PMSM	Permanent Magnet Synchronous Motor
AM	Asynchronous Motor
CV	Constant-Velocity
PC	Personal Computer
DAQ	Data Acquisition Device
DOF	Degree of Freedom
FE	Finite Element
FEA	Finite Element Analysis
RCF	Rolling Contact Fatigue
CoA	Coefficient of Adhesion

List of Symbols

$\dot{\omega}_w$	Wheel angular acceleration $[rad/s^2]$
$\dot{\omega}_r$	Roller angular acceleration $[rad/s^2]$
ω_w	Wheel angular speed $[rad/s]$
ω_r	Roller angular speed $[rad/s]$
$\dot{\omega}_a$	AM rotor angular acceleration $[rad/s^2]$
$\dot{\omega}_p$	PMSM rotor angular acceleration $[rad/s^2]$
ω_a	AM rotor angular speed $[rad/s]$
ω_p	PMSM rotor angular speed $[rad/s]$

k_{s_r}	Roller shaft stiffness $[Nm/rad]$
k_{s_p}	Wheel shaft stiffness $[Nm/rad]$
θ_{s_r}	Roller shaft angular displacement $[rad]$
θ_{s_w}	Wheel shaft angular displacement $[rad]$
$\dot{\theta}_{s_r}$	Roller shaft angular acceleration $[rad/s^2]$
$\dot{\theta}_{s_w}$	Wheel shaft angular acceleration $[rad/s^2]$
T_w	Wheel torque $[Nm]$
T_r	Roller torque $[Nm]$
T_a	AM rotor torque $[Nm]$
T_p	PMSM rotor torque $[Nm]$
F_x	The longitudinal force between wheel and roller $[N]$
r_w	Wheel rolling radius $[m]$
r_r	Roller rolling radius $[m]$
J_w	Inertia of wheel $[kgm^2]$
J_r	Inertia of roller $[kgm^2]$
J_a	The inertia of AM rotor $[kgm^2]$
J_p	The inertia of PMSM rotor $[kgm^2]$
s	Creep $[-]$
w_s	Creep velocity $[m/s]$
E	Elasticity modulus $[kg/ms^2]$
v	Poisson ratio $[-]$
F	Tangential creep force $[N]$
Q	Wheel load $[N]$
μ	Coefficient of friction $[-]$
μ_0	Maximum friction coefficient $[-]$
μ_∞	Friction coefficient at infinity slip $[-]$
ε	Gradient of the tangential stress $[-]$
C	Proportionality of contact shear stiffness $[N/m^3]$

c_{jj}	Kalker coefficient $[-]$
s_x	Slip component on x direction $[-]$
s_y	Slip component on y direction $[-]$
k_A	Additional Polach's parameter $[-]$
k_B	Additional Polach's parameter $[-]$
i_{ds}	Current of d axis $[A]$
i_{qs}	Current of q axis $[A]$
V_{ds}	Voltage of d axis $[V]$
V_{qs}	Voltage of q axis $[V]$
R_s	Resistance of stator windings $[\Omega]$
L_{qs}	Inductance of q axis $[H]$
L_{ds}	Inductance of d axis $[H]$
p	Number of pole pairs $[-]$
ω	Angular velocity of PMSM rotor $[rad/s]$
φ	Amplitude of flux $[Wb]$
ω_{syn}	Synchronous speed of AM $[rad/s]$
s_m	Slip of the AM $[-]$
R_{Th}	Resistance of the AM rotor $[H]$
X_{Th}	Reactance on the stator $[\Omega]$
V_{Th}	Thevenin voltage $[V]$
R_2'	Reflected resistance of the rotor $[\Omega]$
X_2'	Reactance of the rotor $[\Omega]$
r_{nom}	Nominal radius $[m]$
r_{min}	Minimum radius $[m]$
r_{max}	Maximum radius $[m]$
δ_f	Displacement of frame $[m]$
δ_v	Displacement of shaft positions $[m]$

1 INTRODUCTION

From the time of very first usage of railway vehicles, studying on wheel-rail contact mechanics is a very popular area as it significantly affects the rolling properties and so the safety of the passenger transportation and goods. Even though the importance of the contact phenomenon is realized, it is not fully clear in terms of several aspects. Those are intended to be clarified by many theories developed in the literature, but further studies are still desirable to provide more detailed and more certain information about the contact mechanics. As also mentioned above, forces acting in this contact pair are significantly important for safe operations due to a most refrained situation which is stated as derailment. Those also result in wear of wheels and rails, which can reach an extreme level and lead to serious operational dangers. Understanding the rail-wheel contact phenomenon provides avoiding and/or decreasing the effects of such undesired cases.

Studies about wheel-rail contact can be conducted both experimentally or theoretically. Experimental studies can be carried out in the field or in laboratories that can simulate the field scenarios. Various sizes and types of laboratories can be built but a practical and cost-effective solution can be provided by using roller rigs. “Roller Rig” is a term, used in here, for experimental equipment which is used to conduct studies about railway vehicles and components regarding the railway vehicles.

Roller rigs are widely used in the literature as it brings several advantages. Those can be grouped briefly as follows;

- No Field Needs: As known, railways are mostly designed for mass transportation between long distances. So, testing of railway vehicles under all operational conditions also need longer distances which would be extremely expensive and non-cost-effective. However, roller rigs do not need a wide field for service, hence they can be constructed and operated in many technical facilities.
- Construction Flexibility: Construction size, instrumentation, modularity can be determined by experimental needs and available resources. This can provide, energy efficiency, economical solution, multiple uses of components, non-complexity, easy maintenance and repair, adding or excluding components, etc.

- Data Gathering: As known, obtaining data is the most significant part of experimental studies. On a fixed system desired numbers of sensors, readers, counters, etc. can be mounted/placed and this provides a large number and variety of data for processing but on a moving system, it wouldn't be easy to gather this variety of data.
- Parameter Control and Repeatability: On a roller rig setup, all experimental parameters such as friction, contact angles, load, etc can be easily modified. In field work, these cannot be done easily or maybe impossible. Moreover, extreme parameters also can be investigated such as extreme load, friction especially derailment which cannot be repeatable in a real field case.

With the use of roller rigs, many types of research activities can be performed. Some of these main topics can be briefly listed as;

- Investigation of traction and braking properties
- Investigation of wear, damage and irregularities and their effects on the rolling bodies
- Investigation of contact mechanics
- Investigation of vehicle dynamics
- Investigation of operational safety
- Investigation of lifetime
- Investigation of efficiency
- Testing of developed or existing concepts
- Testing of manufactured components
- Developing of control, monitoring and other software related concepts
- Developing intelligent control system

Based on the above-mentioned statements, the measurement accuracy of the roller rigs is vital for reliable studies, experiments, developments, etc. In order to increase the measurement quality of a full-scale tram wheel roller-rig, in this study, several tasks performed which are the determination of the issues regard to the dynamic behaviour and provide solutions to eliminate the effects of them.

Outline

Chapter 1 gives introductory information about the study.

Chapter 2 provides a comprehensive literature survey about roller-rigs. Their history, types, general and specific purposes are briefly given. Also, several key information about methodologies and conducted studies with roller-rigs are mentioned in this chapter.

Chapter 3 provides definitive information about the dissertation objectives and listing of followed methodologies.

Chapter 4 provides the technical specification about the mentioned roller rig. Also, the determination of the issues is stated in this chapter. Then, possible hypotheses for the stated/determined issues are given and applied solution methodologies are explained in detail. Detailed information on the numerical and experimental works was given in this chapter as well. The results of conducted investigations are provided after each part of the study for both experimental and numerical studies.

Chapter 5 deals with the interpretation of the obtained results and provides specific solutions to the mentioned issues.

Chapter 6 summarizes the whole study.

Chapter 7 Recommendations about possible future works are mentioned in this chapter.

2 LITERATURE REVIEW

This chapter contains an extensive literature survey on the usage of roller rigs and technical information about known concepts. Roller rigs and their advantages/disadvantages have been investigated as well. Additionally, an overview of several remarkable studies conducted with roller rigs have been provided.

2.1 Background

Roller rigs are being used from steam-powered locomotives age to validate developed theories, improvement or investigate the new designs/concepts regarding railway vehicles [1–3]. Although, mostly roller rigs have been used for improving the rail vehicle performance, there are also individual varieties developed for specific purposes. However, extensive improvements have been done for simulating the real conditions of the rail vehicles, further improvements are still anticipated. In 1904 Swindon, UK, one of the initial facility built by Great Western Railway which was a full-scale roller rig with adjustable rollers, a braking feature which is used for traction force at different speeds (Figure 1) [1,4]. Since then, both full-scale [5–9] and scaled types [10–13] have been used. Roller rigs are being used for wide ranges of studies including but not limited to, rail vehicle dynamics, adhesion/braking investigations, contact mechanics, derailing, etc [2,12,14–17].

In a chronological aspect, Carter used a scaled test track for his studies in 1920s [2] and in 1950s, in Japan, 1/10 and 1/5 scaled roller rigs are built by the Railway Technical Research Institute. In 1960s, British Railways constructed scaled and full-scale roller rigs for investigating the instabilities of rolling stock. A French company CAFL constructed a roller rig which has hydraulic actuators controlling lateral and vertical motions for investigating lateral, vertical and yaw vibrations. In 1967, Germany, a roller rig developed for studying traction and braking equipment. In 1970, for investigating the derailments of three-piece trucks, 1/5 scaled roller rig built by Princeton University [18]. A full-scale roller rig was constructed by Deutsche Bahn in Munich in the year of 1977. It has vertical, lateral, inclination and rotation controls provided by servo-hydraulic systems which can accurately simulate real track conditions of operating vehicles and capable of reaching 500 km/h speed. This facility has a significant contribution to the development of ICE high-speed trains [1,19]. Between 1984 and 1992, a

particular roller rig operated which has a 13 meters diameter roller, and maximum speed with 250 km/h. With a quarter scaled test bogie, similar conditions to the tangent track is provided. VOCO simulation software has developed by using the results of this roller-rig [19]. Also, another type of roller rig is operated in Linz, Austria which has a 1.5-meter-long rail-part used for rail-wheel contact fatigue. Also, there are scaled roller rigs used widely around the world because of easy build, maintenance and operating costs which are subject to scaling strategies [1,10–12,19–24]. Also, similar to scaled roller-rig concept twin-disc machines are used for some researches [14,25–27]. More detailed information about roller rigs can be found in a study performed by Zhang et al [28].

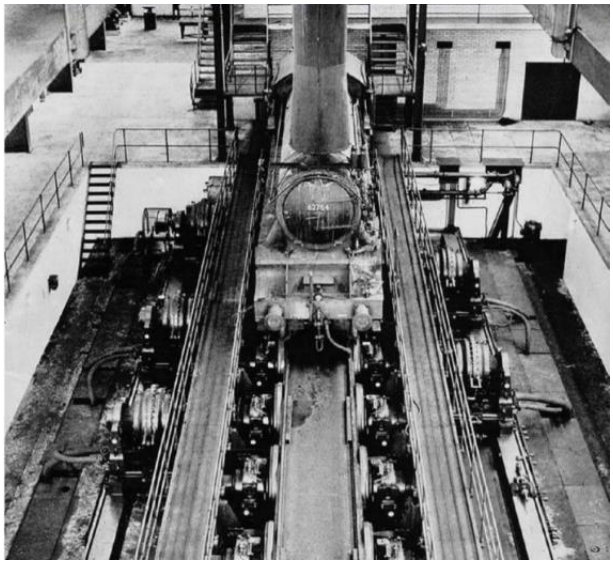

Figure 1. Roller rig for steam locomotives Swindon works Great Western Railway, UK [1]

2.2 Review of Concepts and Functionalities of Roller Rigs

The main criteria for classifying roller rigs can be briefly listed as scale, according to tested specimen and design concept [19,29]. According to the scale, those can be divided into two groups which are scaled roller rigs and full-scale roller rigs. In scaled roller rigs; investment, power consumption, space requirements are lower than full-scale roller rigs and this gives advantages to many institutions for conducting easier experiments. However, this comes with a drawback (i.e. these systems are not fully capable of representing real field operations so there is a need for scaling strategies) [1,29]. For tested specimen classification, grouping can be made single wheel, wheelset, bogie or full car. The complexity of the systems

increases to the given order also conducting experiments are getting complex in the same way [29]. Moreover, conceptual classification can be listed as vertical plane, perpendicular plane, internal roller, and oscillating rail roller rigs. Mentioned concepts are detailly given in the following part. In this study, a full-scale vertical plane roller rig with a single wheel is used.

2.2.1 Single – Wheel Roller Rigs

Single rail test rigs are designed to perform tests for single wheels on a rail structure. Vertical plane roller rig concept is the one of the most favourite type around the world due to easy construction. This concept is also top scored concept in single wheel concepts in the point of view of studying related wheel-rail interaction studies [19,30]. One of the most attractive side of this concept is the cost efficiency. It can be manufactured and operated very cost effectively. Also, on specific topics (i.e. interaction between wheel-rail) the additional parts other than the wheel can create complexity. Additionally, due to small size and less complexity; instrumentation of sensors, constraining and controlling the specimen is much easier compared to other concepts. Nevertheless, there are some drawbacks comes with this concept. Due to single wheel, studies concerning lateral movement (i.e. hunting) are limited. Also, real fielded components such as load systems, rail, side frames, bearings, etc. cannot be used fully and/or need modifications.

2.2.1.1 Vertical Plane Roller Rig

Vertical plane variation is the typical roller rig design with a roller rail and wheel rotating over each other on a common vertical plane. This type is the simplest and most common configuration in study of rail vehicles. Generally, this concept allows to simulate load, attack of angle, rail cant. The roller rail is mostly used to create a steady roll in a specified speed for the planned experiments. It's been reported that some roller rigs are able to perform dynamic vibration actuation while taking measurements using various sensors [30]. An illustration and an example of this concept are given in Figure 2. These types can reach high speeds (in certain cases real vehicle wheels can be used). Force controllers can be mounted easily. Overall, the roller rig could be simply instrumented. As one major drawback of this type can be stated as the rotating rail is not a perfect representation of the straight track. Thus, it can't replicate the

behaviour of straight track. It should be noted that in this study this type of roller rig has been used.

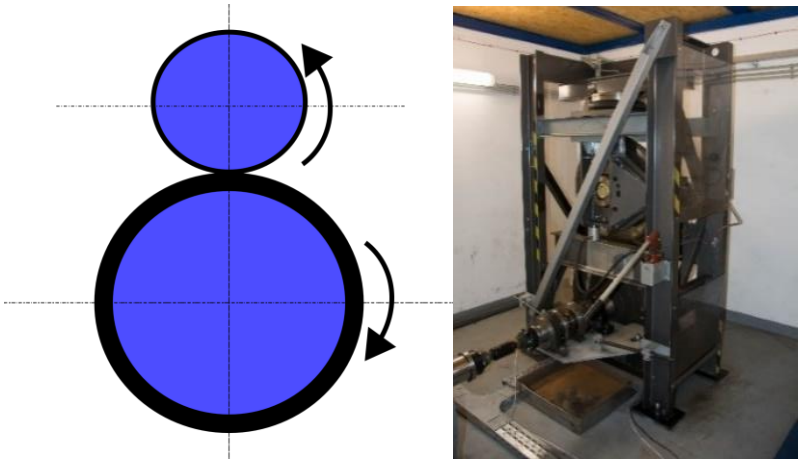

Figure 2. Illustration and an example of vertical plane wheel roller rig

2.2.1.2 Perpendicular Plane Roller Rig

In this configuration, the wheel is placed on a horizontal circle rail. It offers to simulate wheel load, cant angle some additional parameters. Conceptual advantage of this system is to simulate curved track and from point of view contact. It is due to infinite radius on travel direction contact which can be simulated more closely to real cases. Also, rail profile and sub-rail can be modified according to needs. But, due to large horizontal radius of rail, the driving arm and the other components creates a high moment. This limits the speed of the rolling part. A visual illustration and example of perpendicular plane roller rig are given in Figure 3. Another scaled example of this concept can be found in studies [15,31]

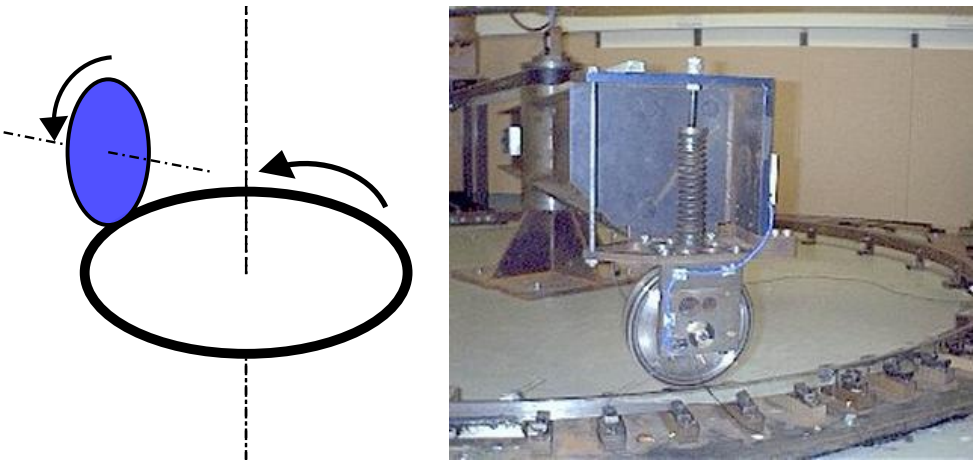

Figure 3. Illustration and an example of perpendicular plane wheel roller rig (Photo credit [32])

2.2.1.3 Internal Vertical Plane Roller Rig

This concept principally same with the Vertical Plane Roller Rig (see 2.2.1.1). This type is used for transit rail and automotive industry [30]. The main difference lies over the radius difference of the roller rail. With a scaled wheel over a high radius of roller rail, geometric interaction can be replicated better than the typical roller rig. However, this comes with a drawback of more demanding space and higher mass than typical one. Illustration and an example can be found in Figure 4.

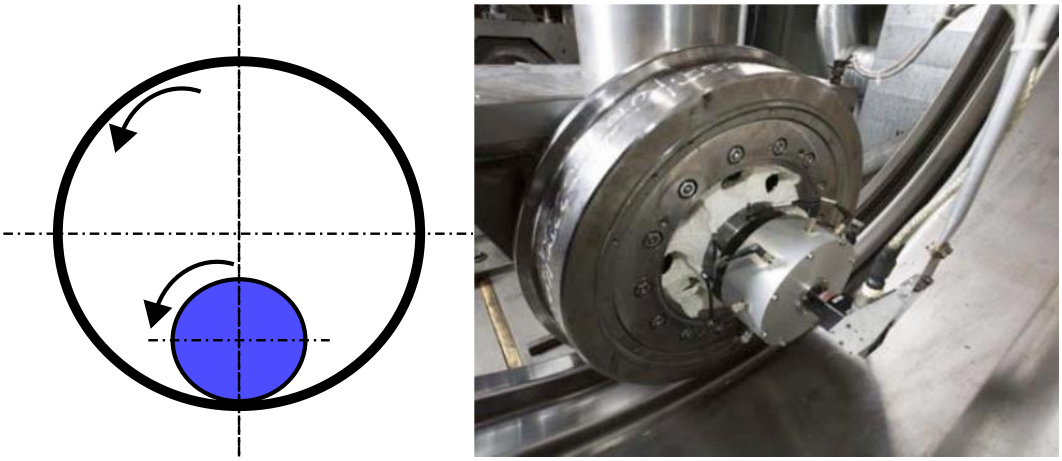

Figure 4. Illustration and an example of internal vertical plane roller rig (Photo credit [33])

2.2.1.4 Oscillating Rail Rig

The main aspect on this type of testing equipment is to perform repeating studies about specific rail parts. Also, they have been used to investigate the rail strength and joint bar fatigue

[30]. In addition to having a simple design, the main advantage of this concept is, fielded rails can be used. Thereby, interaction between roller and rail can be obtained same as in the operational interaction. But naturally it cannot be applied for high speeds or steady state performances. Illustration of the concept and an example can be found in Figure 5.

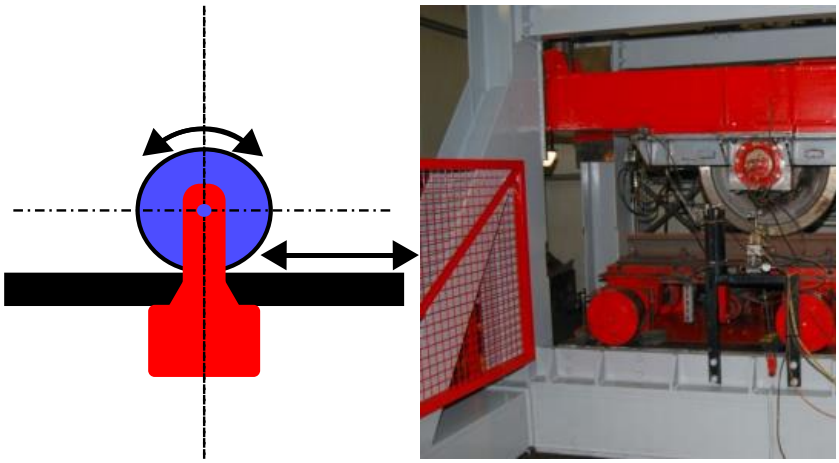

Figure 5. Illustration and an example of oscillating rail setup (Photo credit [34])

2.2.2 Wheelset Type Roller Rigs

This concept provides an experimental setup for investigating wheelset studies. Compared to single wheelset concept, wheelset type has an increased complexity. However, it provides additional studying areas such as suspension design, hunting motion studies, etc. Mainly, it is been used for angle of attack, speed, adhesion-braking, validation of new designs. Also, in this concept, using real field components is much more possible over single wheel concept. (i.e. side frame, bearings, etc.)

It can be briefly described as the doubled version of single wheel concept with a connecting shaft between wheels. The rollers can be independent or connected according to the design and needed outputs. Drum type rollers can be given as an example for dependent roller types [1]. Due to complexity of the system, optional configurations are widely various. Illustrations and examples of both types are given in Figure 6 and Figure 7, respectively.

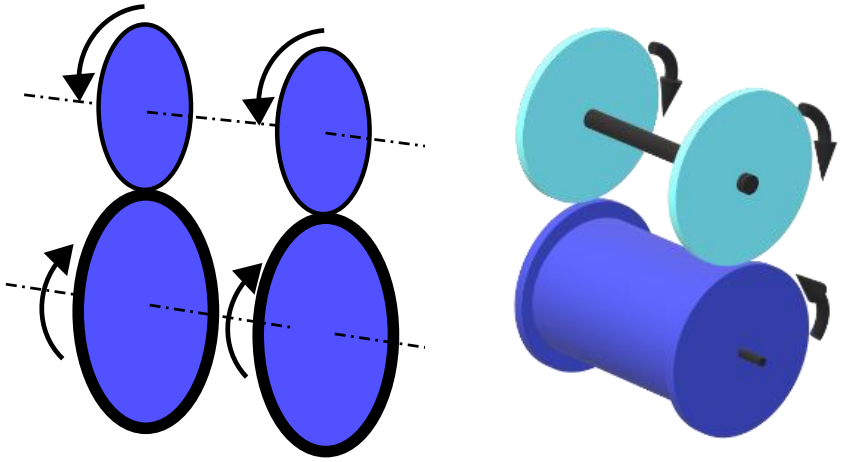

Figure 6. Illustration of vertical wheelset concept design for both type

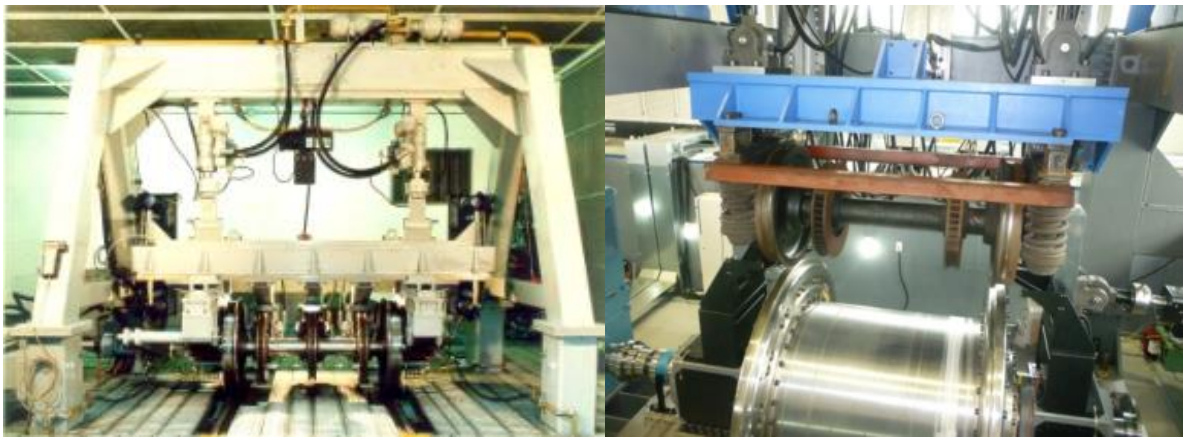

Figure 7. Examples of vertical plane wheelset roller rigs (Left [35], Right [36])

2.2.3 Full Truck Concept Rigs

Full truck rigs are designed for testing full car bodies or bogies. This type facility can be considered as the most complex type in use of roller rigs. However, this complexity provides deep analysis and experiment environment to the researchers especially studies concerning the railway vehicle itself. Full truck rigs allow to investigate complete body dynamics, wheel-rail interaction studies, hunting studies, etc. Moreover, due to possibility of placing a complete car body on a testing rig, all components regarding to vehicle can also be tested. The advantages can be briefly grouped as; (i) loading and constraining conditions may be simulated as field conditions, (ii) bogie and wagon assemble can be tested for curvature conditions, (iii) it allows studies about interaction between body/suspension, bogie/wheelset and combination of both, (iv) it also allows investigation on fielded cars. Nevertheless, it is for sure that there are

drawbacks about this concept. Cost for investment and operation is much higher than over other concepts and sizes. Also, monitoring for specific studies and instrumentation for data gathering are difficult due to physical complexity. One of the most complex full-scale testing facilities in Chengdu, China is given Figure 8.

Although they have a lot of properties in common, it is not possible to make a certain classification about existing full truck roller rigs. Each of them has been designed with different technologies, traditions, budgets, aims, institutions, structures, etc. in order to satisfy different goals. An extensive review study about existing full truck roller rigs may found in the reference by Zhang et al [28].

Figure 8. Full car roller rig in Chengdu, China [28]

2.2.4 Scaled Roller Rigs

It is known that full-scale roller rigs can provide much closer simulations to real field operations than scaled types [37]. However, for deeper investigations concerning specific topics about railway vehicles (i.e. for wheel-rail contact studies using full-truck roller rigs are not efficient tools). Mostly, due to smaller sizes, investment and operation costs are much lower compared to the full-sized roller rigs. Additionally, modifying the parameters of experiments are easier. However, it may be advantageous in some points, scaling factors can’t be neglected [37].

Similarity laws, size effects, and correlated problem of scaling are of interest for the transformation of experimental results from a scaled model to the full scale design [37].

Deriving scaling factors from dimensional analysis can be pointed as an approach which were conducted before some researchers [21,38–40]. Additional scaling approaches may be given such as modifying equations of motion and materials. A detailed study about scaling can be found in reference by Allen [37].

All above mentioned concepts exist in scaled versions designed according to the needs of the facilities and capabilities. Scaled versions of above mentioned concepts are given in Figure 8Figure 9; a twin disc machine (a), scaled vertical plane single wheel roller rig (b), scaled vertical plane wheelset roller rig (c) and scaled bogie roller rig (d) are given in Figure 9.

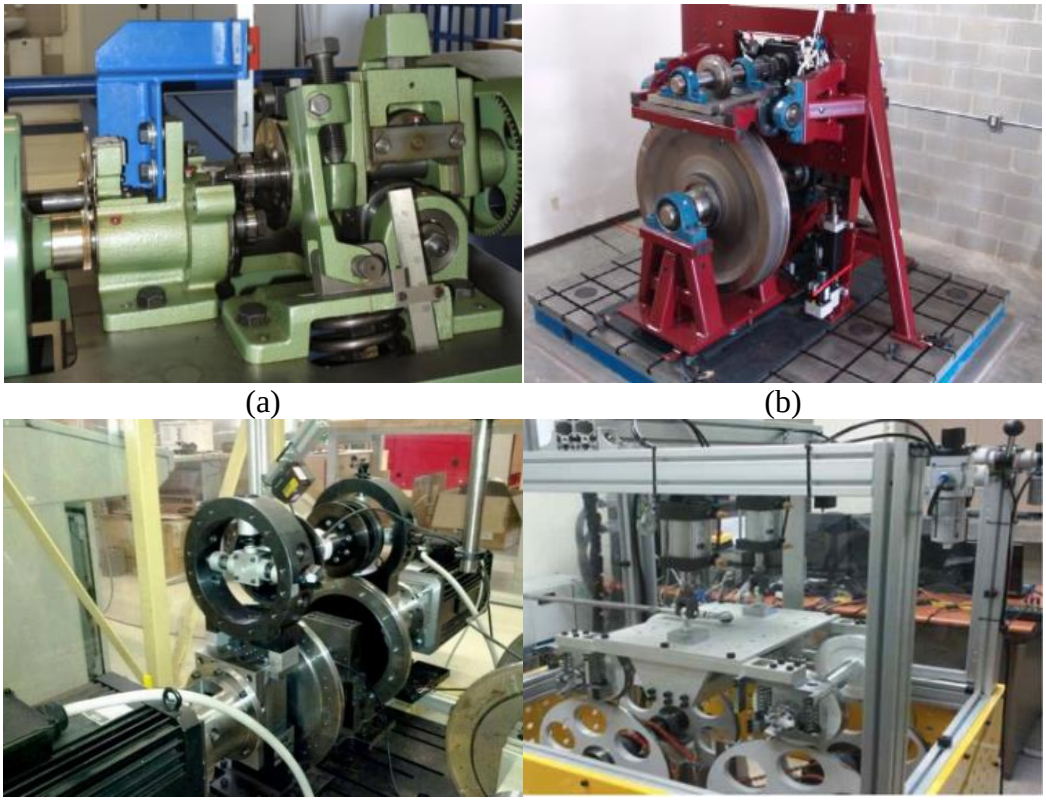

(a) (b)

(c) (d)

Figure 9. Examples of scaled roller rigs (a [41], b [42], c [13], d [16])

2.3 Review of Studies Performed on Roller Rigs

As mentioned above, the roller rigs are widely used tools around the world for studying the matters related to railway applications. In this section, several prominent studies which are conducted on roller rigs have been overviewed according to the topics.

2.3.1 Studies Concerning Wheel – Rail Interaction

Wheel-rail contact is the one of the most popular topics in railway research due to its influence on reliability, efficiency, safety, etc. Also, this interaction is affected by environmental conditions significantly (i.e. rain, snow, leaves, temperature etc.) and the level or duration is highly varying according to the yearly date, climate and geolocation. Thus, these variabilities arise necessity of studies concerned about adhesion itself and characteristics. Some experimental studies about adhesion characteristics conducted on roller rigs are given in [3,23,43–46]. Moreover, theories concerning wheel-rail interaction still not able explain this interaction fully, so it is still demanded study field in railway applications. Several studies concerning wheel-rail contact can be found in [9,17,47–49]. In addition to them, some studies can be found concerning directly about contact patch between wheel and rail [50–53].

Wear and rolling contact fatigue (RCF) are also among the popular topics studied [5,54]. The RCF mechanism is closely related to the wear [5,55]. Researchers have been working on the effects of wear and RCF due to their effects on reliability and durability because of strict relation to the maintenance and repair [56].

2.3.2 Testing of New Designs

It’s known that developed engineering products need to be tested before use. Roller rigs are also being used in validating the new designs, developing innovative solutions. A wide-spread spectrum of study topics is being performed about testing new designs. Several studies about testing new designs can be found such as, guidance for running gears [57], a novel running gear [58], new coatings [59], condition monitoring system [60], slip control system [61], friction modifiers [41], traction control system [13].

2.3.3 Running Safety

Roller rigs are being used also for concerning safety of railway vehicles [28]. In railway operations, one of the most avoided cases are derailments with no doubt. Additionally, critical speed, lateral stability and curving dynamics can be included in safety topic. Several studies about derailment can be found in [62–64]. Studies about lateral stability, critical speed and curving dynamics can be found [65–67], respectively.

2.4 Wheel – Rail Interaction

2.4.1 Normal Contact Problem

One of the earliest studies about contact problem is made by Redtenbacher in 1855. He studied head-crack formation in rail [6,19,68]. In 1882, one of the most significant study about contact has been published by Hertz [69]. In this theory, the contact patch arises around a point and takes form according to the shape of the surfaces. Even so, true shape of the contact cannot be represented with this theory because of the non-constant shape of surfaces but it provides accurate results for continuously curved surfaces. Today it's still being used as a foundation in wheel-rail contact analysis also many studies and developments are based on this theory [1,70,71]. A review study of analytical methods is published by Piotrowski and Chollet [72]. Also; Kik and Piotrowski [73], Pombo et. al. [74], Linder [75] are proposed non-Hertzian methods for contact analysis. Some of them are compared in the study of Sichani et al [76] and compared results are shown in Figure 10.

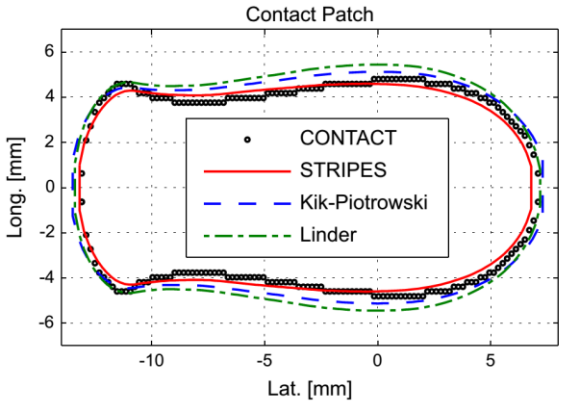

Figure 10. Wheel-Rail contact area compared for different contact models [76]

Nowadays, thanks to the emerging technologies, it’s also possible to study the contact problem with finite element method, which provides faster results [77]. Additionally, Boundary Element Methods are also used [78]. One of the most popular method used in wheel-rail interaction has been studied by Kalker [70]. However, FEM and BEM calculation times are longer over analytical methods due to calculation complexity. Because of this reason, in the further part of this study, contact size and shape calculated with Hertzian approach.

2.4.2 Tangential Contact Problem

For an initial perspective of tangential contact problem, it can be presumed that applying Coulomb's friction law to contacting surfaces can be acceptable. However, it is not a fully proper approach in wheel-rail contact due to defects, force distribution, wear, the strength of materials, etc.

In 1926, Carter propounded a theory about continuous rolling of a wheel on a rail on a bi-dimensional plane [71,79]. In this theory, he assumed that the wheel is cylindrical, and the rail is infinite elastic medium. He defined creepage "as the ratio of the distance gained by one surface over the other, to the traversed" [79]. According to his approach, creepage has a direct relationship with the tangential forces. With increasing torque, the creep and the creep force are also growing until the traction bound, which is roughly considered as the maximum frictional force between surfaces according to Coulomb's friction law. This is named "saturation" in the related literature [1,70,79]. The three dimensional approach was proposed first time by Johnson [80]. In this approach, an elastic sphere is rolling on an elastic plane. He investigated straight rolling motion and the spin of elastic sphere which occurs on circular area of contact. In 1964, Johnson and Vermeulen [81] extended his study to elliptic contact shape and they proposed a saturation law for tangential forces but in their study the effect of spin wasn't considered. In 1973 Kalker extended his work. On his former study, he proposed his famous Linear Theory. With this study, he contributed to the literature a 100 times faster calculation method. Also, he provided longitudinal and lateral forces. In 1982, he published another study which is defining a connection between elastic displacement and traction by tangential flexibility [82]The latest analytic approach to the tangential solution was contributed by Polach [45]. His study was an extension of Freibauer [83]. Polach's study was based on slip velocity depended friction and he added two parameters for adhesion and slip part. Due to good approximation and simple structure, Polach's formula was implemented for tangential solution in this study and the details are given in the related section.

2.5 Differences Between Tangent Rail and Roller Rail

For most of the roller rigs (full scale or scaled types), for the wheel-rail pair, the rail is substituted by a rotating (roller) rail due to inherence of the laboratory conditions. To create a

continuous motion in a laboratory environment an infinite rail must be employed. In this context, a specific contrary example may be given for use of tangent rail can be seen in section 2.2.1.4. Another case for simulating curve track also may be given as the perpendicular plane roller rig which is described in section 2.2.1.2. Apart from these concepts, the roller rigs contain roller rail which is differs from a tangent rail. The main differences between roller rail and tangent rail are geometric parameters.

In real case of wheel- tangent rail contact, the rail is almost flat in longitudinal direction. In contrary, wheel-roller rail contact, the roller rail has a curvature in longitudinal direction. Both situations sketched in Figure 11. This difference directly effects the contact area. So, one of the main parameters which is used for determination of contact condition, change. In lateral direction, maintaining the lateral curvature is mostly possible however, for higher scaled rigs (e.g. 1/20 scaled roller rig, twin disc machine) may not be possible due to small sizes in every direction.

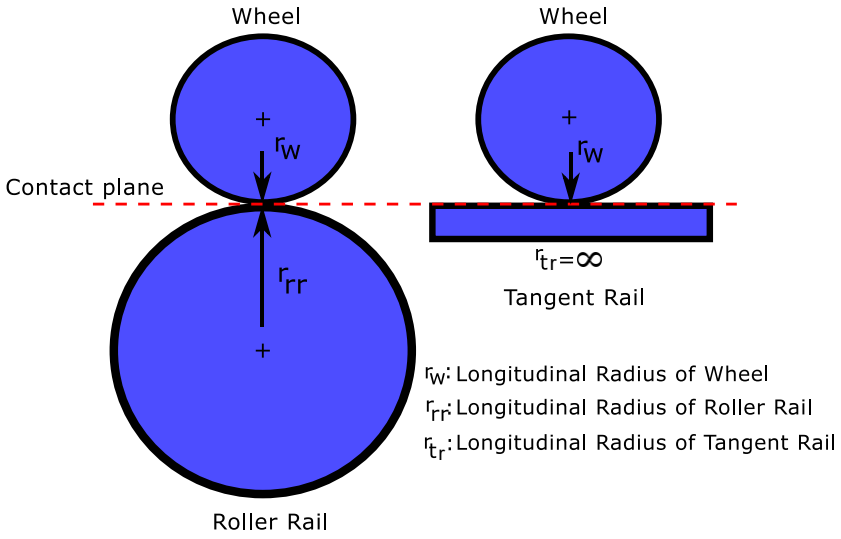

Figure 11. Scheme of longitudinal radius difference between tangent rail and roller rail

A comparative study has been applied in order to see the change of the contact area according to the radius change of the interacting bodies (wheel-rail). Due to easy application and comparison, Hertz Theory employed for determining the contact radii and contact area. Longitudinal wheel radius (r_w) kept constant (350 mm) and longitudinal rail (r_r) radius has been increased from 350 mm to infinity in order to see the effect of the rail/roller radius change. It is assumed that the radius of the roller rail should be higher than the wheel radius. Lateral

radii were also kept constant and taken 300mm and 400mm for wheel and roller/rail, respectively. Both of the bodies are assumed identical from the material properties aspect which are 210GPa for elastic modulus and 0.3 Poisson ratio and the applied load selected as 20 kN.

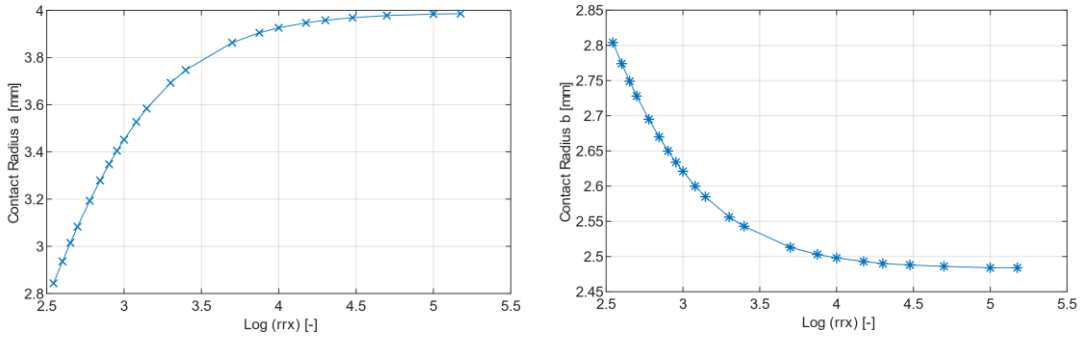

(a) (b)

Figure 12. The effect of rail radius changes in longitudinal direction on contact ellipse radii

In Figure 12 the effect of rail radius change in longitudinal direction is given. Horizontal axis is the logarithmic value of the radii. As it is seen in referred figure, the effect of radius change is significantly small when the logarithmic value of the radius is bigger than 4, which corresponds 10^4 mm (10 meters). The effect of the radius change on the contact area is given Figure 12.

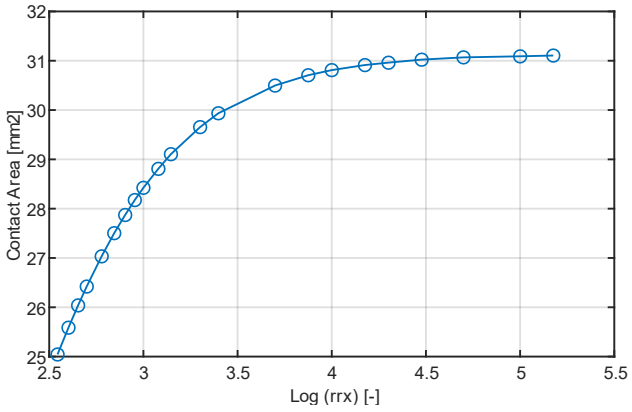

Figure 13. The effect of rail radius changes in longitudinal direction on the contact area

According to the calculation results, the contact area for 10 meters radius is 30.9129 mm^2 and for tangent track is 31.1196 mm^2. The difference between calculated values is ‰7 which is quite acceptable. However, in practical application, designing a roller rail with 10 meters radius non-preferable for most. In this context, to reach a closer contact area an

acceptable solution can be applied by decreasing the wheel radius. However, reducing the radii of rolling bodies brings another issue and in order to overcome this issue several scaling strategies are being used.

3 DEFINITION OF DISSERTATION OBJECTIVES

The overall objective of the dissertation is to improve the quality of the measured data by analysing the dynamic behaviour of a full-scale tram wheel roller rig from the mechanical aspect. In order to achieve this objective, several sub-objectives must be accomplished which can be expressed;

1. The differences between the experimental results and expected results which have been given according to existing well-known wheel-rail contact theories must be identified.
2. Structure and characteristics of the experimental device must be understood and examined in order to understand the weaknesses or possible issues which may cause the inaccuracies.
3. Possible mechanisms of influences which causes the mentioned issues must be formulated.
4. The formulated mechanisms must be tested and validated with experimental procedures and computational tools.
5. Possible solutions for eliminating beforementioned inaccuracies must be proposed.
6. Proposed solutions must be implemented, and their contributions must be verified.

In order to test the accomplish beforementioned sub-objectives, the system is considered as sub-systems. The sub-systems considered as composition of specific parts. A scheme of considered parts and generated solutions are given in Figure 14. These parts must be analysed and investigated with proper tools such as experimental procedures, structural analyses, etc. All those components described under main system are analysed step by step. Possible weakness in these individual components are intended to be revealed. Identification of issues, details of abovementioned roller rig, used methodologies, experimental instruments and initial results will be presented in regarding sections.

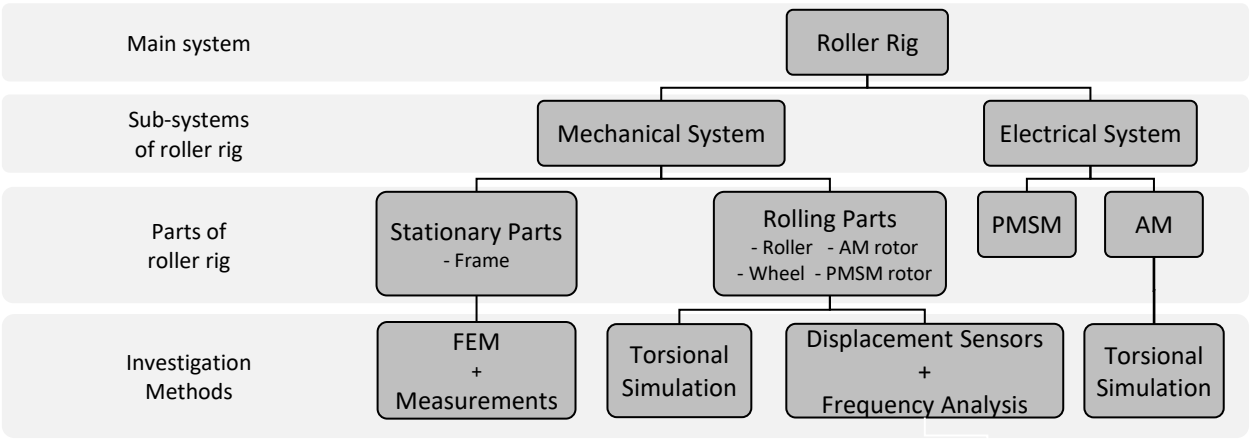

Figure 14. Scheme of sub-systems of roller rig and investigation methods

4 METHODOLOGY AND RESULTS

4.1 Experimental Setup

Before analysing the possible measurement issues in the roller rig, its experimental setup must be examined in detail. The system which are the measurements conducted is a plane type roller-rig placed in Educational Centre in Transport in Doubravice, Pardubice. The stand has a reprofiled tram wheel after extensive using and the roller is a converted wagon-wheel. It has been built by VUKV (Rail Vehicle Research Institute) and its modified according to needs of researches. Roller rig gives the opportunity to conduct adhesion experiments also it's been used for the development of PMSM regulation systems. Several studies performed with this roller rig can be found in [3,46,60,61,84–89]. The roller-rig is given in Figure 15.

Figure 15. Tram Wheel Roller-Rig

4.1.1 Mechanical Design

Wheel and roller are placed on a vertical plane while the roller is connected to the bottom of the frame by two bearings and a plate. The wheel is connected to a single beam on top by a pneumatic spring and swinging arm. Swinging arm is connected to side columns by a journal bearing which does not permit the lateral and yaw movements. The normal force is

applied with pressure control of air spring on top. Schematic representation of the tram-roller rig is given in Figure 16.

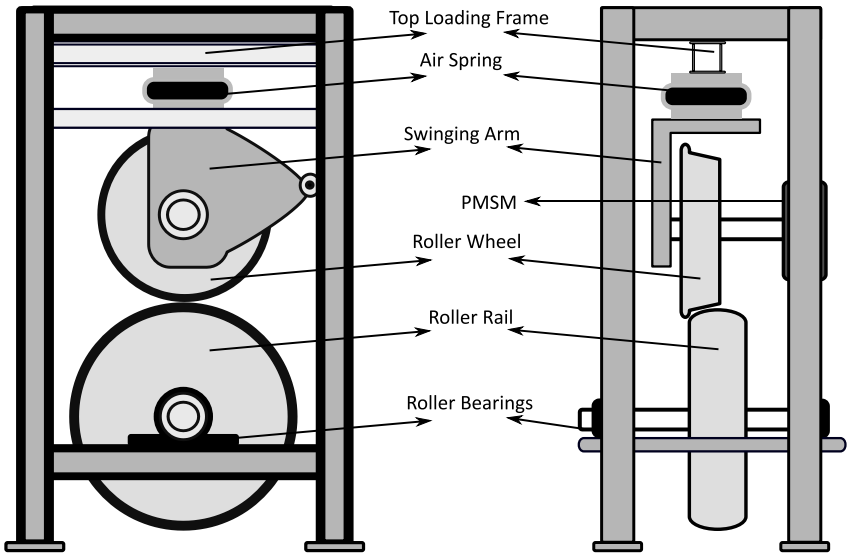

Figure 16. Illustration of tram roller-rig from both-sides

4.1.2 Electrical Design

Wheel of roller rig is driven by a PMSM (Permanent Magnet Synchronous Motor). PMSM has a rotor with attached permanent magnets and rotation is provided by the magnetic field created by the stator. It is controlled with a flux weakening method. The torque is generated by torque request via controller. Electrical scheme of the roller rig is given in Figure 17. Details of the control method and PMSM are explained in other studies [85,90]. Technical properties of PMSM are given in Table 1.

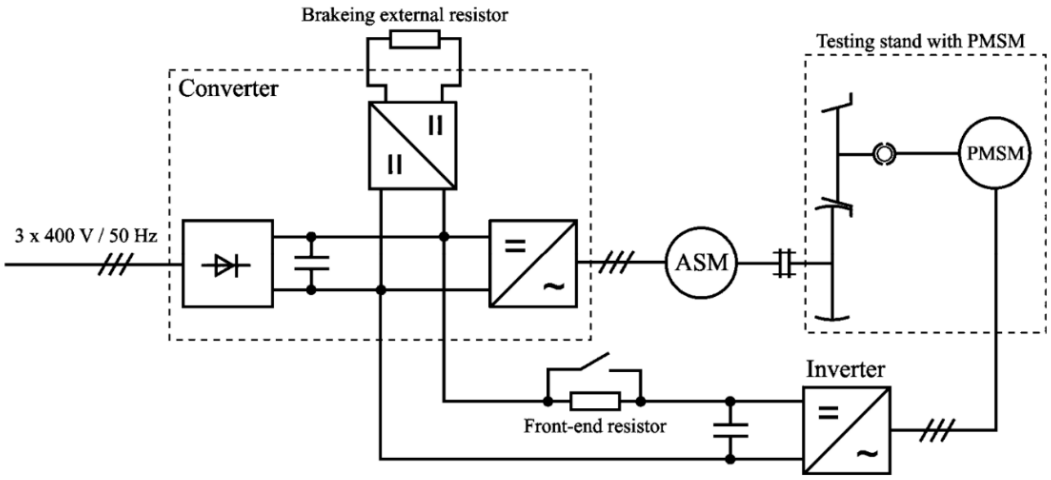

Figure 17. Electrical scheme of the tram wheel roller rig [90].

Table 1. Parameters of PMSM

Power	58 kW
Speed	650 rpm
Nominal Torque	852 Nm
Current	122 A
Flux	0.2 Wb
Number of poles	44

Table 2. Parameters of AM

Power	55 kW
Frequency	50 Hz
Nominal Torque	891 Nm
Current	133 A
Voltage	3x380 V/Δ
Number of poles	10

Roller is driven by AM which is placed out of main frame. Mainly, AM contains two parts which are rotor and stator. The principle of this motor is creating a rotating magnetic field over a squirrel-cage by a stator without any wire connection. The magnetic field of stator and rotor don't rotate synchronously, and the speed control is made by changing the frequency of the current. Roller rail is connected to the motor via torque sensor, CV shaft. Technical properties of AM are given in Table 2.

4.1.3 Data Acquisition System

Controllers and data acquisition scheme is given in Figure 18. Normal force in the system is provided by air-spring with pressure control. The pressure in the spring is monitored with sensor - see element (1) in Figure 18- and stored in PC (9) via DAQ device (7). Wheel torque is provided by PMSM (2) and controlled by PC via PMSM Controller (6). AM (5) is controlled by an independent controller (8) via a converter (10). Angular speeds of the wheel and roller are measured by rotary encoders (3) which are connected to shafts. A torque sensor (4) is mounted on the shaft between the roller and AM for measuring torsional load. The coefficient of adhesion and tangential force is calculated by PC based on the signal of the torsional sensor.

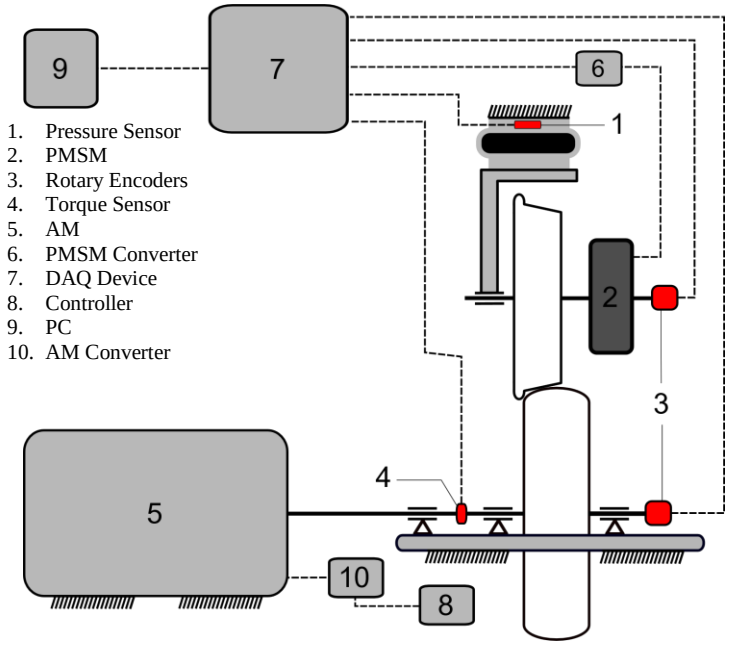

Figure 18. Controllers and data acquisition scheme of Roller Rig

Pressure sensor is DMP331 model and the manufacturer of the sensor is BD SENSORS, Germany. The rotary encoders are produced by LARM and type of encoder is IRC315. The DAQ device is NI USB-6341 model of National Instruments, USA. The data resolution used in the study is 250 Hz.

4.1.4 Procedure of Adhesion Measurements

As mentioned before the main purpose of this roller rig is to conduct adhesion experiments. The procedure during the experiments is summarized as follows;

- The normal force is applied by pressure controlled pneumatic spring.
- The roller is brought to desired constant speed by AM controller so that the wheel starts free rolling.
- A torque request is sent to PMSM then wheel speed starts to increase (traction case) or decrease (braking case).
- Due to the adhesion force between wheel-roller pair, the AM creates a reverse torque.
- System pushed until to the requested torque or a safe slip.

By above-mentioned procedure, the following quantities are obtained;

- Pressure from pneumatic spring (Converted to Normal force).
- Rotary speeds of wheel and roller.
- Torque on the shaft between the roller and AM.

4.2 Determination of Inaccuracies

4.2.1 Dynamic Phenomenon

A dynamic phenomenon has been revealed in the adhesion measurement results which occurs after loss of adhesion with a sudden decrease of requested torque. The phenomenon appears as an oscillation around zero torque with significant overshoots before the system gets the steady state. To identify the dynamic phenomenon, the torque patterns were repeated three times in a test with identical conditions. Sudden increase and decrease of torque values, which resulted in non-random oscillations, were found. Requested wheel torque pattern and measured roller torque are shown in Figure 19. The oscillation around zero torque can also be seen in the referred figure. Additionally, the influence of mentioned oscillation is given on Figure 20.

Additionally, with a closer look to the referred figure, a delay can be seen on the torque values. Especially on the torque-decrease phase the time gap between requested wheel torque

and measured roller torque is significant. Moreover, when the torque request increased to the maximum, an overshoot is visible on the measured roller torque.

The primary objective of this study is to propose a possible explanation and solution for mentioned oscillation, delay and overshoot.

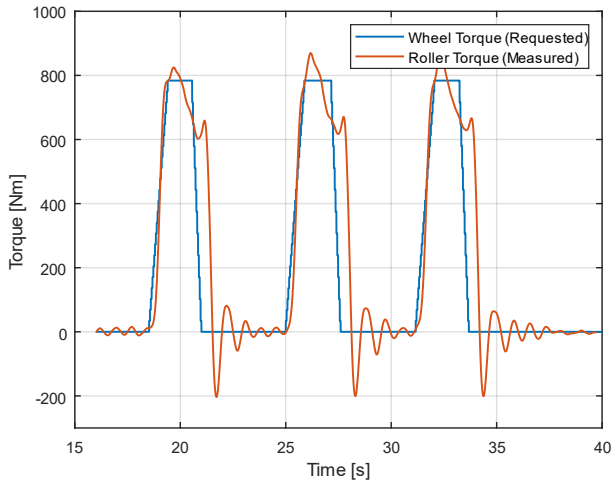

Figure 19. Requested wheel torque and measured roller torque for determining the phenomenon

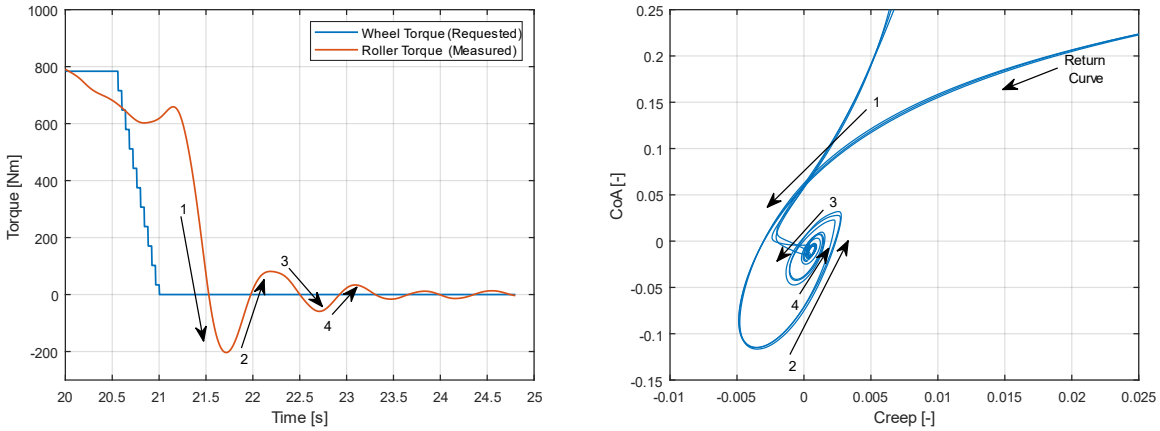

(a) *(b)*

Figure 20. The influence of the torque signal oscillation on Creep-CoA graph

4.2.2 CoA-Creep Inconsistency

An inconsistency in the measured data revealed itself. It is observed that, when torque request decreased after a certain creep level, creep-adhesion curve follows a different path when returning to the steady state. It shows different adhesion levels for same creep values. Figure

21 shows a comparison for dry and wet surface conditions between Polach's theoretical creep-adhesion curves and experimental creep-adhesion curves. (Theoretical curves are obtained with estimated values and fitted to the measurements). Those include creep values corresponding to adhesion.

It has been reported in some literature, after a certain slip, the CoA doesn't follow the same path as theoretical fit [8,87]. It is obvious that the exact match can't be expected between theoretical considerations and experimental results. However, in the dry surface case, the gap between increasing slip curve and decreasing slip curve is relatively high (Figure 21). Especially, on the decreasing slip, when the value gets closer to the zero the CoA drops significantly. In Figure 21, same issue has revealed itself for wet surface condition also. This leads to undesired creep-adhesion results which is an issue for the reliability of the measurement. Providing an explanation and solution for this issue is another objective in this study.

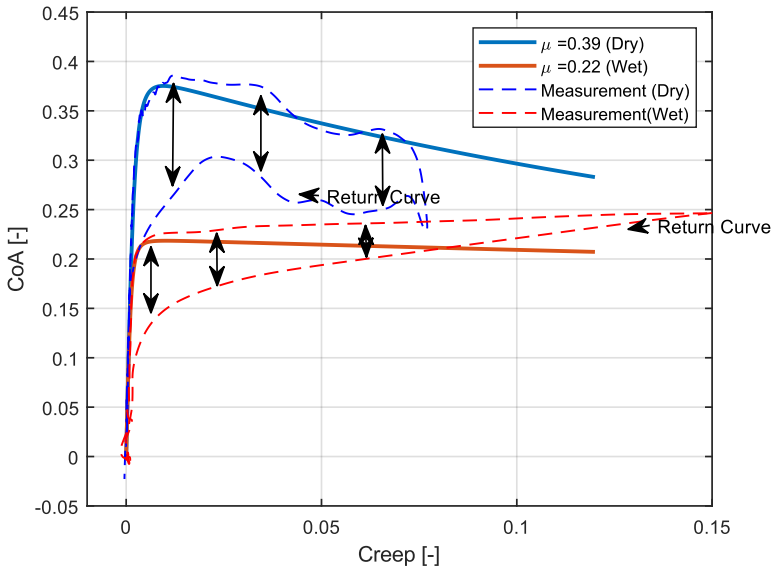

Figure 21. Comparison of theoretical adhesion-creep curve and measurements.

4.2.3 Waving Torque Output Under Free Rolling

Moreover, another issue is found in steady state rolling where there is no traction. As seen in Figure 22, the measured torque value before loading has a waving character around zero

under free rolling. This undesired situation could be due to the out of roundness of one or more rolling elements. It is believed that the out-of-roundness creates a dynamic effect on the global behavior. Also, the mentioned signal may occur due to issues regarding electrical issues or components. An explanation and solution will be searched also for this issue.

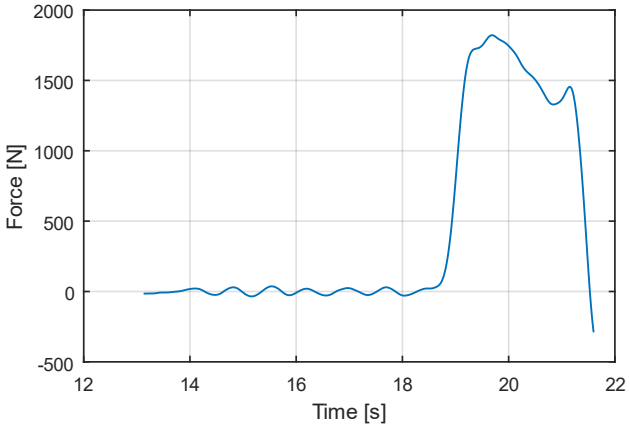

Figure 22. Waving torque signal under free rolling

4.3 Possible Causes of Inaccuracies

4.3.1 Stationary Parts

As it's seen in Figure 19 , there is an oscillation in measured torque signal ending with damping where slip ends. It's believed that one of the reasons of the oscillation may occur due to roller-rig frame flexibility in longitudinal direction. A schematic representation of this possible effect is given in Figure 23. Under traction case, the torque generated by PMSM transfers to the roller rail via the wheel. The transferred force creates a horizontal load between wheel and roller which results in a deflection on the longitudinal direction (δ_f). After releasing the requested PMSM torque sharply, the load on the frame discharges. A sudden decrease of the load would cause an oscillation on the roller rig frame (1). Oscillation of the frame would create a horizontal oscillatory movement of the wheel in longitudinal direction (2). This may be transferred to the torque sensor by the roller rail on over roller shaft (3). Possible reasons of these effects may be low stiffness of the frame components or weak bonding in frame joints.

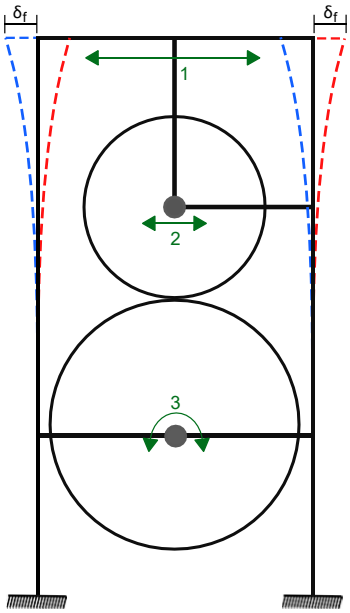

Figure 23. Schematic representation of possible occurance of longitudinal oscillation of frame

4.3.2 Rolling Parts

Another possibility for the cause of the oscillations (Figure 19) can be issues regarding to rolling parts of the system. The inertia of the roller rail is relatively larger compared to the other rolling parts of the roller rig. As it can be seen in the Figure 18, the torque sensor has been placed on the shaft between roller and AM rotor. The diameter of the cross-section of this shaft relatively small compared to the roller size. As mentioned in the section of procedure of adhesion measurements; when the requested wheel torque is decreased, the asynchronous motor torque response is also decreased. Sharp change on the torque request might cause high overshooting of AM torque response due to high inertia. This may be an explanation of the before-mentioned oscillation around zero torque due to the relative motion difference between roller and AM rotor. A schematic representation of the possible cause is given in Figure 24. Another approach is; this relative motion can also occur due to the slow reaction of the overall system to the torque changes. Both possibilities will be investigated in related section.

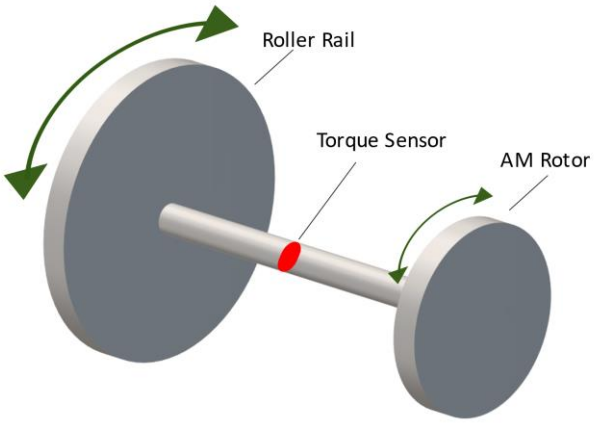

Figure 24. Schematic representation of torque oscillation signal in the roller shaft

When Figure 22 is investigated deeply, the wave signal is repeating under free rolling. From the mechanical point of view, a possible explanation for the reason of the wave signal is can be out-of-roundness of the rolling parts which may produce a signal varies according to the speed. Furthermore, it can be related to the shaft eccentricity or bending due to incorrect positioning of the shaft bearing.

4.3.3 Electric Motors, Control of the Electric Motors and Data Acquisition System

Another possibility for the cause of the oscillations (Figure 19) may be the motor and controller responses. However, it is known fact that PMSMs are widely accepted electric motors due to their robustness [91]. Moreover, field oriented control (FOC) provides great improvement on dynamic response of the motor [92]. Because of the robust characteristic of the PMSM and its control method, it is believed that the abovementioned issues are not connected with PMSM nor control methodologies.

However, the AM in the roller-rig is controlled by open loop voltage frequency control strategy. It is stated that, open loop voltage frequency is the most popular control strategy of squirrel cage AC motors [93] due to less complexity and relatively lower cost. On the contrary, the biggest disadvantages are the speed dependence on the external load torque, mainly for AM, and reduced dynamic performance [94]. Thus, the abovementioned dynamic phenomenon may occur due to the dynamic performance of the AM and/or its control strategy.

Also, issues in the resultant data may be created by the data acquisition system, noises in electronic parts and disturbing frequencies of moving parts.

4.4 Investigation of the Stationary Parts

4.4.1 Numerical Study

Stationary parts of the roller rig have been numerically modelled in Solidworks® software environment in order to investigate the dynamic behaviour of roller-rig frame. As an initial approach, a static solution has been generated. The frame is rigidly fixed in six directions from bottom ends of all four columns. Bonding types were neglected in the initial model so, all components were modelled as fully connected joints. Experiments are planned in two groups which are aimed to measure the response of selected parts of the roller rig frame under vertical and horizontal loads. In this regard, two loading cases have been simulated statically. These are vertical-for normal load simulation, horizontal-for the tangential force simulation. 20 kN, which is the maximum force generated by the pneumatic spring, is applied vertically. Simultaneously, 2 kN applied horizontally is estimated from past adhesion measurements for the initial model. The vertical load has been applied over a plate from the bottom surface of the top beam which is similar to loading plate between pneumatic spring and the top beam. The bottom plate is loaded with reaction force from two sides with plates which are similar to the bottom of bearings of the roller shaft. Statically loaded frame in FE software shown in Figure 25.

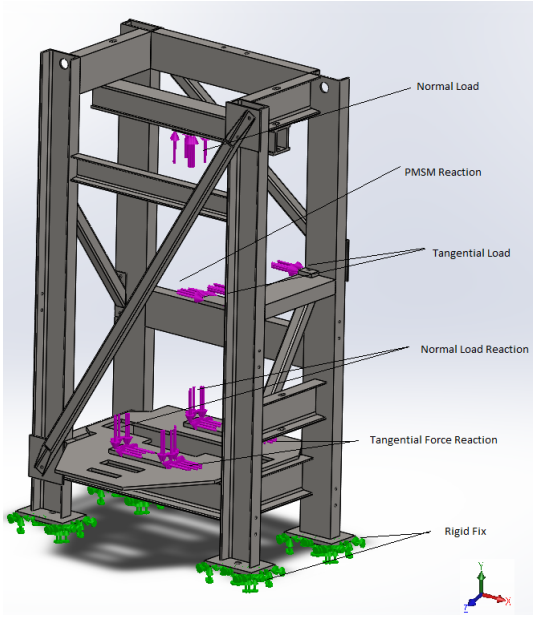

Figure 25. Loading and fixtures scheme of roller rig in FEA software

As expected, under vertical loading, the top beam (loaded one) has a bending response. Maximum stress has been found around the midpoint of the beam. FE model and response of the roller rig frame under vertical loading shown in Figure 26.

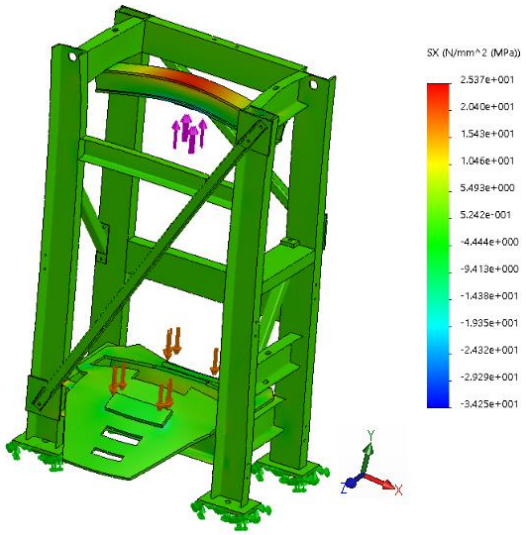

Figure 26. The response of frame under vertical load

The response of the model under horizontal and vertical load shown in Figure 27. The locations near to swinging arm connection on the vertical beams had the maximum stress.

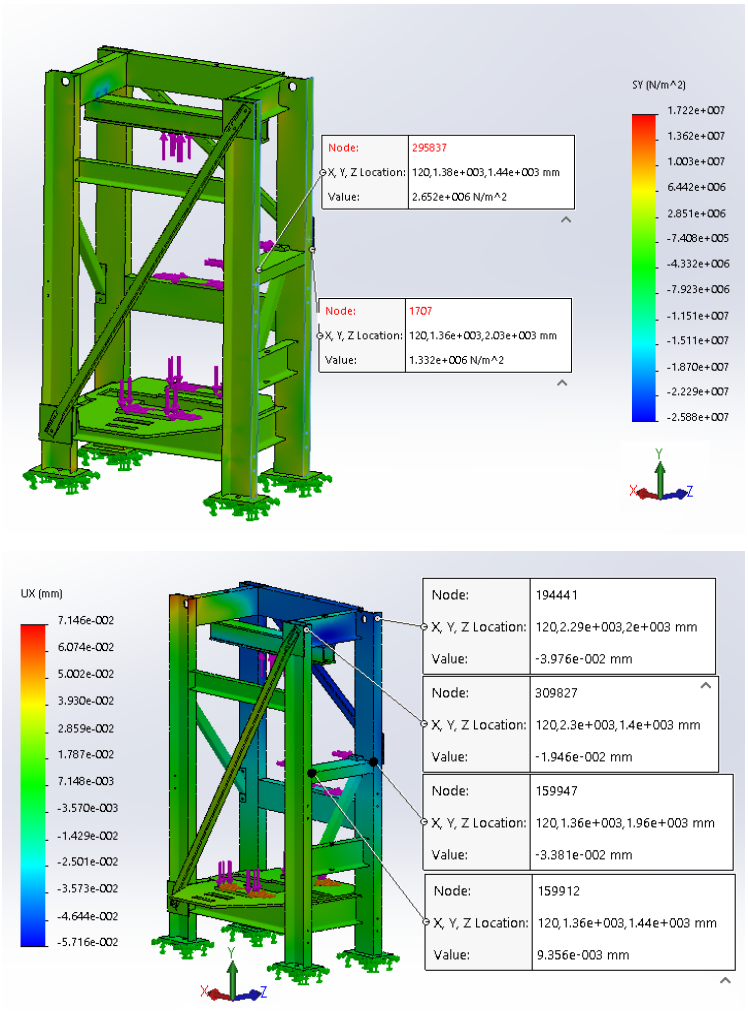

Figure 27. Response of frame under horizontal and vertical load

4.4.2 Experimental Study

For validating the results of the initial FE analysis, a measurement procedure has been applied. The locations of maximum stresses had been selected and measured with strain gauges. Locations of the strain gages are given in Figure 28 (left) and application of strain gages are given in Figure 28 (right).

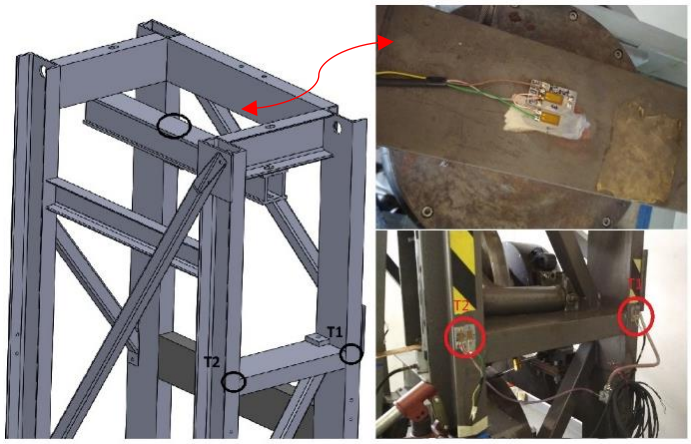

Figure 28. Determined strain gauge locations and instrumentation

4.4.3 Measured Data

In order to discard the noises from the results and obtain a smooth curve, a smoothing filter (Loess method) has been applied to the measured data. An example is visually presented with measured data and smoothed curve for 10 kN in Figure 29.

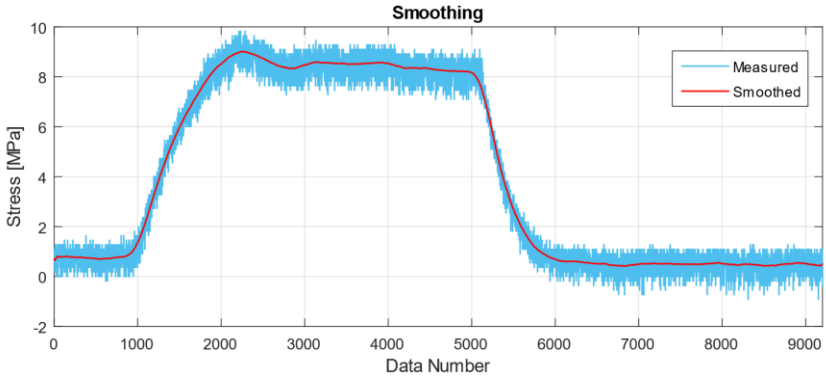

Figure 29. Smoothing procedure of measured signal

Measured data and static FEM results were compared in order to verify the model results. The mechanical stress generated by 20 kN vertical load has been measured from the same place (i.e. top of the beam). The comparative results are provided in Figure 30. A close relation was found between measurement and FEM result. The differences between monitored stresses and calculated stresses were found relatively low which shows the efficiency of the FE solution.

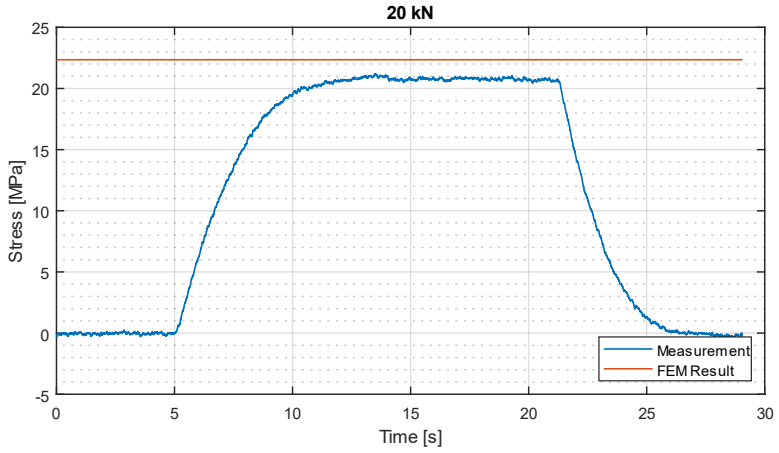

Figure 30. Comparison of FEM and Measurement

As seen in Figure 31, the three identical loading cases were applied for this particular case (horizontal load under 30 km/h). Even though there is a small difference in the amplitude of the measured data for repeated conditions, those have an insignificant impact on the global response. As referred in depicted figures, the experimental response is compared with the one obtained from the numerical solution. It should be noted that the stress corresponding to the position of the strain gauge is estimated by averaging the surrounding nodes. In the FE solutions, the results yield higher values for the right side of the frame (i.e., short braced side in Figure 27) while a lower value was found for the opposite side. When the results are investigated in depth, both experimental and numerical response is in close correlation. On the other hand, the measured stress values are very low which adversely affect both model accuracy and experimental measurement. Thus, each model and experimental result together with the relation between experimental and numerical results should be interpreted heedfully for this particular case. Since the measured stress value under normal force is higher than the one from traction, comparing the model accuracy with the case with normal force could yield better construal.

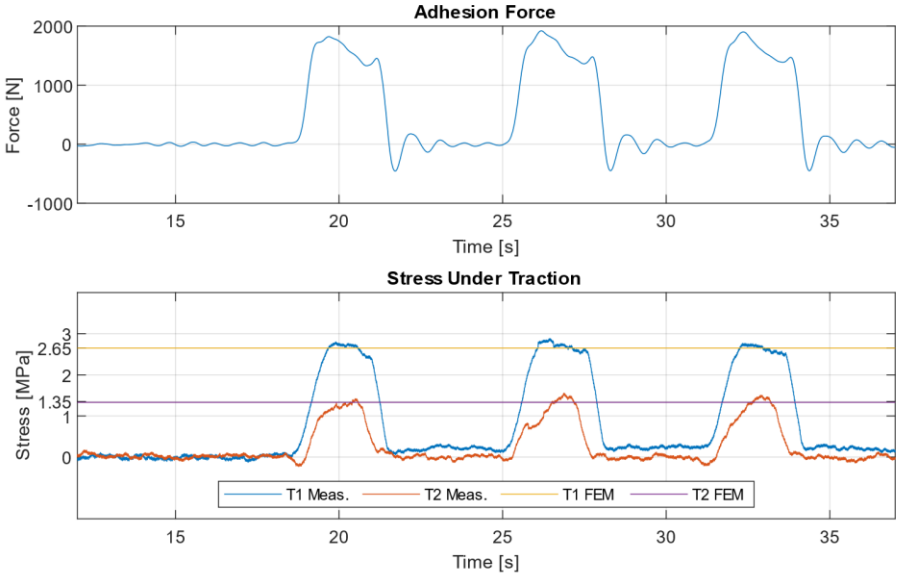

Figure 31. Compared results of FEM and measurement under traction load

The measured and calculated stresses (i.e., experimental and FEM) for traction forces were found quite low even for the most forced/stressed places. It can be, therefore, pretend that the frame is not forced much during the motion of two rolling bodies or under traction state. The horizontal deformation on the top of the roller-rig frame was not measured during traction load. On the other hand, those can be obtained from the validated FE model. The deformation values lie around 0.04 mm in the places where it deforms maximum (see Figure 27). Thus, as the computed horizontal displacement at the top-end is ignorable it can be interpreted that the frame exhibits a firm performance. Overall, the horizontal displacement value was found very low, which has nearly no impact on the global response. It's concluded that the dynamic behaviour of the frame has no influence or negligible influence on the mentioned inaccuracies. Therefore, the point of the view for investigating the solution is changed to rolling parts.

4.5 Investigation of Rolling Parts

4.5.1 Torsional Dynamic Model

Due to measured small forces in the frame, it's concluded that its structure has no or insignificant effects to stated problems mentioned in section 4.2. For investigating the responses of rolling parts, a torsional dynamical model has been developed. This model simulates the

adhesion experiments in MATLAB environment under different surface, loading and traction conditions. The simulation consists of seven rotating elements which are a PMSM stator, PMSM rotor, wheel disc, wheel tyre, rotating rail, AM rotor, AM stator. Mountings of the AM and PMSM stators are modelled with a torsional element which have high torsional stiffness. The rubber connector between wheel disc and wheel tyre were also modelled in order to obtain more realistic response. An illustration of the generated model is given in Figure 32. The related equations of the model are given in 4.1-4.14.

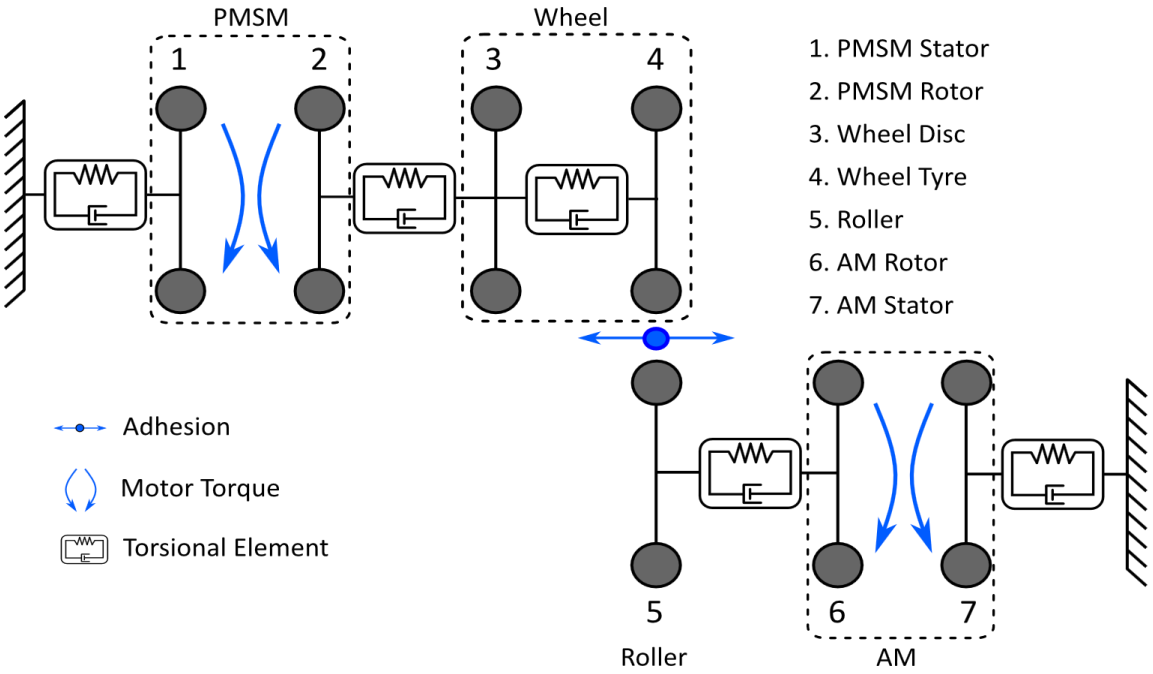

Figure 32. Illustration of torsional dynamic model of roller rig

$$\alpha_1 = \frac{-T_{01} - T_{12}}{J_1} \tag{4.1}$$

$$\alpha_2 = \frac{T_{12} - T_{23}}{J_2} \tag{4.2}$$

$$\alpha_3 = \frac{-T_{23} - R_{03} + T_{34}}{J_3} \tag{4.3}$$

$$\alpha_4 = \frac{-T_{34} - A_x \cdot r_{wx}}{J_4} \tag{4.4}$$

$$\alpha_5 = \frac{T_{56} - A_x \cdot r_{rx} - R_{05}}{J_5} \quad 4.5$$

$$\alpha_6 = \frac{-T_{56} + T_{67}}{J_6} \quad 4.6$$

$$\alpha_7 = \frac{-T_{67} + T_{70}}{J_6} \quad 4.7$$

$$T_{01} = k_{01}.\theta_{01} + b_{01}.\dot{\theta}_{01} \quad 4.8$$

$$T_{23} = k_{23}.\theta_{23} + b_{23}.\dot{\theta}_{23} \quad 4.9$$

$$T_{34} = k_{34}.\theta_{34} + b_{34}.\dot{\theta}_{34} \quad 4.10$$

$$T_{56} = k_{56}.\theta_{56} + b_{56}.\dot{\theta}_{56} \quad 4.11$$

$$T_{70} = k_{70}.\theta_{70} + b_{70}.\dot{\theta}_{70} \quad 4.12$$

$$R_{03} = N * f_g \quad 4.13$$

$$R_{05} = (W_r + N) * f_g \quad 4.14$$

where, $\dot{\omega}_1, \dot{\omega}_2, \dot{\omega}_3, \dot{\omega}_4, \dot{\omega}_5, \dot{\omega}_6, \dot{\omega}_7$ are rotational accelerations and $J_1, J_2, J_3, J_4, J_5, J_6, J_7$ inertias of PMSM stator, PMSM rotor, wheel disc, wheel tyre, rotating rail, AM rotor and AM stator respectively. T_{01} and T_{70} are reaction torques of PMSM and AM stator respectively. T_{23} and T_{56} are transmitted torques over shafts generated by PMSM and AM, respectively. T_{12}, T_{67} are torques generated by AM and PMSM respectively. r_{wx}, r_{rx} are longitudinal radius of wheel and roller and $A_x$is adhesion force between wheel and roller. R_{03} and R_{05} are the bearing resistances of the wheel and rotating rail, respectively. $k_{01}, k_{23}, k_{34}, k_{56}, k_{70}$ are torsional stiffnesses, $b_{01}, b_{23}, b_{34}, b_{56}, b_{70}$ are torsional damping ratios respectively. $\theta_{01}, \theta_{23}, \theta_{34}, \theta_{56}, \theta_{70}$ are angular displacements and $\dot{\theta}_{01}, \dot{\theta}_{23}, \dot{\theta}_{34}, \dot{\theta}_{56}, \dot{\theta}_{70}$ angular speeds of PMSM mounting, wheel shaft, rubber layer, roller shaft and AM mounting respectively. N is the normal force and W_r is the weight of the rotating rail and its components. A flowchart of the torsional dynamic simulation model with submodules is given in Figure 33.

4.5.1.1 Wheel-Roller Contact Geometry and Normal Contact

As an initial step of obtaining the contact area and shape, contact parameters must be found. Hertz theory [69] is widely used for calculating the shape of the contact area between the wheel-rail pair. The calculation procedure of the Hertzian contact is given in the book by Shabana et al. [95]. Also, a similar study can be found in the study of Onat et al.[96]. The geometric parameters used in the calculation of the contact area between the wheel-roller pair is given in section 4.5.1.3.

Additionally, the Poisson ratio is taken as 0.3 and the tensile modulus is taken as 210 GPa. According to the abovementioned method and parameters, contact area and stress under 4300 kN are given in Figure 34.

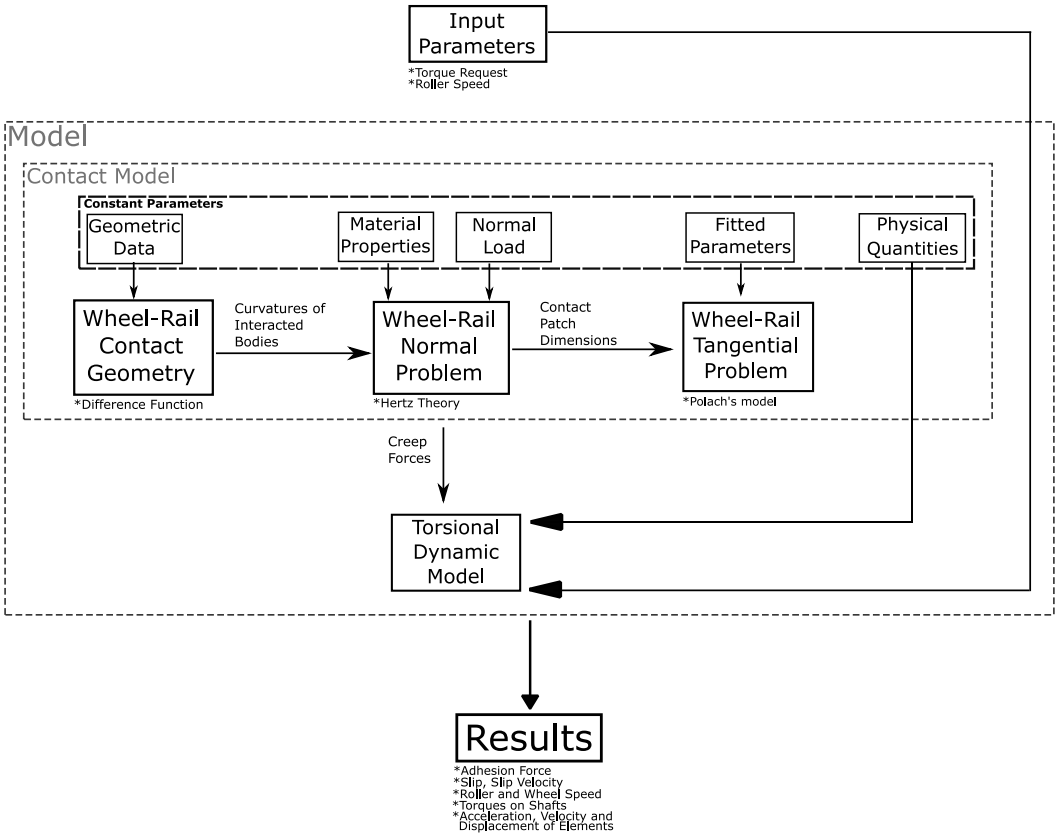

Figure 33. Block diagram of the torsional dynamic simulation model

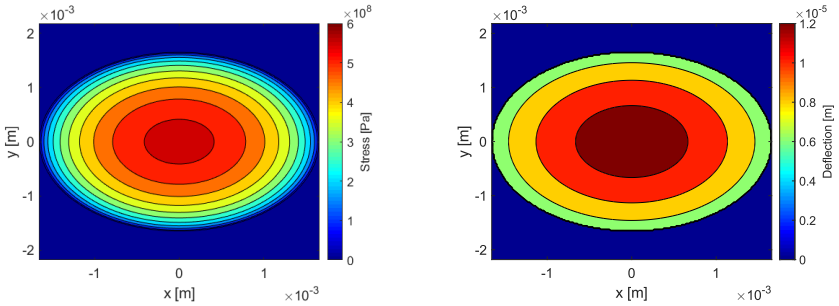

Figure 34. Stress and deflection plots for Hertzian contact under 4.3 kN

4.5.1.2 Creep Forces

In order to model the forces between wheel – roller pair under rolling conditions, a creep model is needed. Relatively recent model proposed by Polach [45] is used in dynamic simulation. For calculating the creep forces according to Polach's model, Kalker's coefficients are needed. These coefficients are tabulated data with respect to combined Poisson's ratios of interacting bodies and semi-axes of contact patch. The tabulated data is given in Kalker's study [97] which should be mathematically fitted for using in the model. In this dynamic model, polynomial fit used in reference by Onat [98].

The tangential creep force defined by Polach [45] is;

$$F = \frac{2Q\mu}{\pi}\left(\frac{\varepsilon}{1+\varepsilon^2} + arctan\varepsilon\right) \tag{4.15}$$

where Q is the wheel load, μ is the coefficient of friction and ε is the gradient of tangential stress in the area of adhesion and expressed as,

$$\varepsilon = \frac{2}{3}\frac{C\pi a^2 b}{Q\mu}s \tag{4.16}$$

where a and b are half-axis of contact ellipse and C is proportionality coefficient characterizing the contact shear stiffness. This coefficient can be derived from Kalker's linear theory [97].

$$\varepsilon_x = \frac{1}{4}\frac{C\pi abc_{11}}{Q\mu}s_x \tag{4.17}$$

Then;

$$s = \sqrt{s_x^2 + s_y^2} \tag{4.18}$$

where s is total creep and s_x and s_y are the components of creep in x and y directions, respectively. It should be noted that in the model only longitudinal creep is considered.

The friction coefficient (μ) mentioned in equation 4.19 is variable friction depended on slip velocity. Details about variable friction depended on slip velocity can be found in related literature [8,99]. This can be formulated as,

$$\mu = \mu_0[(1 - A)e^{-Bw} + A] \tag{4.19}$$

where B is the coefficient of exponential friction decrease and A is the ratio of limit friction coefficient at infinity slip velocity (μ_∞) and maximum coefficient of friction (μ_0). Besides, in the mentioned study, it's been referred to the additional studies, there are such parameters that affects the adhesion. (i.e. temperature, third layer between surfaces). To model these effects, two additional parameters, k_A and k_S are used in the area of adhesion and in the area of slip, respectively. With the addition of these two parameters the equation can be rewritten as,

$$F = \frac{2Q\mu}{\pi}\left(\frac{k_A\varepsilon}{1+(k_A\varepsilon)^2} + \arctan(k_S\varepsilon)\right), \qquad k_S \leq k_A \leq 1 \tag{4.20}$$

Parameters of the creep model have been obtained by fitting the measurement results from the roller rig. An example of fitting for the Creep-CoA model for non-contaminated wheel/rail contact has been given in Figure 35.

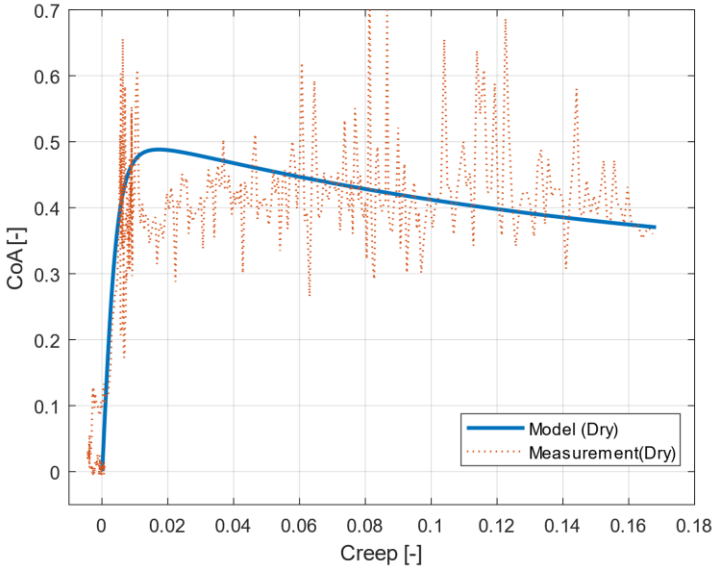

Figure 35. Fitted adhesion model (dry case) from experiments

As mentioned above, creep forces are depended on the slip and slip velocity. Slip ratio and slip speed are implemented into the model by equations 4.21 and 4.22.

$$s = \frac{\omega_w \cdot r_w - \omega_r \cdot r_r}{\omega_r \cdot r_r} \tag{4.21}$$

$$w_s = \omega_w \cdot r_w - \omega_r \cdot r_r \tag{4.22}$$

4.5.1.3 Model Parameters

The parameters used in the torsional dynamic model are given in Table 3. In this model, the shaft stiffness is critical due to investigation of shaft oscillation (Section 4.3.2). The shaft in the roller-rig is a multi-component shaft that is compiled with a CV shaft, torque sensor, roller shaft and additional binding component. In order to determine the shaft stiffness, the dimensions of the components were obtained. It was aimed to determine the part with lowest stiffness and using that value as torsional stiffness of the roller shaft.

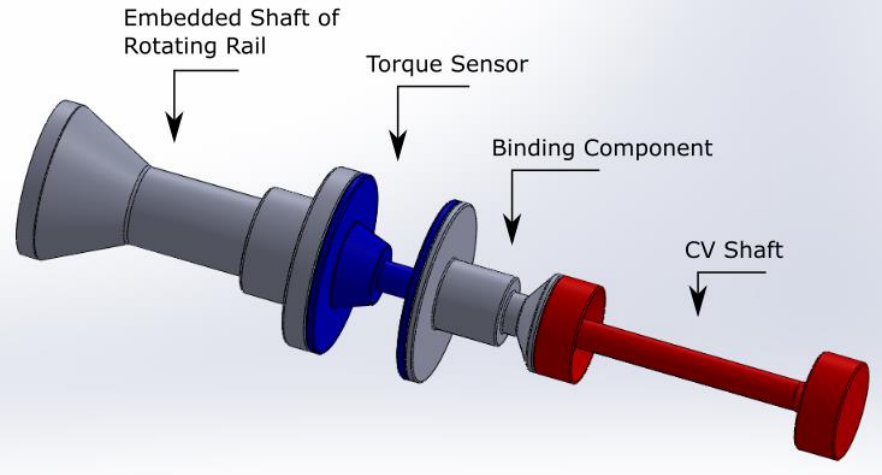

Figure 36. Dimensions of the roller shaft components

CV shaft has been manufactured by GKN Automotive Limited with the model code 108/21 and its torsional stiffness is 43.5 kNm/rad [100]. CV shaft is the longest part of the configuration with a small cross-section. The other possible weak sections were calculated also, however, the CV shaft was found as the weakest part. Hence, the stiffness of the shaft between roller and AM has been taken as CV shaft's torsional stiffness. Some of the other physical parameters have been provided by the facility and/or obtained from former studies.

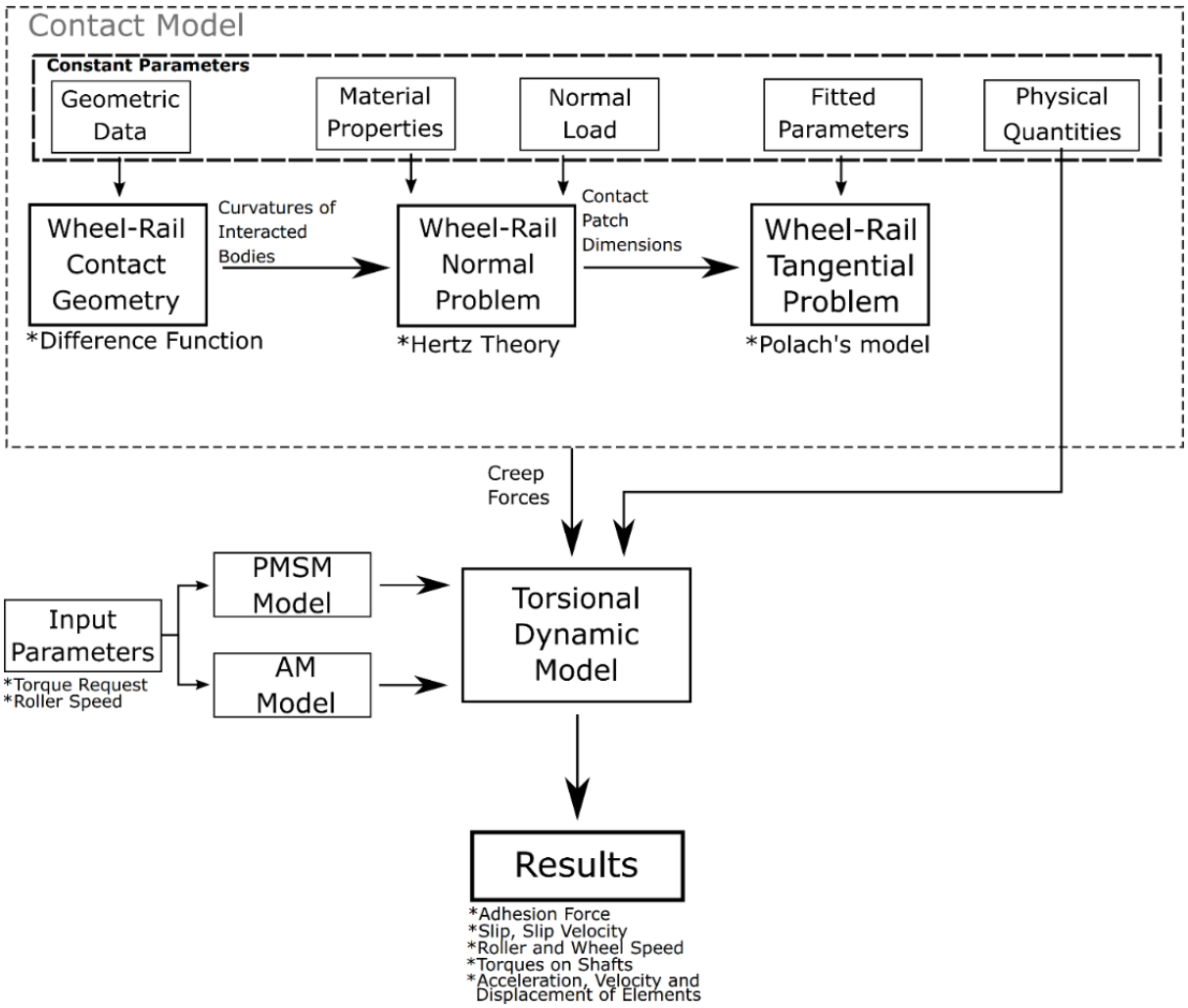

4.5.1.4 Electric Motors

In order to simulate the behaviour of the electric motors, both permanent synchronous motor and asynchronous motor which are driving the wheel and roller have been modelled and implemented into the dynamic simulation.

4.5.1.4.1 Permanent Magnet Synchronous Motor Model

An equivalent dynamic model of permanent magnet synchronous motor has been implemented to the simulation. Dynamic equivalent model on the rotor reference frame is given as follows;

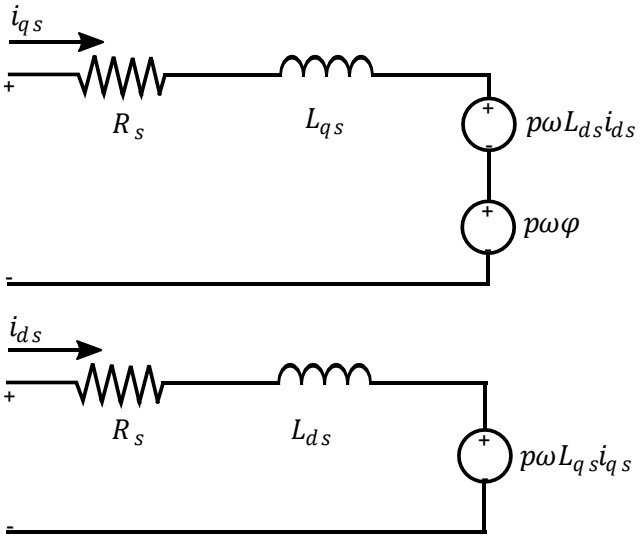

Figure 37. The dynamic equivalent circuit of the PMSM

Dynamic equations of the stator currents are given the following equations,

$$\frac{d}{dt} i_{ds} = \frac{1}{L_{ds}} V_{ds} - \frac{R_s}{L_{ds}} i_{ds} + \frac{L_{qs}}{L_{ds}} p\omega i_{qs} \tag{4.23}$$

$$\frac{d}{dt} i_{qs} = \frac{1}{L_{qs}} V_{qs} - \frac{R_s}{L_{qs}} i_{qs} + \frac{L_{ds}}{L_{qs}} p\omega i_{ds} - \frac{\varphi}{L_{qs}} p\omega \tag{4.24}$$

where i_{ds} and i_{qs} are d and q axes currents, $V_{ds}$and V_{qs} are d and q axes voltages, L_{qs} and L_{ds} are d and q axes inductances, R_s is the resistance of stator windings, p is the number of pole pairs, φ is the amplitude of the flux induced by permanent magnet of the rotor in the stator phases and ω is the angular velocity. Electromagnetic torque generated by PMSM can be calculated from,

$$T_p = 1.5p\left[\varphi i_{qs} + \left(L_{ds} - L_{qs}\right) i_{qs} i_{ds}\right] \tag{4.25}$$

The electrical speed and angular position of the rotor are calculated from,

$$\frac{d}{dt} \omega_e = \frac{p}{J_p} \left(T_p - F_x r_w \right) \tag{4.26}$$

$$\frac{d}{dt} \theta_e = \omega_e \tag{4.27}$$

4.5.1.4.2 Asynchronous Motor Model

As mentioned before, the AM creates an opposing torque against the PMSM torque request in order to maintain a stable speed. For determining the opposing torque according to the angular velocity, an equivalent circuit model should be obtained by some tests. Thevenin equivalent circuit has been selected for the AM model. This method is used in the railway sector and there are many studies concerning this matter [101]. In this study, parameters for the equivalent circuit are obtained from another study [98]. On the roller rig, the AM is controlled with an open-loop volts per Hertz. The principle of this control method is based on keeping the flux constant. The line voltage must be decreased proportionally to a certain frequency so, the V/f ratio can be kept constant [93]. The equivalent circuit for different frequencies can be seen in Figure 38 and the mathematical expression of the Thevenin equivalent circuit is given in equation 4.28. In the study of Onat [98], it is stated that the Thevenin equivalent circuit parameters are validated.

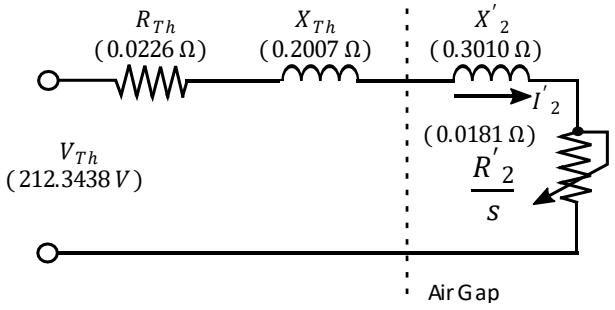

Figure 38. Thevenin equivalent circuit of the asynchronous motor (Redrawn from [98])

$$T_{th} = \frac{3}{\omega_{syn}} \frac{V_{Th}^2}{\left(R_{Th} + \frac{R_2'}{s_m}\right)^2 + (X_{Th} + X_2')^2} \frac{R_2'}{s_m} \tag{4.28}$$

where s_m and ω_{syn} is the slip and synchronous speed of the electrical motor, respectively. R_{Th}, X_{Th}, V_{Th} are the resistance of the rotor, reactance on the stator side and Thevenin voltage, respectively. R_2' and X_2' are reflected resistance and reactance of the rotor, respectively. The details of the Thevenin equivalent circuit and obtaining the values can be found in the related work [93]. Torque-speed characteristic of a typical asynchronous motor is given in Figure 39.

In a simulation, it is impossible to reflect the mechanical characteristics of an actual system completely. In real operations, the behavior of the mechanical systems, are open to being affected by environmental conditions, age of the components, non-exact material properties, non-exact geometrical properties, non-exact characteristic, non-available measurements, control sensitivity, etc. Hence, mostly it is needed to be the use of some additional methods in order to obtain more realistic results. These additions may be a single parameter or a complex equation which differs according to the needs.

It is reported in the literature, the voltage-frequency control method has a poor dynamic performance which creates overshoots and response delays against the load changes [102–107]. Also, it is mentioned that the open-loop control method increases the effect of these handicaps due to the inherent of the no-feedback system [108–110]. Delays, response characteristics and other additional effects can not be modelled exactly. However, the response delay of the AM can be implemented by a simplification. Hence, in order to represent the response delay of the AM and controller, a discrete-time low-pass filter applied as;

$$T_a = c_{lp} T_{th} + \left(1 - c_{lp}\right) T_{ap} \tag{4.29}$$

where, $c_{lp}$is time constant, $T_{ap}$is the previous torque value. A similar application of this method can be found in the studies by Spriyagin et al. [111,112].

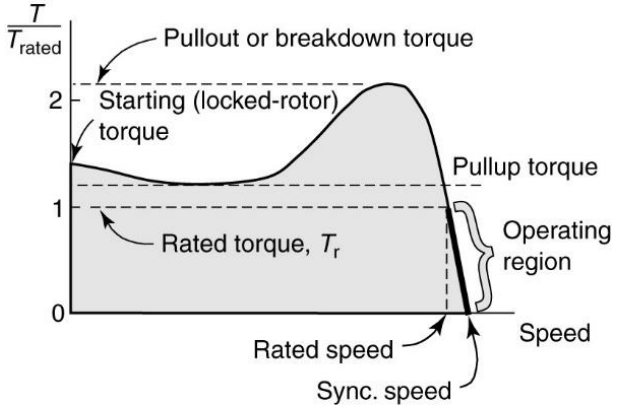

Figure 39. Torque-speed characteristic of an induction motor. [113]

4.5.1.5 Model Parameters

Notation	Definition	Value
J_1	Moment of Inertia of PMSM Stator	$3\ kgm^2$
J_2	Moment of Inertia of PMSM Rotor	$0.95\ kgm^2$
J_3	Moment of Inertia of Wheel Disc	$5.1\ kgm^2$
J_4	Moment of Inertia of Wheel Tyre	$11.6\ kgm^2$
J_5	Moment of Inertia of Rotating Rail (Roller)	$45\ kgm^2$
J_6	Moment of Inertia of AM Rotor	$6.6\ kgm^2$
J_7	Moment of Inertia of AM Stator	$35\ kgm^2$
k_{01}	Torsional Stiffness of Mounting	$5 \cdot 10^5\ Nm/rad$
k_{23}	Torsional Stiffness of Wheel Shaft	$3.85 \cdot 10^5\ Nm/rad$
k_{34}	Torsional Stiffness of Rubber Between Wheel Disc and Tyre	$3.70 \cdot 10^5 Nm/rad$
k_{56}	Torsional Stiffness of Rotating Rail Shaft	$0.435 \cdot 10^5\ Nm/rad$
k_{70}	Torsional Stiffness of AM Mounting	$5 \cdot 10^5\ Nm/rad$
b_{01}	Torsional Damping of PMSM Mounting	$10^5\ Nms/rad$
b_{23}	Torsional Damping of Wheel Shaft	$1\ Nms/rad$
b_{34}	Torsional Damping of Rubber Between Wheel Disc and Tyre	$10^3\ Nms/rad$
b_{56}	Torsional Damping of Rotating Rail Shaft	$1\ Nms/rad$
b_{70}	Torsional Damping of AM Mounting	$10^5\ Nms/rad$
v	Poisson Ratio	*0.3 [-]*
f_g	Coefficient of Friction for Bearings	*0.007 [-]*
r_{wx}	Longitudinal Radius of Wheel	*348 mm*
r_{wy}	Lateral Radius of Wheel	*291 mm*
r_{rx}	Longitudinal Radius of Roller	*452 mm*
r_{ry}	Lateral Radius of Roller	*1890 mm*
W_r	Weight of the roller subsystem	*5000 N*

4.5.1.6 Simulation Results

In order to verify the mathematical model, simulations have been executed under the same conditions as the experiments. The comparative results between simulation and experiment are presented for both 30 km/h dry surface condition and 10 km/h wet surface condition. Those related to 30 km/h dry surface condition are presented in Figure 40a-f. The reference torque requested in the experiment and the generated torque by PMSM in the simulation are given in Figure 40a. It should be noted that the reference (blue) is the same with

torque request in the experiment and the torque plot (orange) is generated torque by PMSM model in the simulation. It can be seen that generated torque has oscillation around the reference signal. This occurs due to the switching of the inverter of the PMSM. The Polach's model parameters were adapted from adhesion measurement for the Creep-CoA relationship (Figure 40b). Note that, the existing noise in the experimental measurements were not eliminated in the corresponding graph. Figure 40c and e present comparison the wheel and roller speeds with simulated and experimental results, respectively. When the results are investigated in depth, a good match can be seen between experimental and simulation results. Moreover, the oscillated motion experienced in the tests was well captured by the simulations. This shows the efficacy of the model in terms of prediction capability. The graphs of simulated and recorded data almost overlap for creep velocity (Figure 40d). The predicted response in adhesion force including ascending and descending branches is quite similar to the experimental values. By the increasing torque request, a linear, steep increment in the adhesion force is followed by a nonlinear response with several peak values. Those were well characterized by the simulated model. In the place where the maximum adhesion force is monitored, the experimental response was first descending nonlinearly up to certain value and then continued with increasing trend under same torque request. After that, when the torque request becomes zero, a sudden decrement in the adhesion force has been experienced. This can be seen in Figure 40f. The oscillations which occur right after rapid torque change can be seen clearly in adhesion force and roller speed measurement graphs. The adopted model was also capable of capturing the oscillated response which occurs around zero. The repeatability of the measurement and simulation was also provided. The test was repeated three times and similar responses in torque requested/unrequested cases were monitored during measurement. The simulated results were also capable of generating the same response.

Figure 41 compares the dynamic model results with experimental measurements at the roller peripheral speed of 10 km/h and wet surface condition. Note that, the velocity and requested torque in this particular case are lower than the previous one; moreover, the surface condition is selected as water contaminant which decreases the coefficient of adhesion. As it can be seen in Figure 41a-f, the simulation was able to predict closer values for response variables (outcome variables). All of them were well characterized by the generated model.

Overall, the match between the simulation and experimental results were found quite satisfactory.

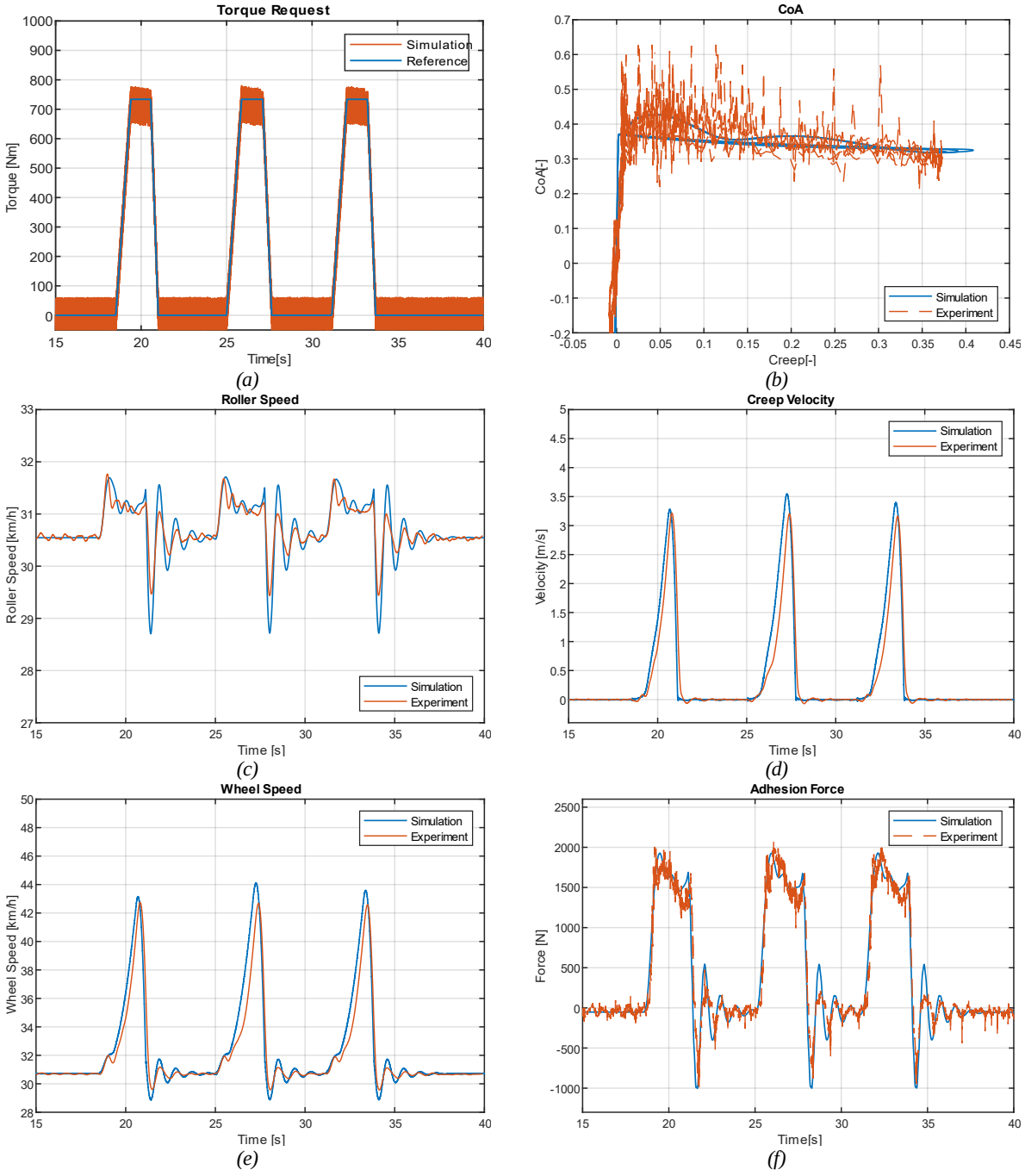

Figure 40. Simulation results at 30 km/h dry condition

The change in the ascending and descending branches of the curve, where the maximum adhesion force is monitored, has been observed very rapidly and clearly. On the other hand, the simulated response follows an almost constant path after reaching the maximum value (Figure 41f). The reason for this most likely seems to be cleaning effect, which increases the friction coefficient [87]. This statement was also supported by the CoA-Creep plot (Figure 41b). As seen in the corresponding figure, CoA value has increased gradually with the increase of creep during the experiment. On the other hand, the model was not designed in order to predict such a response which is unnecessary for this study, due to it does not have a relative impact on the investigated response variables (outcomes of the study). Similar to the previous case, the oscillated motion in the transition area of adhesion force (i.e., area around zero adhesion force) has been predicted by the model (Figure 41f). However, the amplitude of the data is lower than previous case (Figure 40f). The reason lies over the lower speed and less torque request. These parameters significantly change the dynamic response in terms of amplitude.

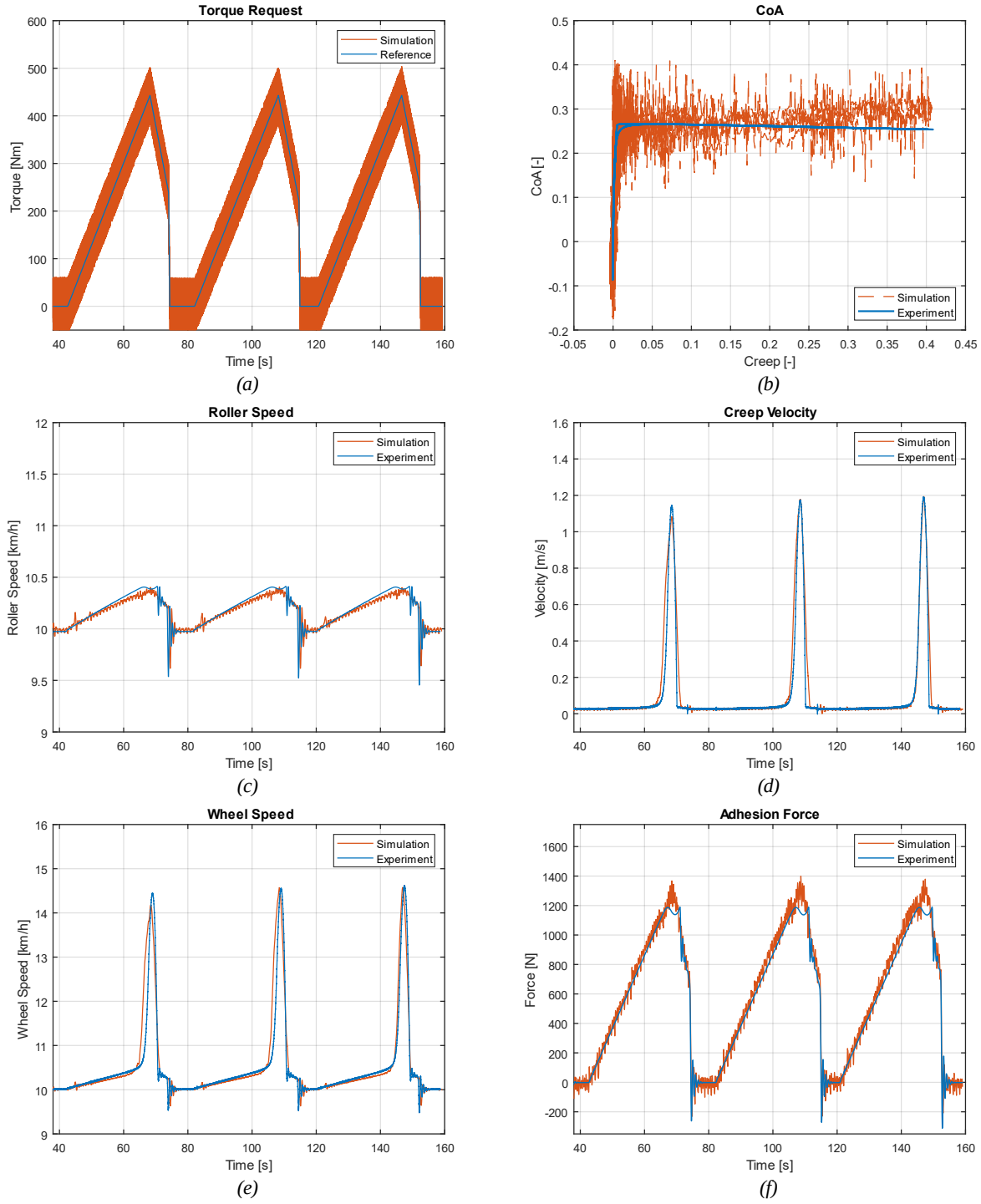

Figure 41. Simulation results at 10 km/h water contaminated surface

4.5.1.7 Effect of the Roller Shaft Torsional Stiffness

In order to determine the effect of the torsional stiffness of the roller shaft on the behavior a parametric study has been performed. For this specific section, the dynamic characteristics of the electric motors have been idealized and it has been assumed that their control is fully robust in order to solely obtain the effect of the torsional stiffness. As mentioned in previous section the torsional stiffness has been obtained as $43500\ Nm/rad$. The result of adhesion force obtained from simulation and comparison of measurement has been given for the obtained value of stiffness in Figure 42.

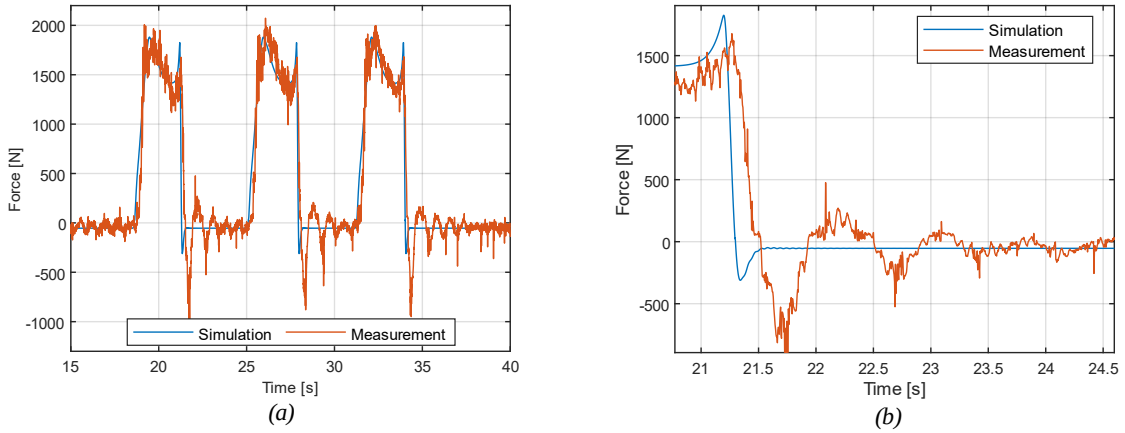

Figure 42. Simulated adhesion force with obtained value of torsional stiffness (a), Specific section of oscillation (b).

As seen in Figure 42b a small oscillation that occurs around zero adhesion force has been obtained in simulation. Even it is a small oscillation, for avoiding possible undesired dynamic influences, the effect of stiffer shafts has been examined. Starting from the original value ($43500\ Nm/rad$), the stiffness value has been increased by $20000\ Nm/rad$ in every simulation. The simulation results of the parametric study and the relative amplitude change (torque request decrease section) according to the torsional stiffness change are given in Figure 43.a and b, respectively.

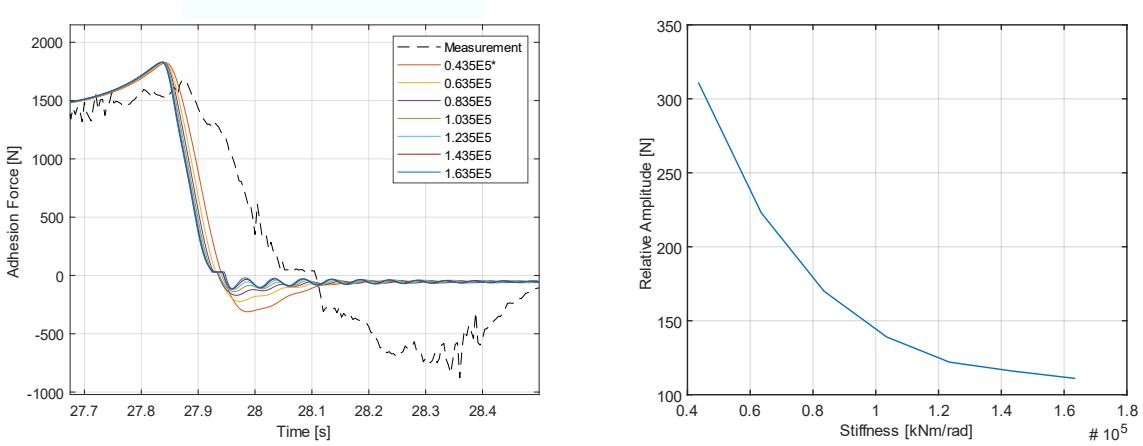

(a) *(b)*

Figure 43. Effect of shaft stiffness on dynamic phenomenon (a), Relative values of amplitudes (b).

4.5.1.8 Effect of the Asynchronous Motor Response

In order to understand the effect of asynchronous motor torque characteristic on the mentioned issue, the motor torque characteristic has been modified by the low-pass filter. In this specific section, the torsional stiffness value has been taken as the original value and PMSM characteristic is idealized in order to solely obtain the effect of the AM torque characteristic change on the dynamic behavior of the roller.

In theory, from the torque-speed characteristic aspect, the induction motors operate in an almost linear range (Figure 39) but, due to the inherent of the practical operations, it is not completely possible to obtain the same theoretical operation range. Also, beside AM itself, there are additional components which influences the dynamic behavior such as controller and inverter.

Torque-speed characteristic of the AM has been obtained by the measured torque and rotary encoder speed. The effect of the torsional stiffness of the roller shaft has been neglected due to its small influence (Section 4.5.1.7.). Hence, it has been assumed that the roller speed reflects the true rotational speed of the AM roller. In Figure 44, the measured torque-speed characteristic of the AM is given for the same experiment in Figure 39. As seen on the Figure 44 the torque-speed characteristic of the AM is far from expected linear operating region.

A linear torque-speed character has been fitted between the range of synchronous speed and maximum torque and the fitted characteristic is given in Figure 45. Besides the linear model, in order to create the realistic AM torque-speed characteristic, a response delay has been applied via discrete low-pass filter. Best behavior has been searched by parametric study and the possible realistic torque-speed characteristics have been investigated. The results of the delayed characteristics have been given in Figure 46.

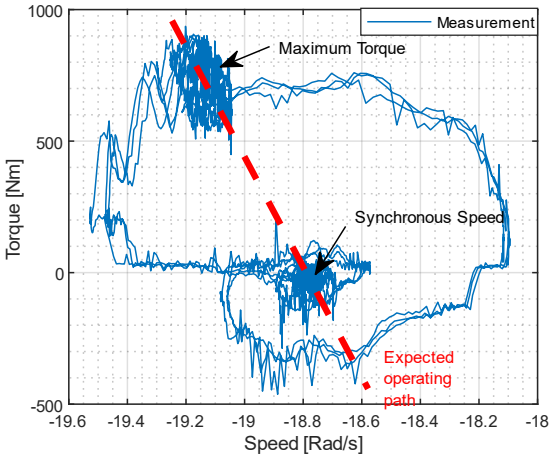

Figure 44. Measured torque-speed characteristic of AM

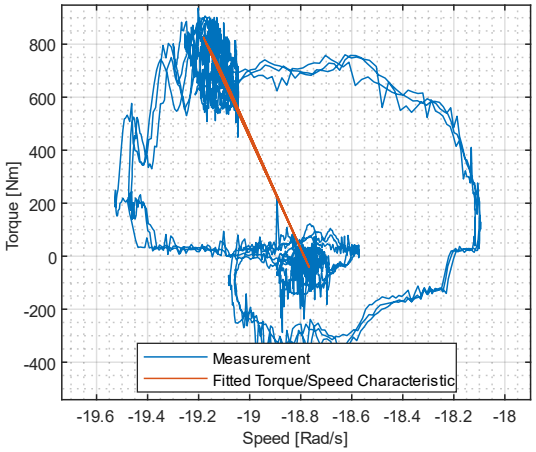

Figure 45. Linear fit of torque-speed characteristic

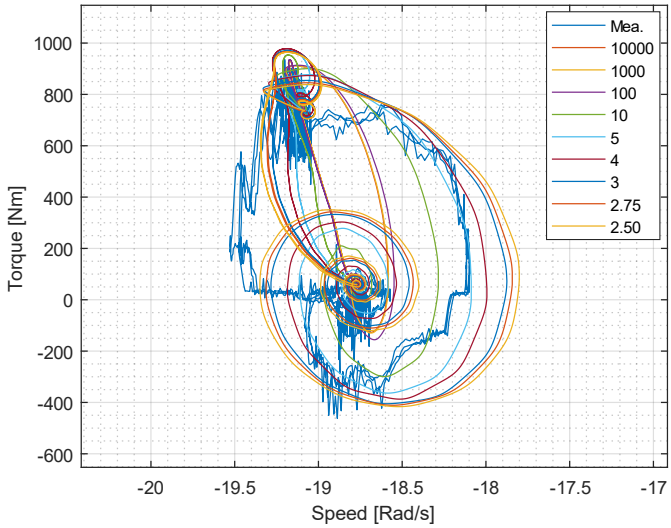

Figure 46. Obtained torque-speed characteristics via response delay

The applied low-pass filter parameters are given in Figure 46 . In this simulation 10^{-4}step time has been used. Hence, with 10^4 control parameter, zero response delay has been obtained. A close torque-speed characteristic has been obtained with a significantly lower control parameter (2.75). Additionally, the influence of the same application on the adhesion force is given in Figure 47.

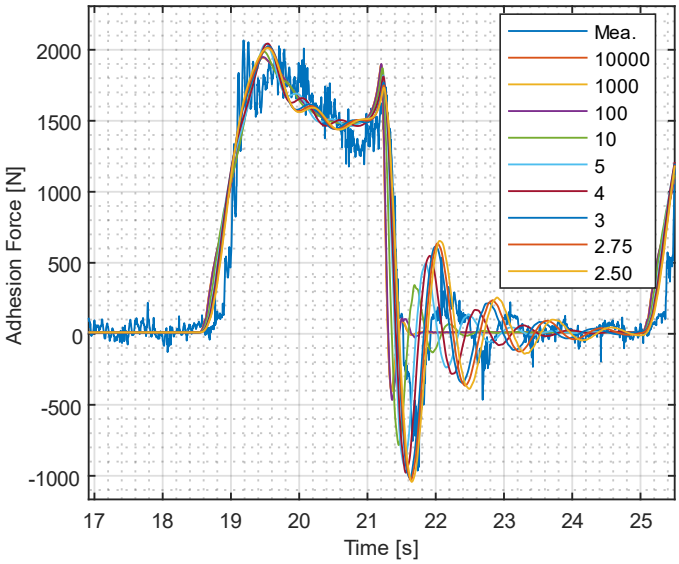

Figure 47. The influence of the response delay on the adhesion force

It has been concluded that the main reason of the issue mentioned in section 4.2.1 is response delay of the AM. Additionally, the stiffness of the shaft between roller and AM rotor has an auxiliary effect on the mentioned issue. In order to provide an improvement on the behavior of the roller rig, a simulation has been applied with no response delay and higher torsional stiffness of the roller shaft. The stiffness of the roller shaft has been selected from the catalog value of the same manufacturer type 108/32 which has a $174\ kNm/rad$. The results of the improved behavior is given Figure 48. When the results are investigated in depth, it can be seen clearly, the mentioned dynamic phenomenon has been eliminated with the increase of the torsional stiffness and zero value of response delay. Additionally, in Figure 49, a quicker response can be seen in the both of the transition areas (increase and decrease of torque request). It should be noted that, in the corresponding figure, the blue line represents the torque request however its value is multiplied with the wheel radius in order to make an easier comparison.

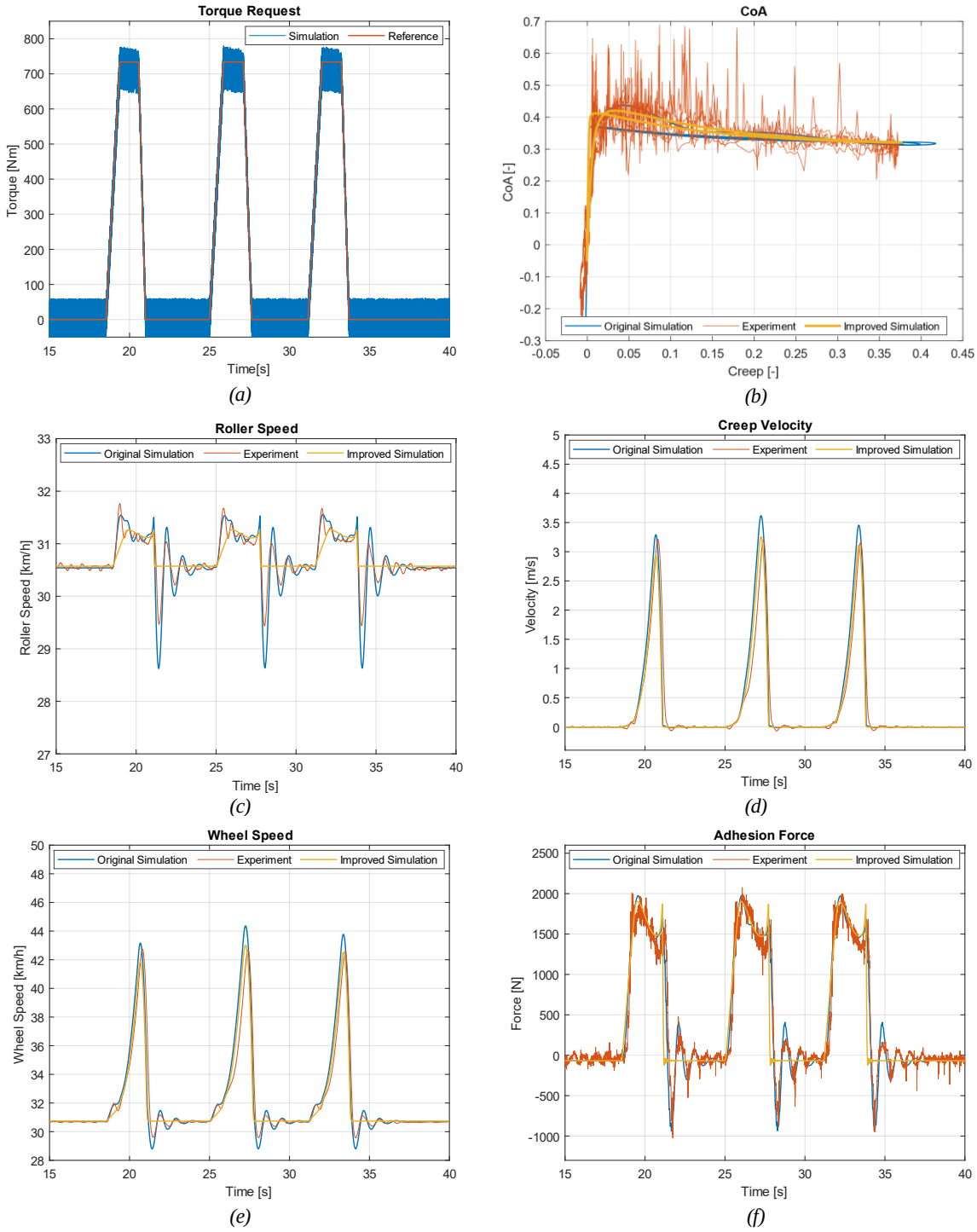

Figure 48. Comparison of original simulation, experiment and improved simulation results

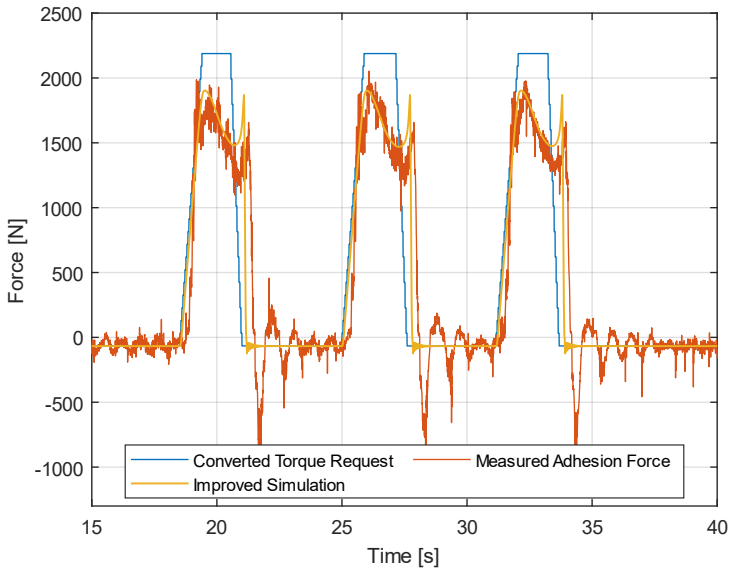

Figure 49. Comparison of response delay

4.5.2 Analysis of Rolling Disorders

In order to generate a solution to the waving torque signal, the rolling parts have been investigated for radial eccentricity. It's been presumed the effect of the out-of-roundness of the rolling parts may create a waving signal. Illustration of out-of-roundness is given in Figure 50.

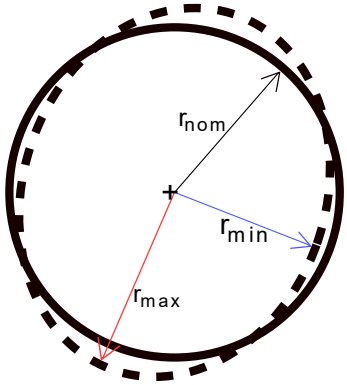

Figure 50. Illustration of out-of-roundness

It is believed that the disturbing signals has been created by difference of the radiuses in several points on the wheel, roller or shaft. In order to identify these differences, rolling radiuses has been manually measured by displacement gauge (Figure 51).

Figure 51. Manual measurement with displacement gauge

Deflection measurements with manual displacement gauge conducted on three different locations on the roller-rig. Those are roller, wheel and in the place where torque sensor is attached on the roller shaft. Measurement of the wheel and roller has been conducted from several locations. The maximum value of out-of-roundness in the radius has been obtained as 0.02 and 0.03 mm for the wheel and roller, respectively. However, those obtained for torque sensor lied around 0.17 mm which is relatively higher than the other values. Also, the vertical movement during measurements due to the out-of-roundness of the shaft has been distinguished easily by visual observation. It's been considered that the wave signal may occur due to the shaft eccentricity. Illustration of the possible effect of the above-mentioned deflection phenomenon is visually presented in Figure 52.

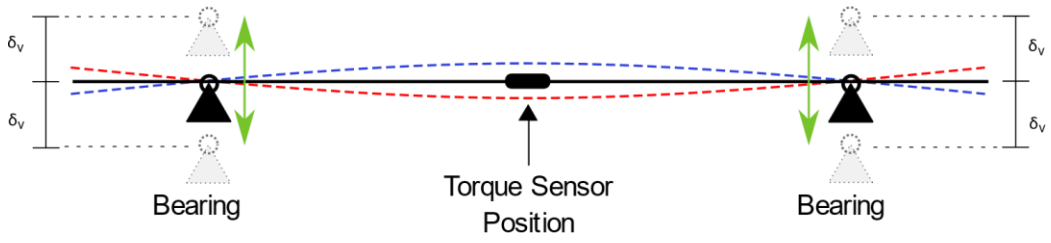

Figure 52. Illustration of shaft eccentricity

Based on the initial measurements conducted by the manual displacement gauge, an issue due to the deflection of the shaft was revealed. This may affect the reliability of the roller rig measurement results. Thus, more detailed measurements are required to identify such an adverse effect. For this reason, an experimental setup was designed to measure the vertical

movement of bearings on both sides and torque sensor which is explained in the following section.

4.5.2.1 Experimental Setup

Three laser displacement sensors have been positioned over the shaft connecting the roller and AM. The illustration of the laser displacement sensors positioning is given in Figure 53. The LK-H 055 were used on bearings and LK-H 087 was used on the torque sensor. Both of the sensors have been manufactured by the company Keyence. The maximum displacement gauges of the sensors are 50 and 80 millimeters with an accuracy of ±0.02% [114]. HBM Quantum MX 840A universal data acquisition module with 19200 Hz speed has been used for data gathering [115]. DAQ device, LK-H055 and LK-H087 displacement sensors are given in Figure 54 a, b and c, respectively. The measurements were conducted with a sampling rate of 600 Hz. The measurements were conducted with a sampling rate of 600 Hz. The application of the displacement sensors on the roller-rig shaft is shown in Figure 42. Also, in order to verify the time consistency between the roller-rig and laser sensors, a duplicate of the torque signal has been recorded parallel with laser displacements.

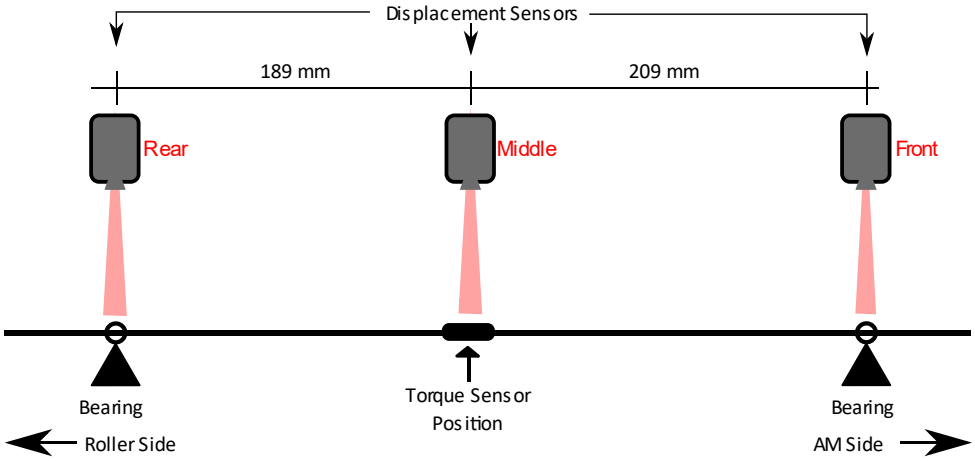

Figure 53. The illustration of laser displacement positioning

a) MX-840A-P DAQ device b) LK-H055 c) LK-H087

Figure 54. Used equipment in experiments (a [115], b [116], c [117])

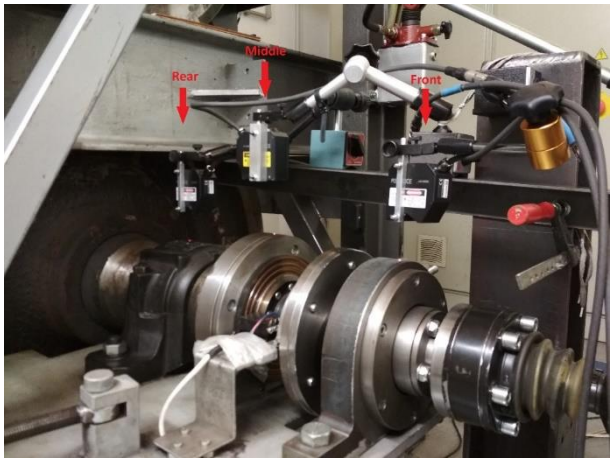

Figure 55. Application of laser displacement sensors on roller shaft

4.5.2.2 Measurement Results

The measurements have been conducted under different speeds (5, 10, 20 and 30 km/h) and under different loads (4.3, 10 and 20 kN) in order to obtain the behavior of the shaft under different conditions. The measurement results for different speeds under 4.3 kN loads are given in Figure 56-Figure 59. Relative movements of the measured positions are compared in each graph. As seen in the corresponding figures, movement of the rear bearing is significantly small, and the movement of the torque sensor and front bearing is relatively higher.

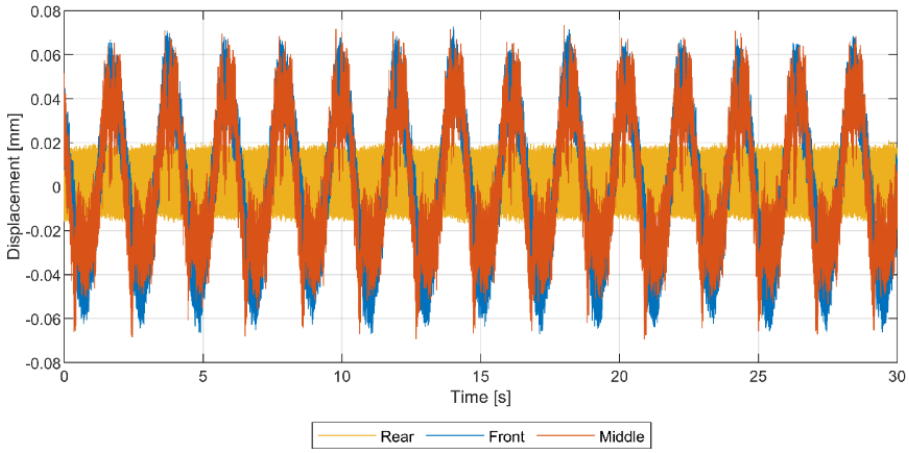

Figure 56. Displacement measurement results for 5 km/h under 4.3 kN normal load.

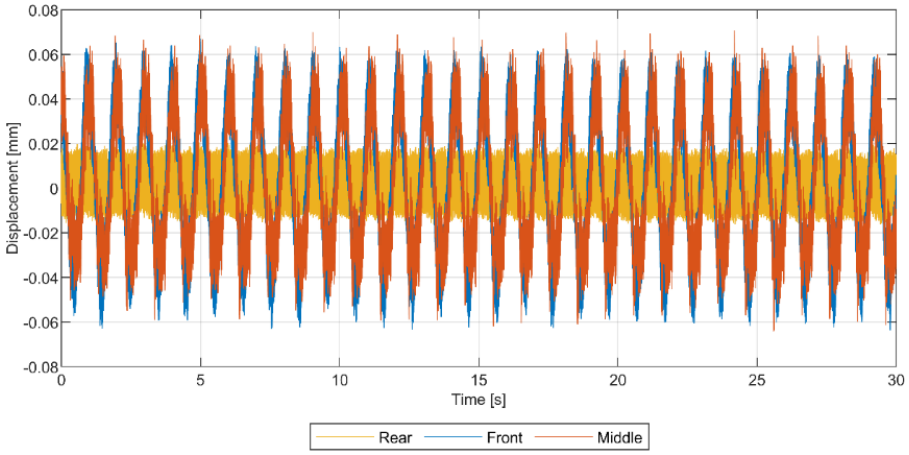

Figure 57. Displacement measurement results for 10 km/h under 4.3 kN normal load.

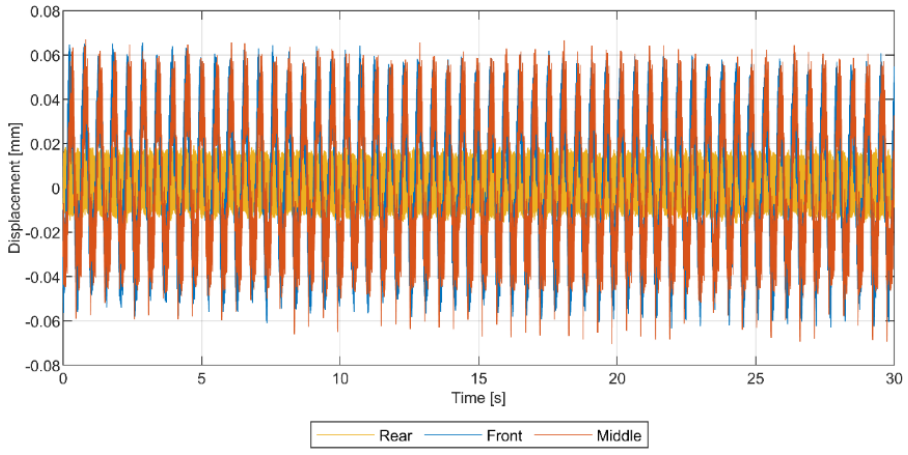

Figure 58. Displacement measurement results for 20 km/h under 4.3 kN normal load.

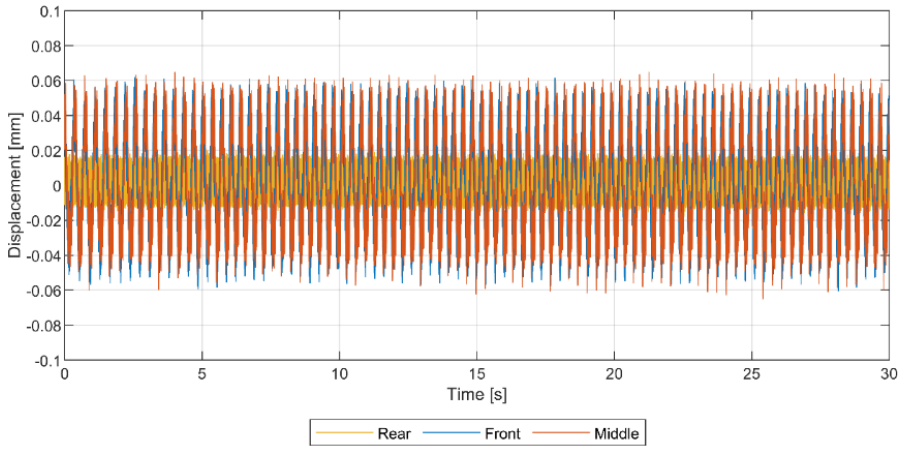

Figure 59. Displacement measurement results for 30 km/h under 4.3 kN normal load.

As it is seen in Figure 56 - Figure 59 the relative displacements for front bearing and torque sensor are between 0.12 mm and 0.15 mm which are close to the manual measurement. It is noticed that increasing the normal load doesn't affect the vertical oscillation rate. However, it relatively changes the amplitude of the oscillation. However, it was noticed that the trend is quite small.

Also, as expected, the oscillation of the bearing and the torque sensor increased proportionally to the speed. For more comparative results, the signal should be analyzed deeply. This will provide a reliable assessment of the signal. Moreover, a relation between the rolling disorder of the shaft and output signal of the roller rig measurement will be revealed. For this reason, a frequency analysis has been applied to the displacement results so that the most influential signal can be outlined. The details of the frequency analysis is given in the following section.

4.5.2.3 Frequency Analysis of the Displacement Data

Discrete Fourier Transformation has been applied to the output data. The signal has been converted from time the domain to the frequency domain and the dominant frequencies in the signal were obtained. The frequency analysis of the data from laser sensors has been done in MATLAB® environment. Results of frequency analysis are given in Figure 60 - Figure 63 for different speeds.

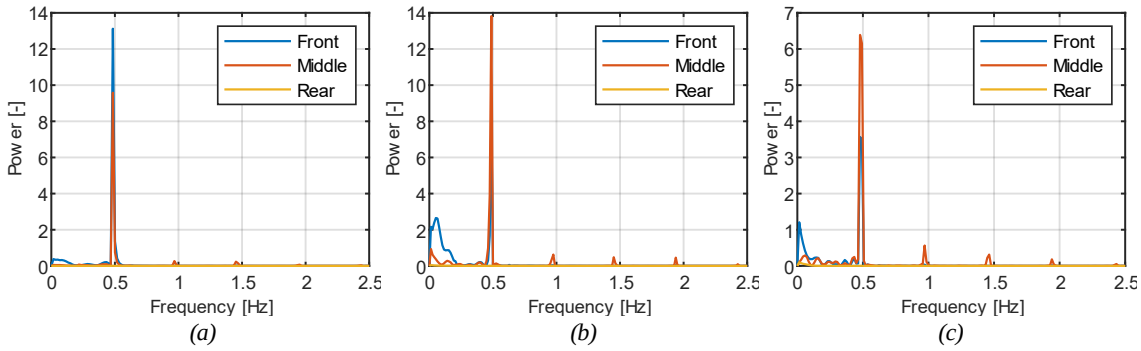

Figure 60. Frequency analysis of displacement sensors for 5 km/h in frequency domain under different loads; (a) 4.3 kN, (b) 10 kN and (c) 20 kN.

For 5 km/h under different loads, frequency analysis of the laser displacement sensors has been presented in the frequency domain (Figure 60), The dominant frequencies of the vertical movement for front bearing and torque sensor are found 0.484 Hz. Also, it is seen that the load increase did not affect the frequency of the oscillation remarkably. Higher-order harmonics of 0.484 Hz was also noticed in small power. Measured raw signals are given in appendix B.

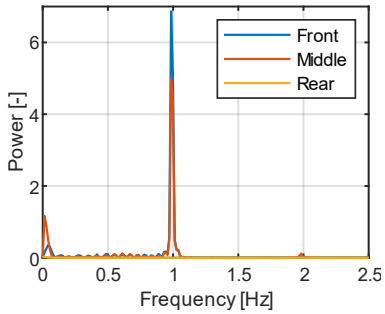

Figure 61. Frequency analysis of displacement sensors for 10 km/h in frequency domain under 4.3 kN normal loading.

In Figure 61, frequency analysis of the laser displacement sensors has been presented in the frequency domain for 10 km/h under normal load. The dominant frequency of the vertical movement for front bearing and torque sensor are found 0.973 Hz. Due to load increase have not affected the frequencies, other loading conditions have not been given. Higher-order harmonics of the 0.973 Hz is also noticed in small power.

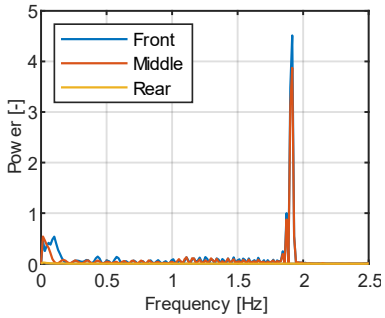

Figure 62. Frequency analysis of displacement sensors for 20 km/h in frequency domain under 4.3 kN normal loading

In Figure 62, frequency analysis of the laser displacement sensors has been presented in the frequency domain for 20 km/h under 4.3 normal load. The frequency of the vertical movement for front bearing and torque sensor was found 1.95 Hz. Yet again, the frequency does not depend on the change in the load values.

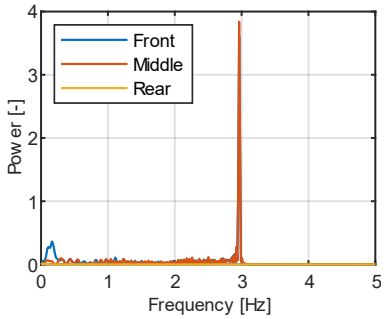

Figure 63. Frequency analysis of displacement sensors for 30 km/h in frequency domain under 4.3 kN normal load.

In Figure 63, frequency analysis of the laser displacement sensors has been presented in the frequency domain for 30 km/h under 4.3 kN normal load. The frequencies of the vertical movement for front bearing and torque sensor were found at 2.99 Hz. Yet again, the other loading conditions have not been given due to the independency of the frequencies in load change.

4.5.2.4 Frequency Analysis of Roller-Rig Data from Torque Sensor

In order to compare the dominant frequencies between the displacement sensors and the output signal of the roller-rig, a Discrete Fourier Transformation has been applied to roller-rig output signal as well. Results of the frequency analysis are given in Figure 64 - Figure 67.

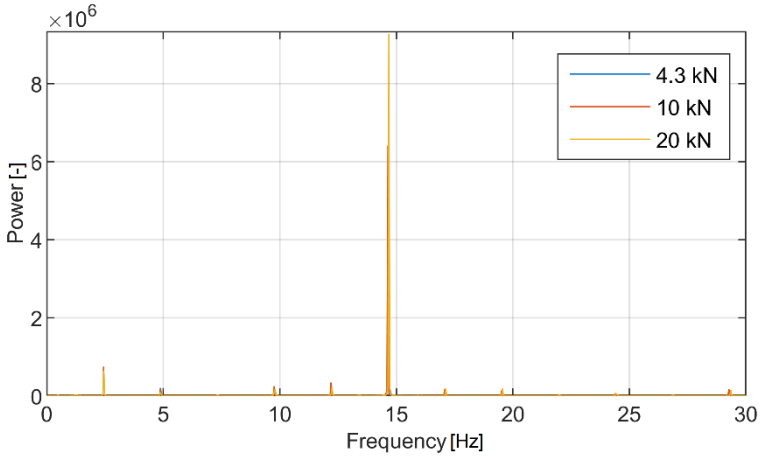

Figure 64. Frequency analysis of the torque signals from the roller-rig for 5 km/h in frequency domain under different loadings.

In Figure 64, frequency analysis of the torque signals measured from the roller-rig for 5 km/h and under different loads has been presented in the frequency domain. The comparison of the results is presented in Figure 64d. It was noticed that increasing the normal load did not change the dominant frequencies, however, the amplitudes of the oscillations were slightly increased.

For 5 km/h, the mechanical frequency of the AM rotor is 0.487 Hz which corresponds to 2.433 Hz for the electrical frequency of the AM. The observed frequencies are the higher order harmonics of the asynchronous motor electrical frequency. The observed harmonics of the AM electrical frequency are given in Table 3.

Table 3. Obtained frequencies from frequency analysis for 5 km/h

AM El. Freq. (Hz)	*Harmonics (Hz)*										
2.433	*4.897*	*7.299*	*9.792*	*12.215*	*14.645*	*17.095*	*19.56*	*22.030*	*24.460*	*26.839*	*29.312*

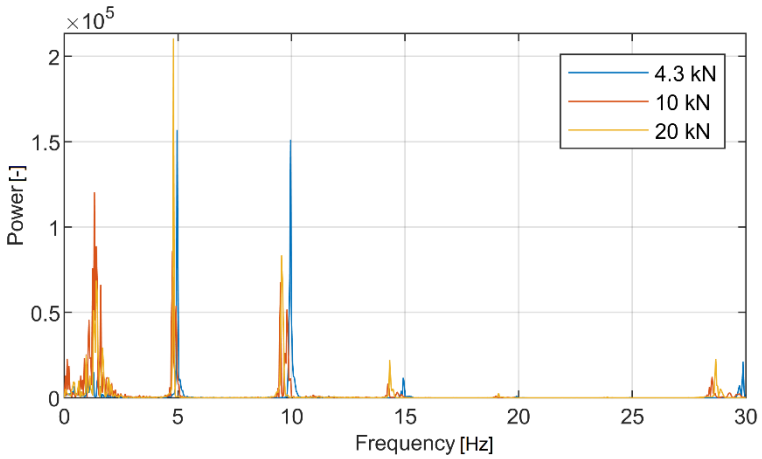

Figure 65. Frequency analysis of the torque signals from the roller-rig for 10 km/h in frequency domain under different loads.

In Figure 65, frequency analysis of the torque signals measured from the roller-rig for 10 km/h and under different loads has been presented in the frequency domain. The comparison of the results is presented in Figure 65d. It was noticed that increasing the normal load did not change the dominant frequencies, however, the amplitudes of the oscillations were slightly decreased.

For 10 km/h, the mechanical frequency of the AM rotor is 0.9728 Hz which corresponds to 4.864 Hz for the electrical frequency of the AM. The observed frequencies are the higher-order harmonics of the asynchronous motor electrical frequency except for 1.333 Hz. The observed harmonics of the AM electrical frequency are given in Table 4.

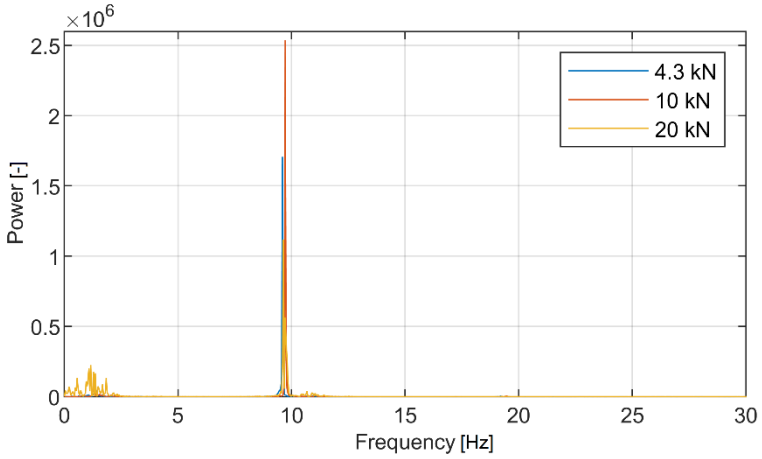

Figure 66. Frequency analysis of the torque signals from the roller-rig for 20 km/h in frequency domain under different loads.

Table 4. Observed frequencies from frequency analysis for 10 km/h

AM El. Freq. (Hz)	*Harmonics (Hz)*		
4.864	*9.732*	*14.580*	*29.162*

In Figure 66, frequency analysis of the torque signals measured from the roller-rig for 20 km/h and under different loads has been presented in the frequency domain. The comparison of the results is presented in Figure 66d. It is noticed that increasing the normal load did not change the dominant frequencies, however, the amplitudes of the oscillations were slightly changed.

For 20 km/h, the mechanical frequency of the AM rotor is 1.7933 Hz which corresponds to 8.9665 Hz for the electrical frequency of the AM. Unlike previous cases, there are no harmonics observed in 20 km/h case. 1.333 Hz is also observed in this case.

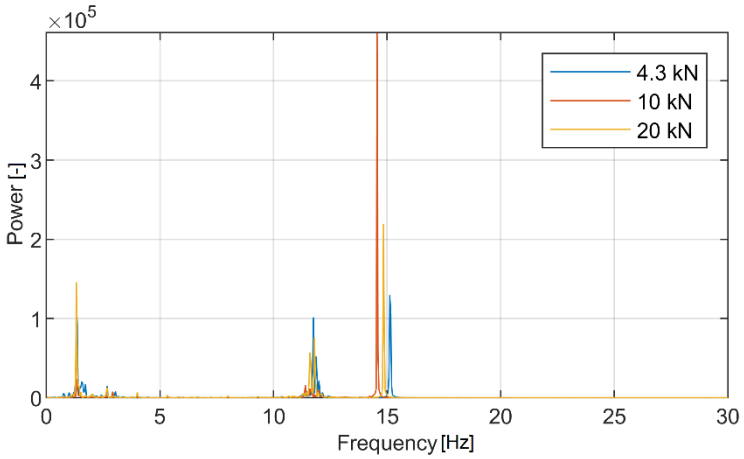

Figure 67. Frequency analysis of the torque signals from the roller-rig for 30 km/h in frequency domain under different loads.

In Figure 67, frequency analysis of the torque signals measured from the roller-rig for 30 km/h and under different loads has been presented in the frequency domain. The comparison of the results is presented in Figure 67d. It is noticed that increasing the normal load did not change the dominant frequencies, however, the amplitudes of the oscillations were slightly changed.

For 30 km/h, the mechanical frequency of the AM rotor is 2.9343 Hz which corresponds to 14.6713 Hz for the electrical frequency of the AM. The other observed frequency is the 4th

order harmonic of the asynchronous rotor frequency. 1.33 Hz is also observed in this case. It should be noted that, in Figure 67d, the differences in the frequency around 15 Hz occurs due to the speed setting of the roller rig. Maintaining the exact same speed for different cases at high speeds is relatively hard.

When the torque signal, laser displacement sensor data and frequency analysis of both were compared, no correlation has been found between the disturbing torque signals and shaft oscillation. Also, amplitudes of the signals have been slightly changed under different vertical loads however there was no correlation found between the vertical load and torque signals nor shaft oscillation. All measured raw data is given in appendix A.

As a result of the conclusions reached, it was decided that filtering is the best solution for eliminating the wave motion on the torque signal. Suitable filters have been examined and a suitable filter method has been applied and optimized to solve the waving signal.

4.5.2.5 Filter Selection

The frequency analysis revealed that almost all of the disturbing frequencies in the output signals were generated by the asynchronous motor. Other disturbing frequencies are notably less than those produced by AM. The mentioned signals produced by AM vary according to the operation speed. It is planned to design a filter in order to eliminate the disturbing signals that change depending on this speed and to obtain a more useful and smoother test result. In this section; considered filters, selection of filter type, selection of parameters and method of application are explained. Common filters used in the literature has been analysed from various aspects. Their contributions and handicaps have been examined and the most suitable filter has been applied.

In its simplest form; the expectation from a filtering procedure is that it yields the best output with minimal data loss. In this respect, how fast and frequently the data change in the time domain is one of the most important factors affecting the outcome. When a filter is applied to a high-frequency data group with low amplitude (noise) and a low-frequency data group with high amplitude (spike), it is not possible to get the same level of successful result output. Therefore, there is a need for a type of filter that can adapt to noise and spikes.

In measurements, it has been observed that the signals have high-frequency oscillations in steady and transient parts of the data. Also, according to the measurement scenario on the roller-rig, there are various types of spikes with different sizes and repeats. In order to find a suitable filter that provides a smooth output, various types of filters applied to the roller-rig data. Common filter algorithms such as Butterworth, Moving Average, Gaussian, Savitzky-Golay, Local Regression filters, have been selected for the application. Local Regression filters have been applied with different versions such as 1^{st}, 2^{nd} degree polynomials and different weightings. Except for Butterworth filter all other filters are also known as smoothing filters.

Butterworth is a type of filter designed to obtain a frequency response as flat as possible in the passband [118]. Designed Butterworth filter for 1st, 2nd and 3rd order is given in Figure 68. The selected cut-off frequency is 1.2 Hz which can be the minimum to eliminate noises and keeping low-frequency data. As seen in Figure 68. the noises in the have been eliminated in the steady part. A comparison of frequency analysis of filtered data and raw data is given in Figure 69. With a closer look, it can be seen that there is a significant difference between the filtered data and the raw data in the transition regions. The filter with the 1st degree followed the spikes slightly. The 2nd and 3rd order filters did not catch the spikes in the transition part and caused their complete elimination. Moreover, there is a considerable delay in the filtered data. The reason for this delay is the ratio of the derivative of the phase response to the frequency [118]. As a result, it is concluded that the Butterworth low-pass filter is not a suitable filter for this application.

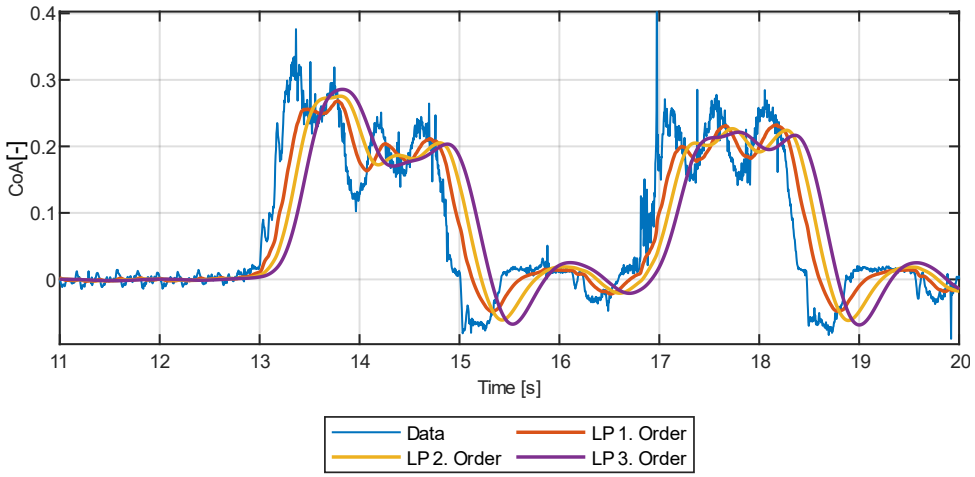

Figure 68. Butterworth filter results for 1th 2nd and 3rd order

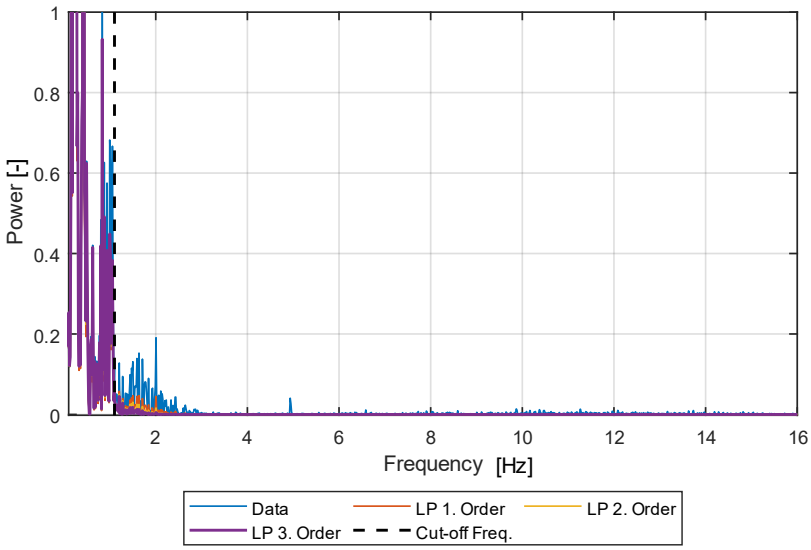

Figure 69. Frequency analysis of applied Butterworth filters

Local regression is one of the most popular methods in statistics. Local regression smoothing filters are the application of classical local regression method to the data by dividing the data into specific parts. Also, robust types of these both versions exist, and they are designed in order to be resistive against the extreme outlier data pieces. In Figure 70, the LOWESS application on the selected data with various window lengths (data number) is given. Due to the incapability of the filter, the application could not succeed in both of the data parts (steady and spike) at the same time. However, the LOESS (2nd order polynomial) filter has performed better on smoothing (Figure 71). With the 131-window length, it succeeded to eliminate the

noises in the steady part, and it has managed to follow the spikes much better than the LOWESS method in the transient parts.

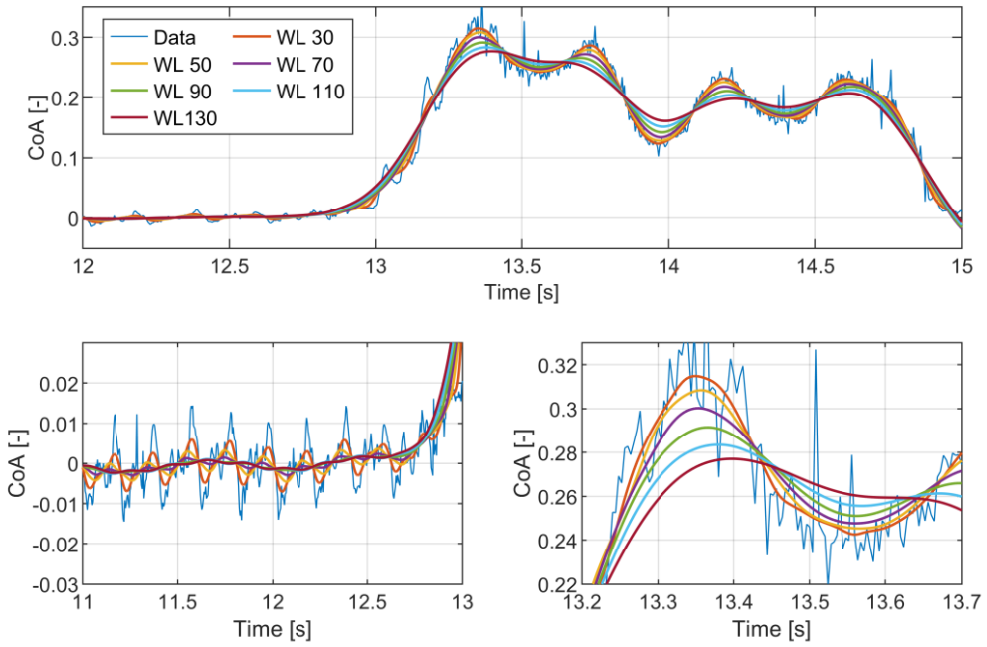

Figure 70. LOWESS filtering on the raw data for various window lengths

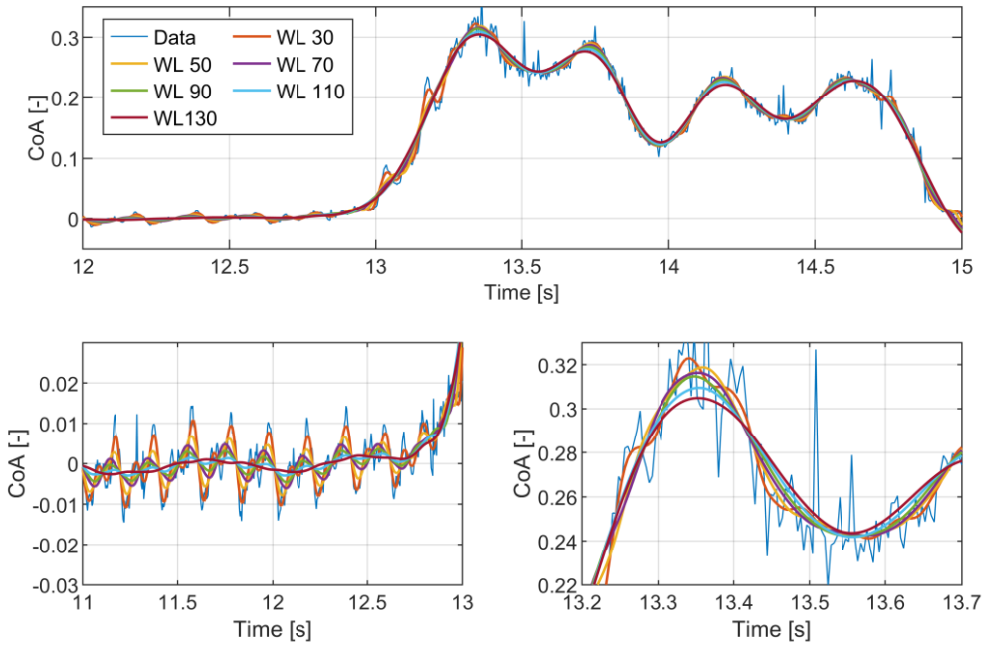

Figure 71. LOESS filtering on the raw data for various window lengths

Robust versions of both LOWESS and LOESS methods have been also applied. Both results are given in Figure 72 and Figure 73, respectively. In the robust LOWESS filtering application, due to the calculation method, window length kept much lower than the original method (~%50). As it is seen in the related figures, the robust types of Local regression smoothing filters were not able to provide an acceptable solution.

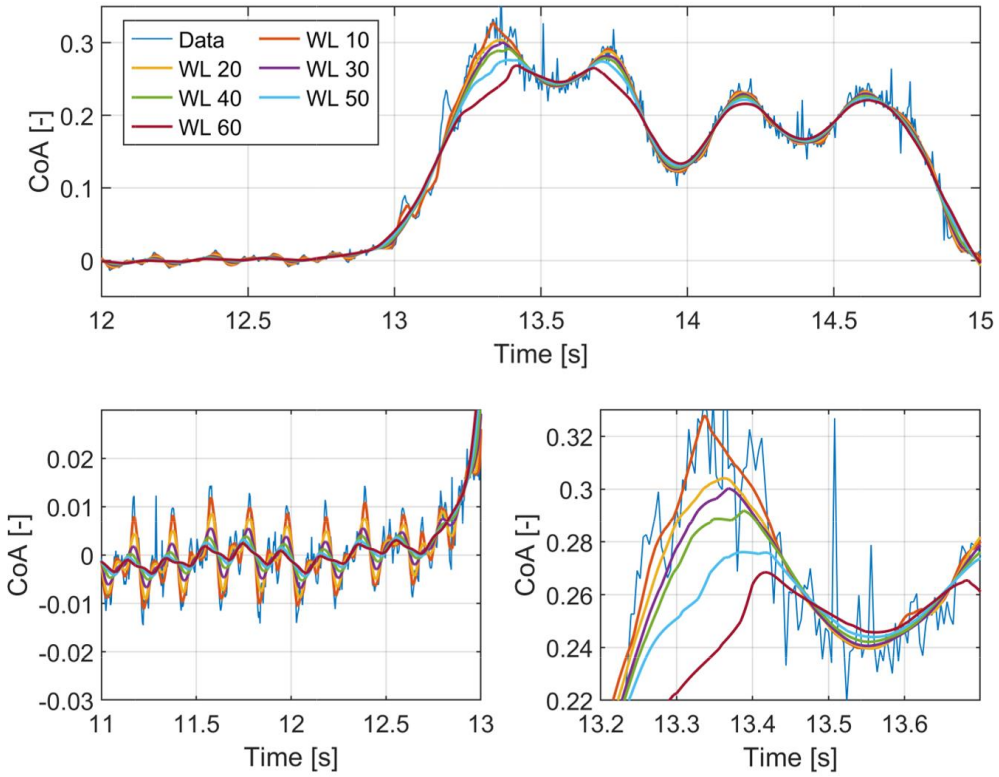

Figure 72. Robust LOESS filtering on the raw data for various window lengths

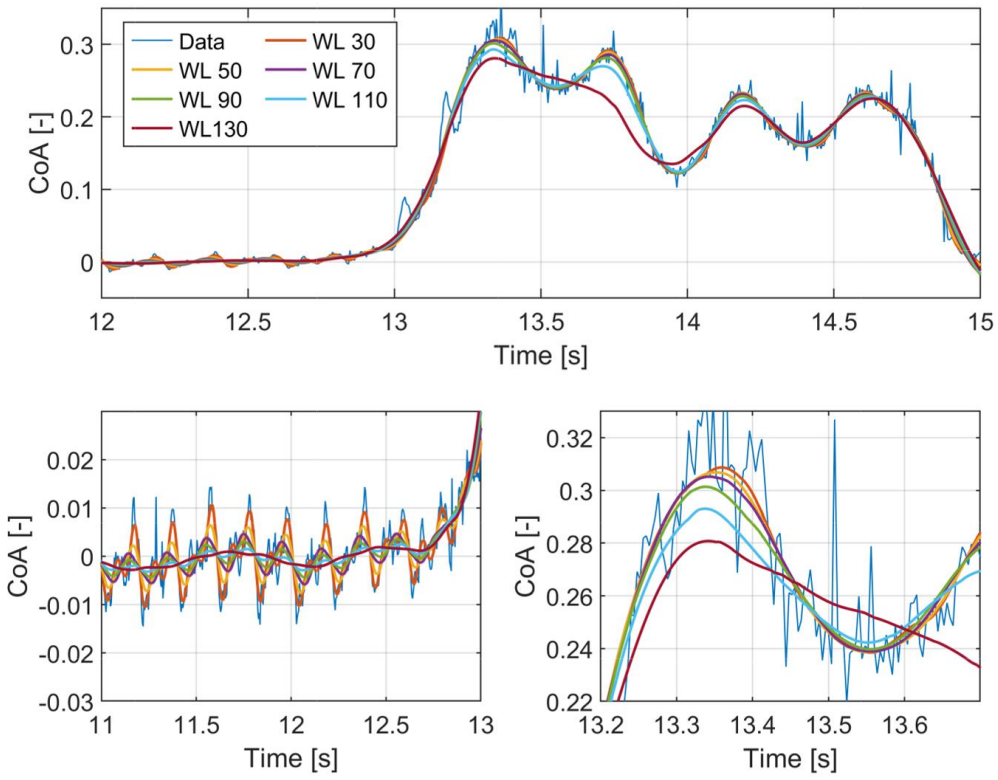

Figure 73. Robust LOWESS filtering on the raw data for various window lengths

Gaussian weighted average filter is a popular noise filter mostly preferred in image processing. It is preferred mainly because of low group delay and calculation simplicity. The results of the Gaussian filter are given in Figure 74. As it is seen in the related figure, the filtering procedure was not successful to provide results for both data parts. With a wider window length, it caused a lot of data losses in the transient parts and it was not able to follow the spikes properly.

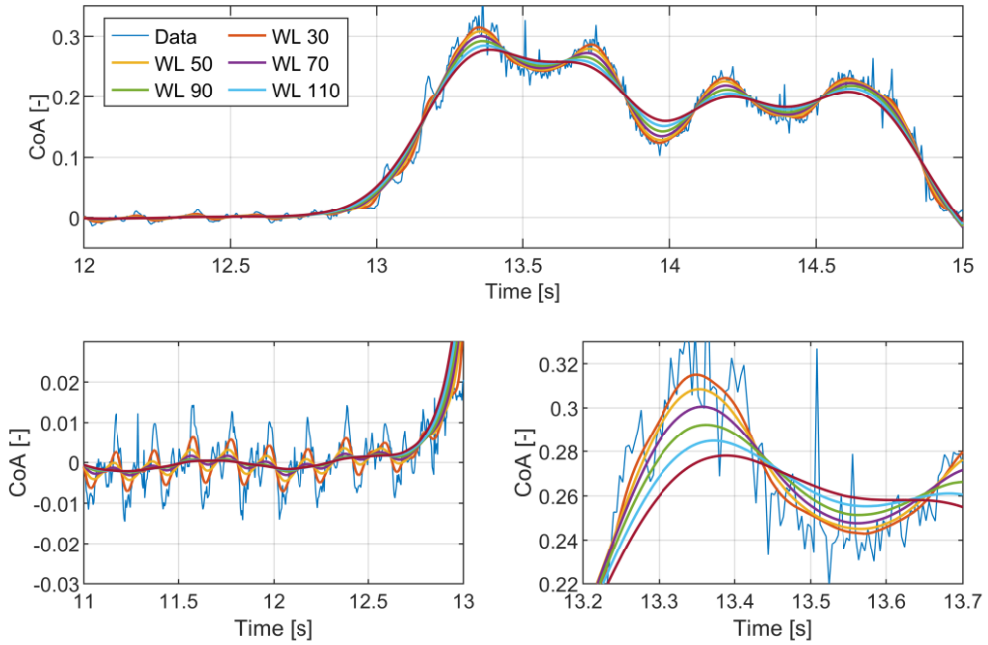

Figure 74. Gaussian weighted average filtering on the raw data with various window lengths

Moving average filters are the most popular smoothing filter in data filtering. It has an easy procedure of calculation and in many cases, especially in steady data series, it provides reliable solutions. As seen in Figure 75, it provided good results on the transient parts also, acceptable results in the steady parts. However, when the results in the steady part tried to be improved by increasing the window length, it caused the removal of the spikes in the transient areas. It is concluded that the moving average filter is acceptable for certain window lengths, however, the search for a better solution has continued.

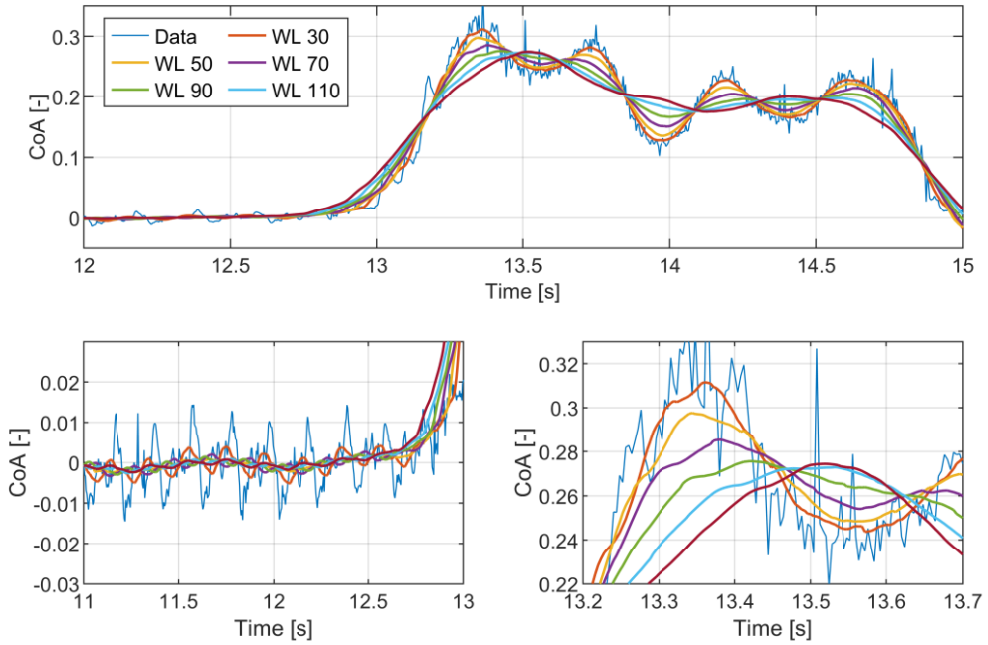

Figure 75. Moving average filtering on the raw data with various window lengths

Savitzky-Golay filter considered one of the strongest filtering methods, due to the preservation of important features of the original time series, like the relative widths and heights which are usually flattened by other averaging techniques [117]. Figure 76 shows the results of filtered data with 2nd degree of Savitzky-Golay with different window lengths. As it is seen from the corresponding figure, the noise has been reduced to an acceptable level in the steady part also the values in the transient parts (spikes) were preserved better than the other filters.

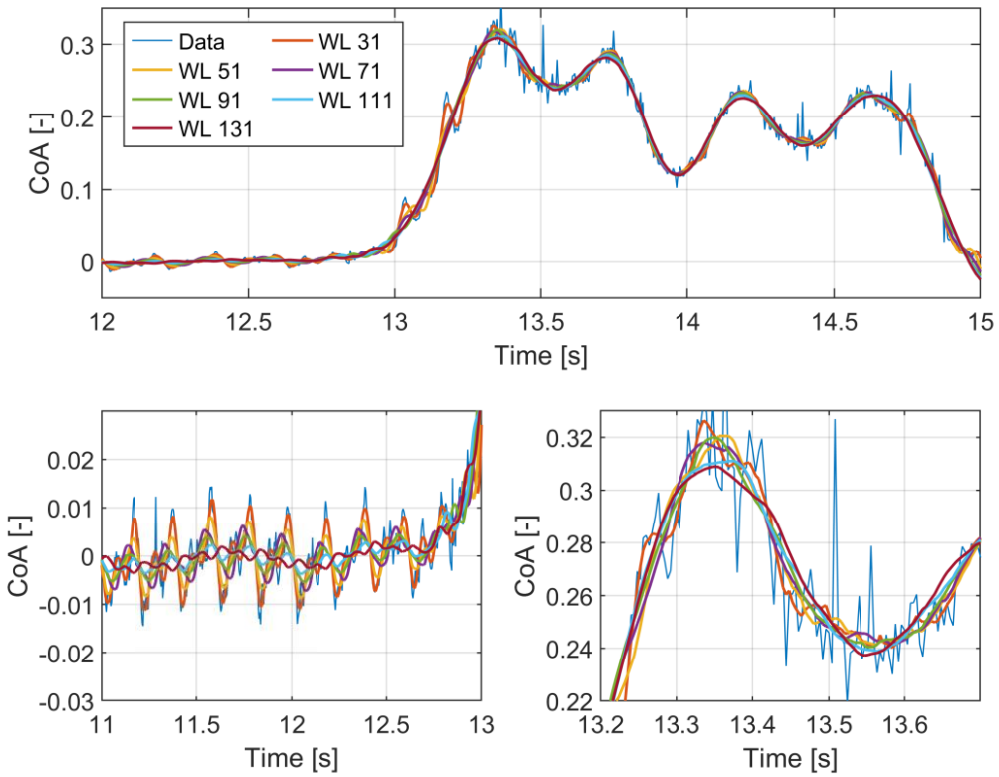

Figure 76. 2nd degree Savitzky-Golay filtering on the raw data with various window lengths

4.5.2.6 Savitzky-Golay Filter

Savitzky-Golay filter is suggested to reduce the effect of noise by suppressing the noise component on the signals while retaining the salient features of the polynomials [119]. The general filter equation Savitzky-Golay explained in [120] is given following. Considering for the moment group of $2M + 1$ samples centered at $n = 0$, the coefficients of a polynomial are obtained as;

$$p(n) = \sum_{k=0}^{N} a_k n^k$$

That minimizes the mean-squared approximation error for the group of input samples centred on $n = 0$,

$$\varepsilon_N = \sum_{n=-M}^{M} \left(\sum_{k=0}^{N} a_k n^k - x[n] \right)^2$$

Savitzky-Golay filter needs two additional inputs different from the raw data which are the order of the polynomial and frame size (window length). The best fit values for order and window length are generally estimated by trial and error [121]. Comparative graphs of Moving Average and Savitzky-Golay filters are given in Figure 77. Both methods have been applied to the raw data (top) with the same window length (33) and the S-G method (bottom) performed noise filtering with keeping the spikes in the data better than MA (middle). It is noted that MA performed better from the point of view of noise filtering. In S-G filtering, this drawback can be eliminated by increasing window length for some cases. Additionally, increasing the order number (degree) can provide better results on transient parts of the data. In Figure 78, 2nd,4th and 6th degree of filtering with 65 window length presented. It is noticed that increasing filter order and window length provides better results in data smoothing.

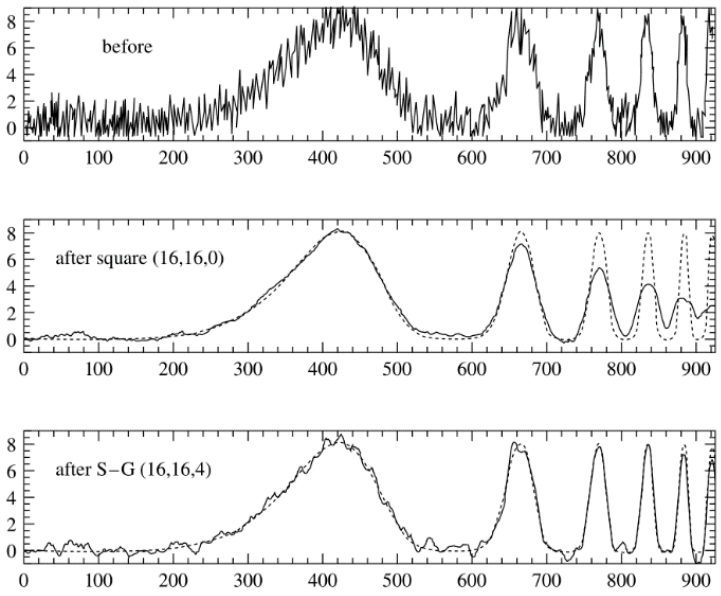

Figure 77. Comparison of S-G filter and Moving average filter. The x and y axes indicates the number of data and value of the data, respectively. [122]

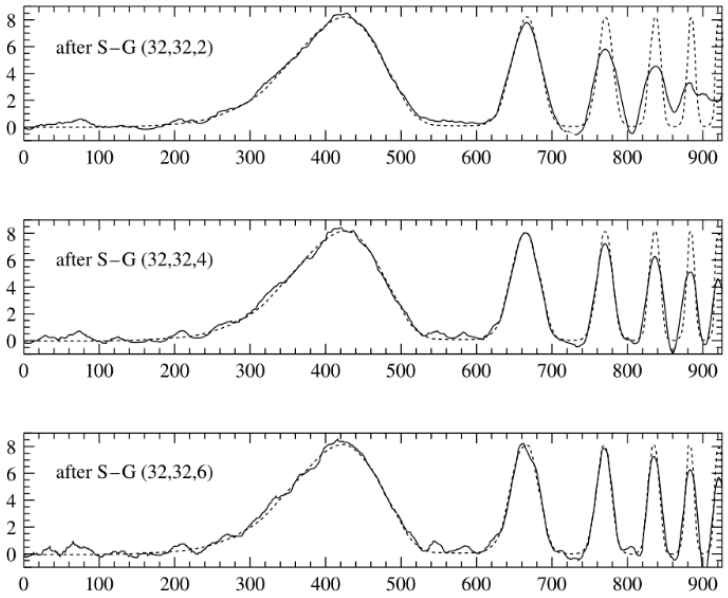

Figure 78. Effect of window length and filter order. The x and y axes indicates the number of data and value of the data, respectively. [122]

A Savitzky-Golay filter has been designed in MATLAB® environment. The designed filter has been applied to various speed data (10, 20 and 60 km/h) in order to verify that it can be applicable for different speeds. Also, normal load differences have not been taken into account due to the insignificant effect on the disturbing frequencies (See section 4.5.2.3 and 4.5.2.4). In order to provide an optimized filter, different orders and window lengths have been applied also. In all figures, steady and transient parts of the data are given in zoom at the bottom of each figure.

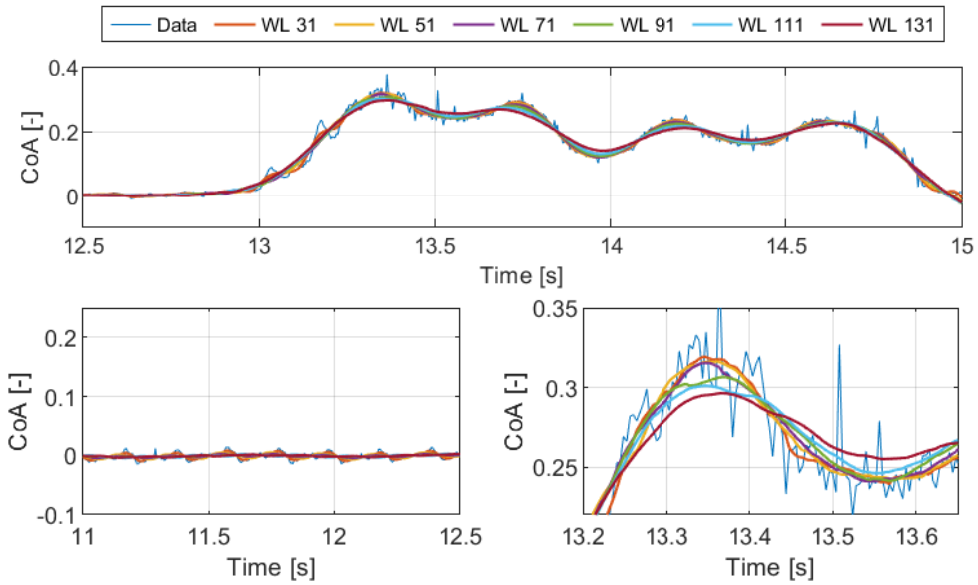

Figure 79. Application of 2nd degree S-G filter to 10 km/h data

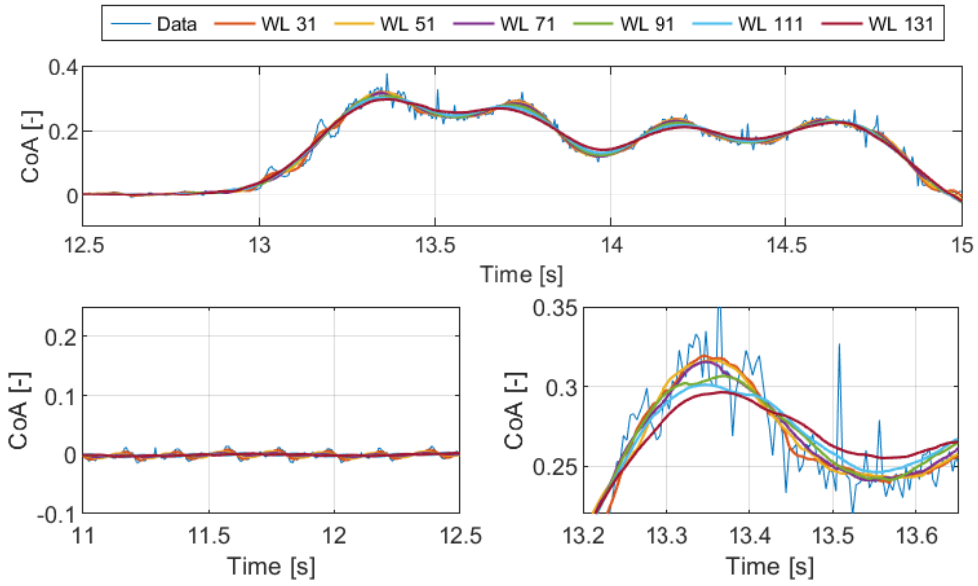

Figure 80. Application of 3rd degree S-G filter to 10 km/h data

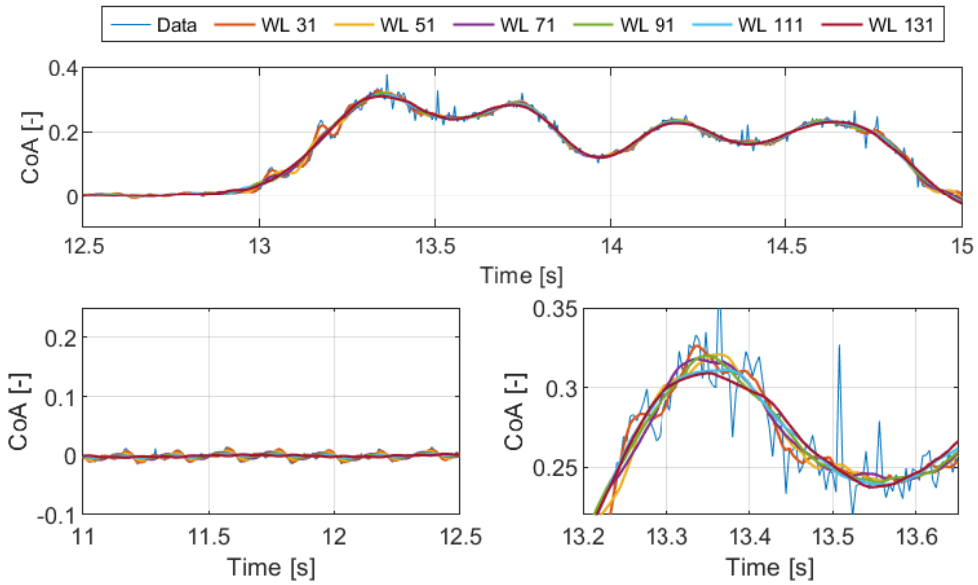

Figure 81. Application of 4th degree S-G filter to 10 km/h data

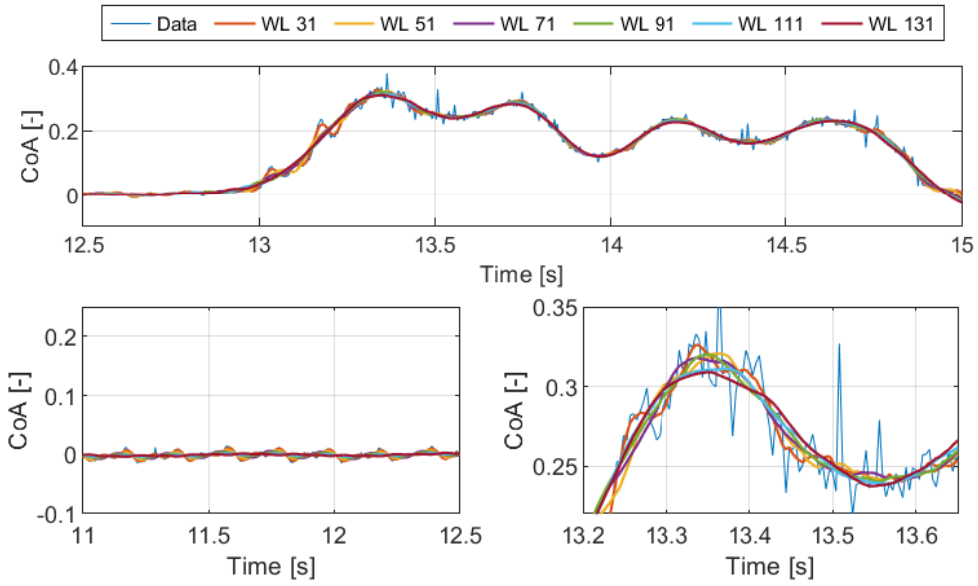

Figure 82. Application of 5th degree S-G filter to 10 km/h data

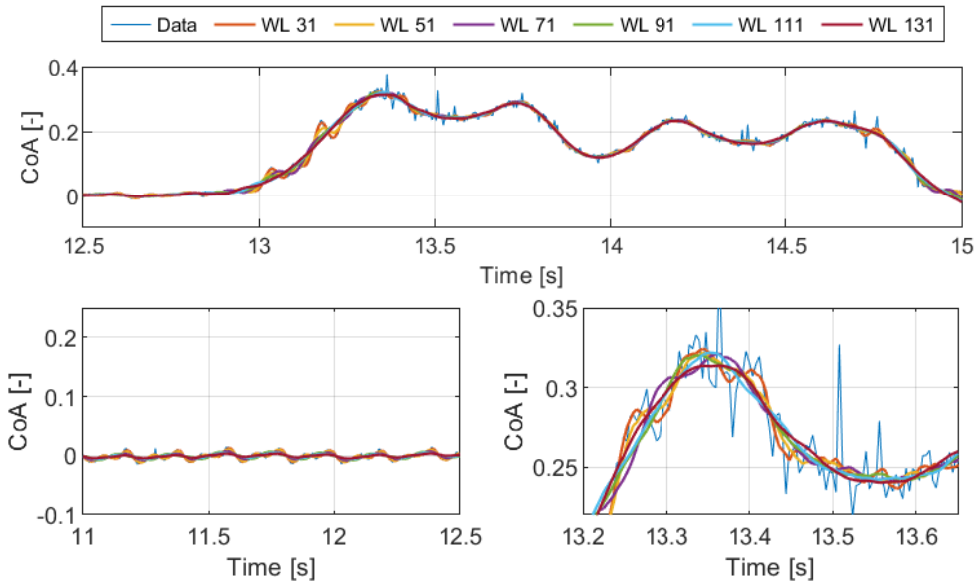

Figure 83. Application of 6th degree S-G filter to 10 km/h data

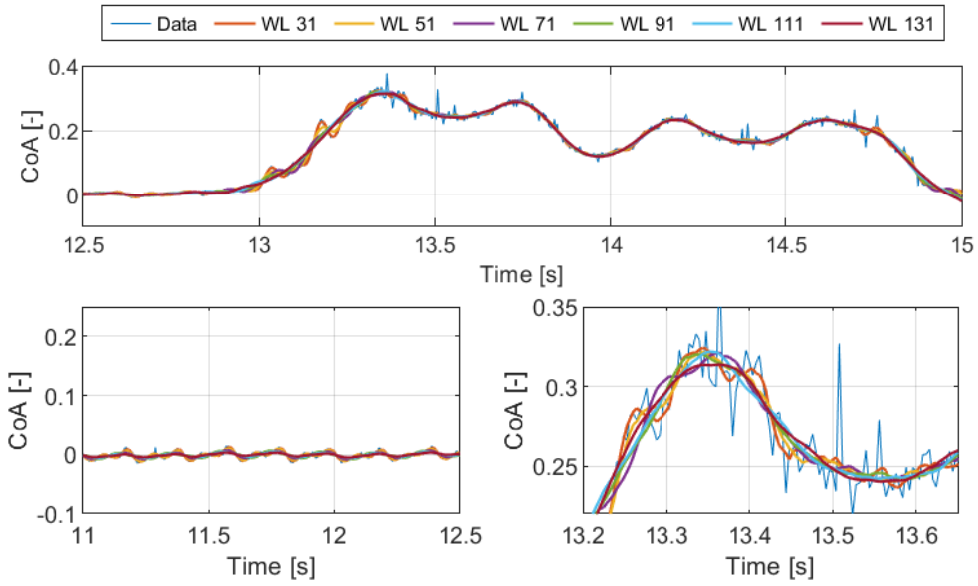

Figure 84. Application of 7th degree S-G filter to 10 km/h data

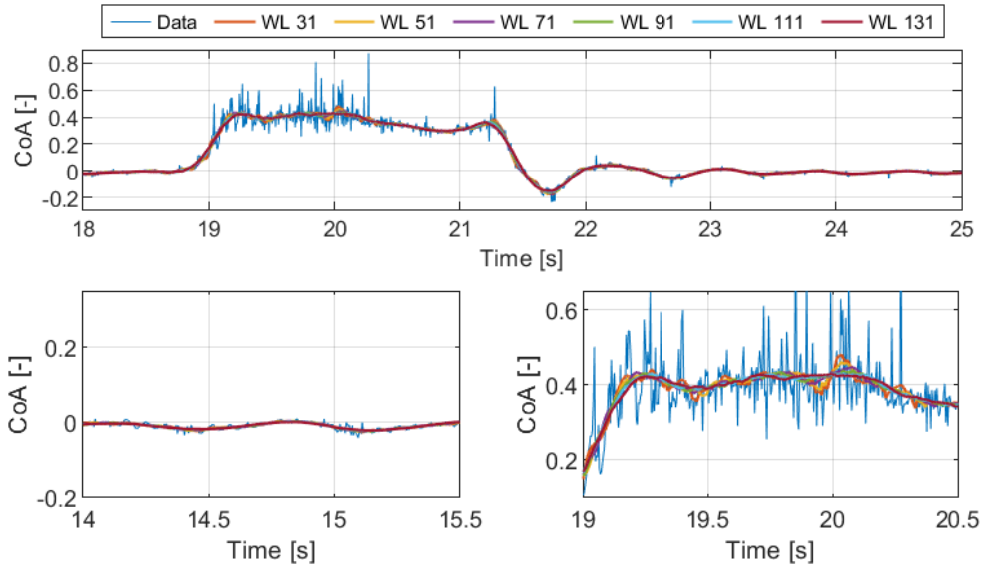

Figure 85. Application of 2nd degree S-G filter to 30 km/h data

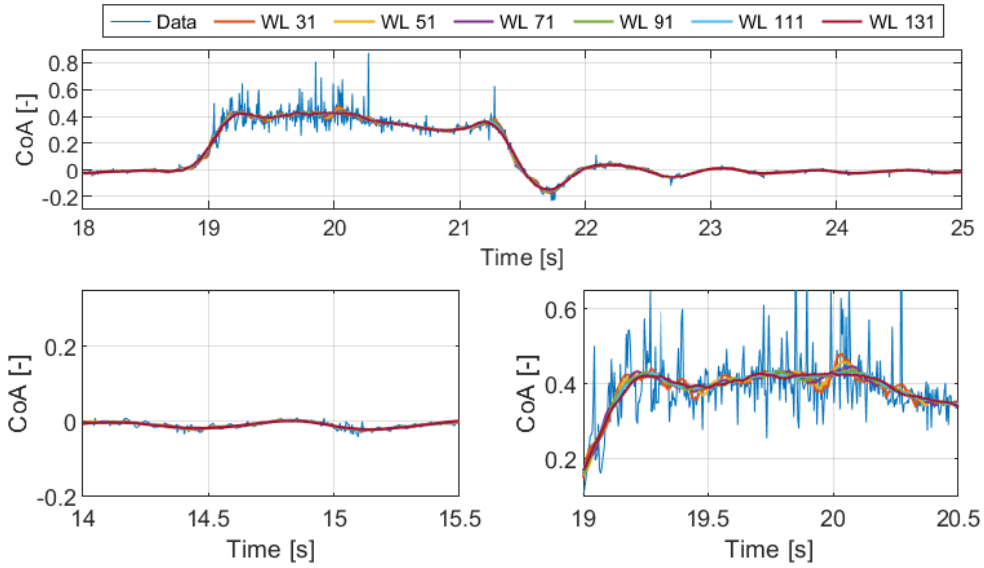

Figure 86. Application of 3rd degree S-G filter to 30 km/h data

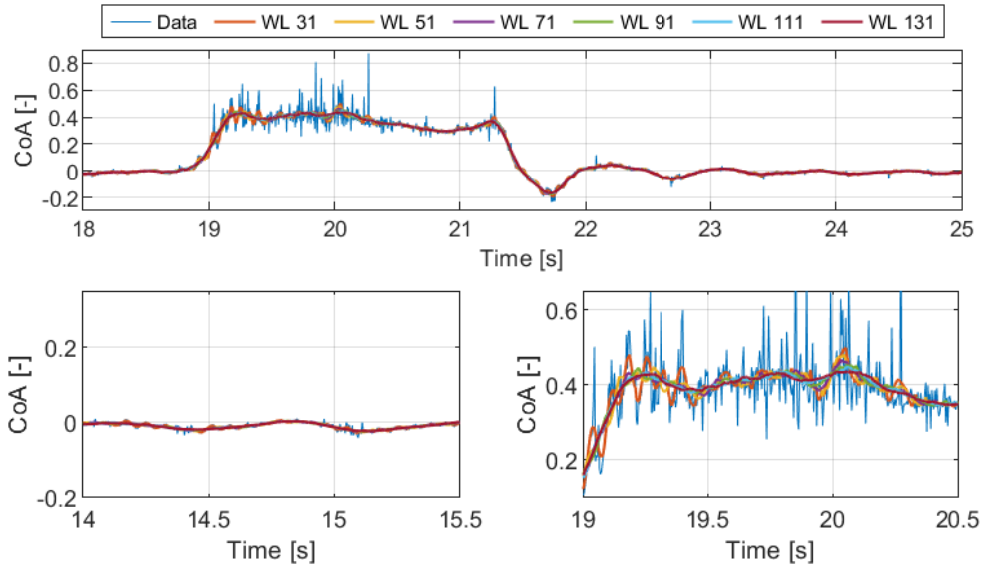

Figure 87. Application of 4th degree S-G filter to 30 km/h data

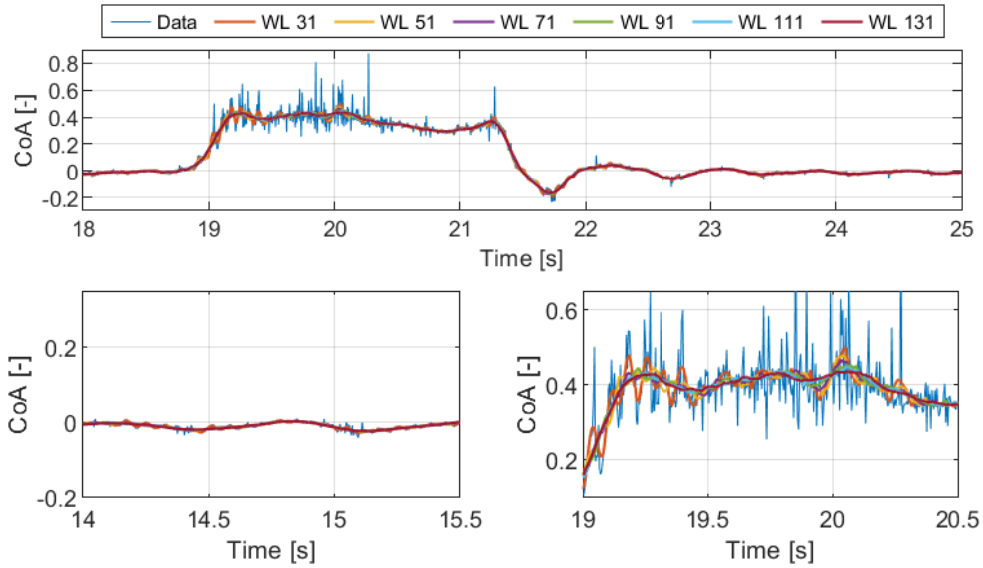

Figure 88. Application of 5th degree S-G filter to 30 km/h data

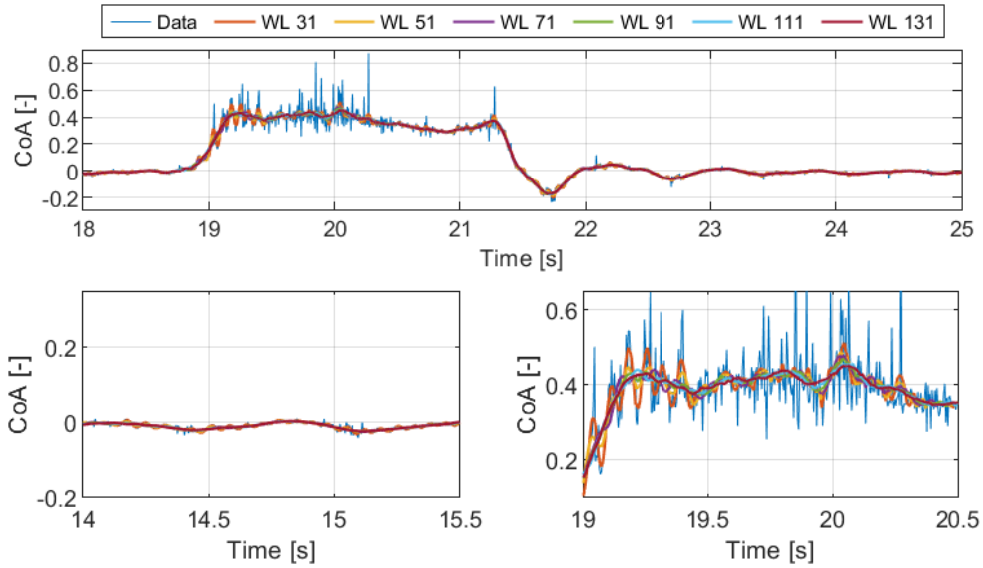

Figure 89. Application of 6th degree S-G filter to 30 km/h data

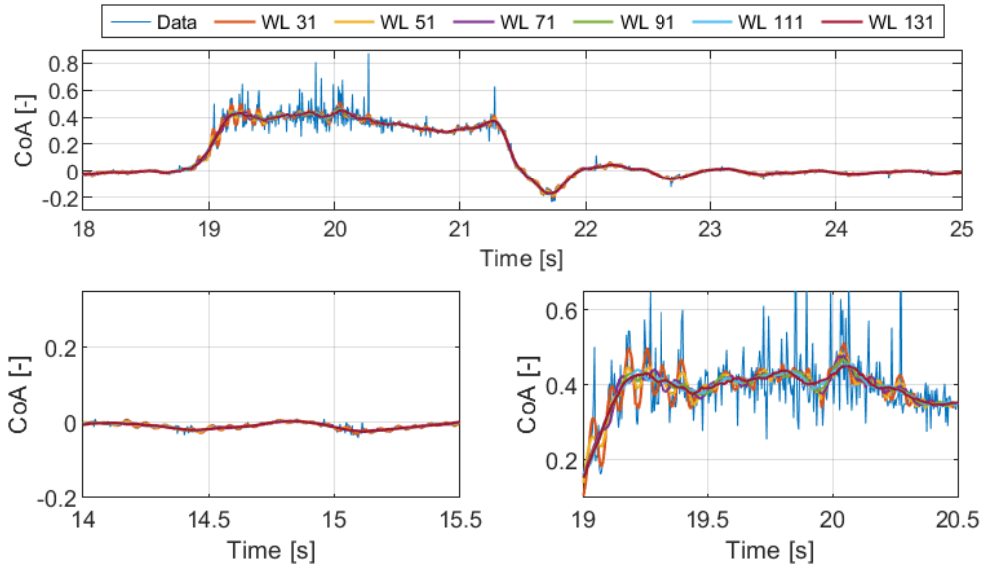

Figure 90. Application of 7th degree S-G filter to 30 km/h data

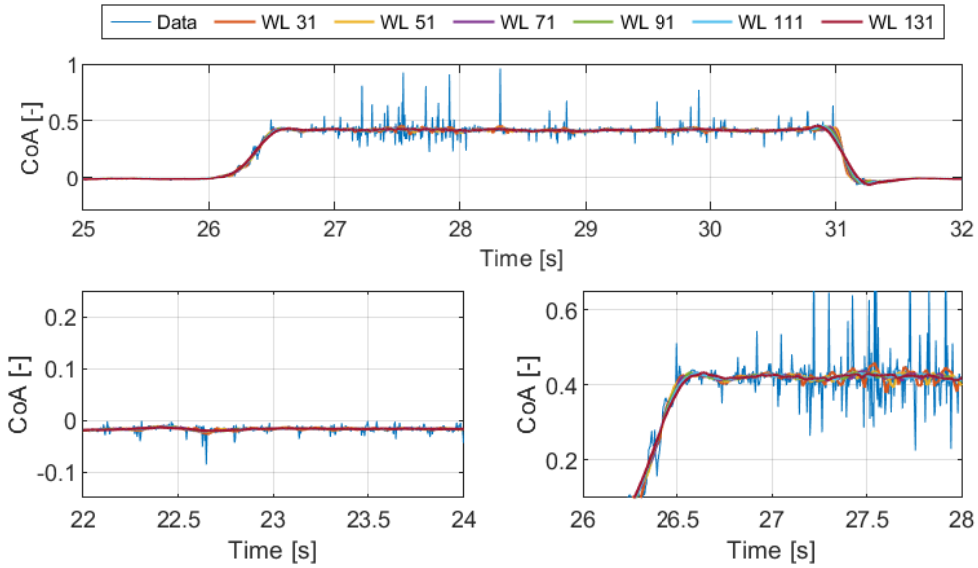

Figure 91. Application of 2nd degree S-G filter to 60 km/h data

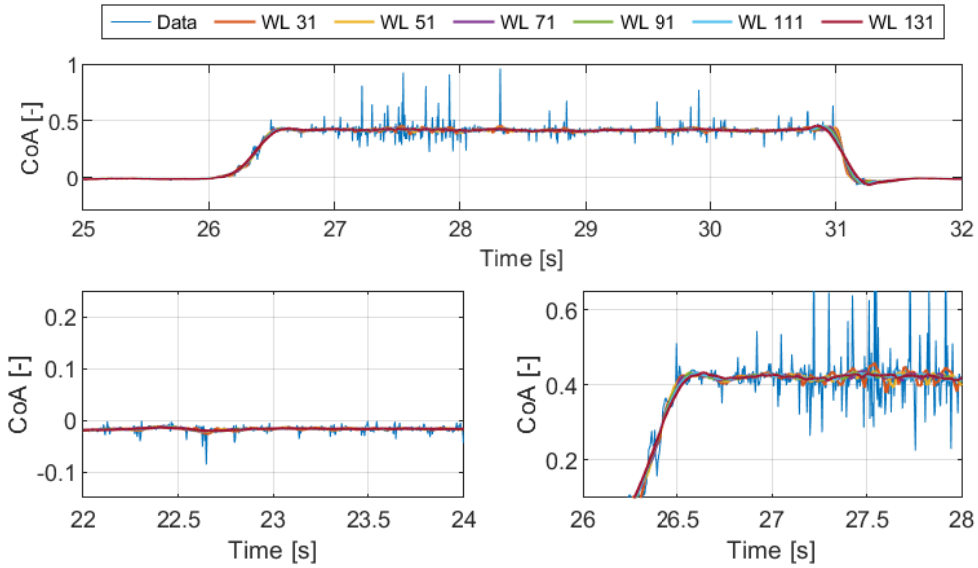

Figure 92. Application of 3rd degree S-G filter to 60 km/h data

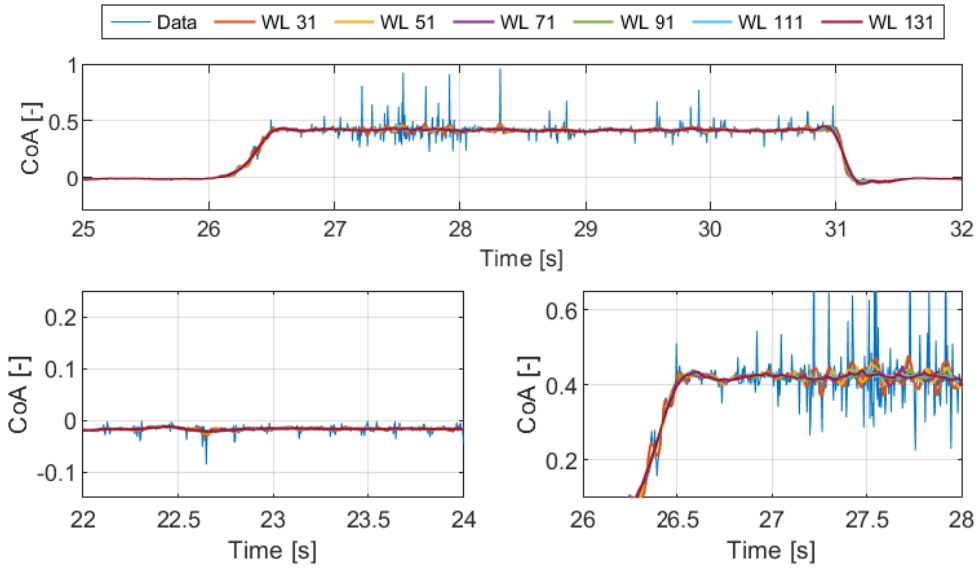

Figure 93. Application of 4th degree S-G filter to 60 km/h data

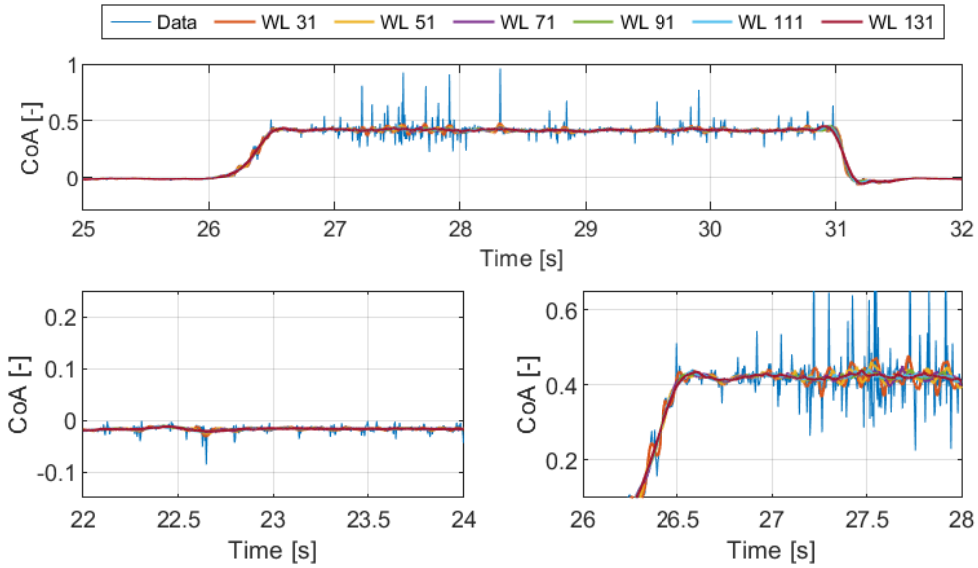

Figure 94. Application of 5th degree S-G filter to 60 km/h data

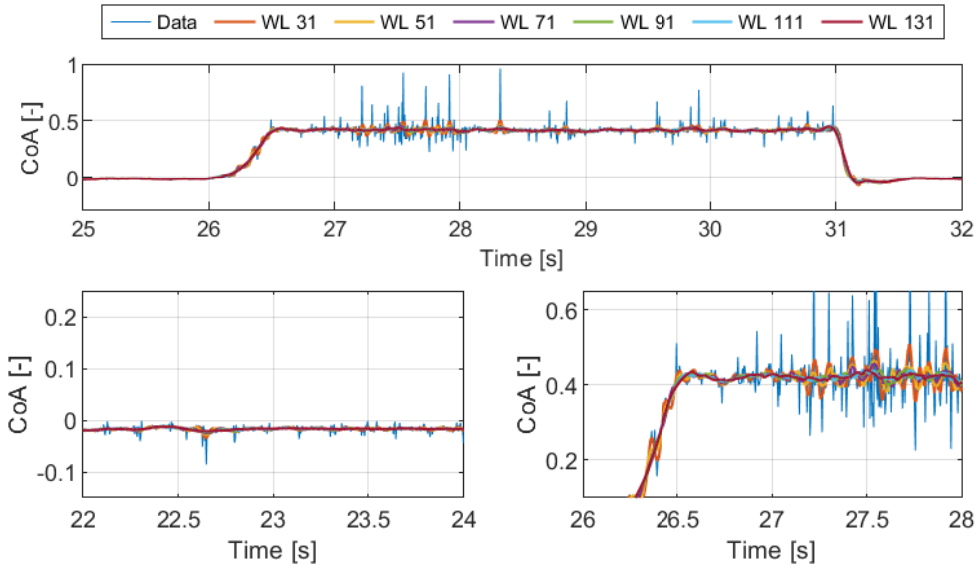

Figure 95. Application of 6th degree S-G filter to 60 km/h data

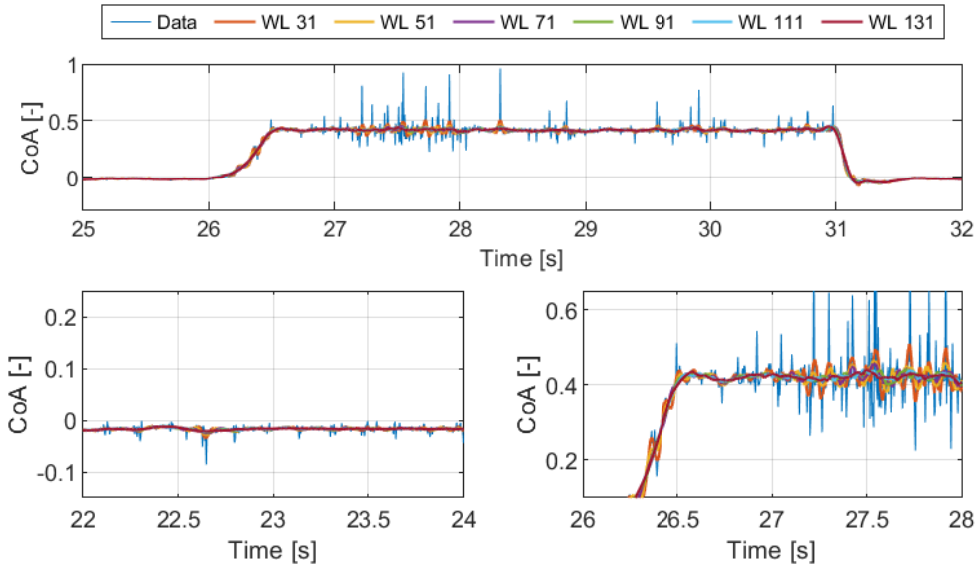

Figure 96. Application of 7th degree S-G filter to 60 km/h data

Comparative results of applied S-G filter for different speeds (10, 20 and 60 km/h) are given in Figure 79-Figure 96. Filter orders have been applied from 2nd to 7th order. The filter characteristics after the 3rd order are same in every two degrees. (4th and 5th orders or 6th and 7th orders). When the filtered results investigated in-depth, it is seen that 4th and 5th degree of polynomial filters are provided better results than lower order filters. Less degree of filters (i.e. 2nd or 3rd) were not capable to follow signal peaks in some cases (Figure 79 and Figure 80).

Also, 6^{th} and 7^{th} order filters were able to follow the peaks more often, which can lead undesired results in the area of data jumps caused by measuring system. In Figure 83 and Figure 84, mentioned data jumps can be seen. In Figure 85-Figure 90 and Figure 91-Figure 96, the data in the steady part is less noised compared to Figure 79-Figure 84, which is occurred due to the operation speed. Decrease of the noise amplitude was also mentioned in the frequency analysis section (See section 4.5.2.3 and 4.5.2.4).

The window length (WL) is also a parameter must be determined. The window lengths are marked on the corresponding figures as WL. In Figure 87 and Figure 88, in the steady part lower window length couldn't provide acceptable results. The reason of this outcome is connected with the amplitude and frequency of the noise signal. According to the mentioned figures, it is concluded that, for a wide speed range (i.e. 10, 30, 60 km/h) a S-G filter with 4^{th} and 5^{th} degrees of polynomials and 111 data window length produces satisfying noise reduction. However, for each speed range, different orders and window lengths may be specified according to the specific needs of the experimental results. As expected, lower window lengths and lower polynomial orders were not able to provide useful results.

5 DISCUSSION

5.1.1 Stationary Part of the Roller Rig

The stationary part (frame) of the roller rig has been investigated with numerical and experimental procedures in order to identify the behavior under traction and normal loading. It has been aimed to find a relation between the behavior of the roller-rig frame and the oscillation of torque signal which occur during measurements. Normal load and traction load have been applied to the FE model of the roller-rig frame. With this FE model, the most forced places have been determined and the reaction of the frame against the loadings has been found. Also, these places have been used for placing strain gauges and the experimental procedure has been applied. The loading values have been selected according to the maximum forces which can be created by pneumatic spring and adhesion.

In the FE analysis, the frame has performed a robust behavior against the applied loads and the reliability of this performance has been verified by the experimental study (See 4.4.2 and 4.4.3). During the tests; the loading has been repeated three times and the frame performed a robust behavior against the traction force. The findings from measured and model results showed that there is no relation between the oscillation signal and frame behavior under horizontal or vertical loading. Therefore, the hypothesis about the possibility of the dynamic phenomenon related to the robustness of the roller-rig frame in section 4.3.1 is **falsified**.

5.1.2 Rolling Parts of the System

A mathematical model has been generated for simulating the rolling parts of the roller rig. The dynamic model contains 7 rotating masses, which are PMSM mounting, PMSM rotor, wheel disc, wheel tyre, rotating rail, AM rotor and AM mounting. Moreover, rolling contact model, PMSM motor model and AM motor model have been implemented to the system (See section 4.5.1). Rolling contact model has been fitted with measured parameters from simulated cases. With the dynamic model, the system responses have been simulated well (See Figure 40, Figure 41). With deeper analysis, it has been revealed that the AM response characteristic and the low torsional stiffness of the shaft cause the dynamic phenomenon which is mentioned in section 4.2.1. One of the main findings is that the effect of the low stiffness of roller shaft is

smaller than the effect of the AM response characteristic. The effect of the AM response delay is the main reason for the dynamic phenomenon: This delay has been simulated via a discrete-time low-pass filter which has been used for simulating the systems which has response delays in traction systems in railway studies [111,112]. The mentioned delay occurrence has been verified by comparing the measured and simulated torque-speed characteristic of the AM. Therefore, the hypothesis about the possibility of the dynamic phenomenon related to the AM dynamic response and torsional robustness of the roller shaft has been **verified**.

It has been concluded that two significant improvements may be proposed in order to improve the behavior of the roller-rig. The first one is to eliminate the response delay of AM which is the main cause of the dynamic phenomenon in section 4.2.1. It is known from the corresponding literature (4.5.1.4.2) the induction motors with voltage frequency control has a poor dynamic behavior. The most simple approach in order to eliminate the oscillation, the AM motor may be replaced with a servo motor which has a higher control sensitivity [123]. Another, improvement may be achieved by using a familiar system which is speed controlled PMSM [124]. Thus, the delayed response of the rotating rail motor may be eliminated or substantially decreased. However, designing, simulating, applying such a motor with its characteristics and control methodology is under the field of electrical/electronic engineering which is out of the scope of this study.

The second one may be achieved by increasing the torsional stiffness of the roller shaft. Due to the measurement of the adhesion has been obtained by the torque sensor on the roller shaft, it is inevitable to make a measurement without the effect of dynamic responses of the AM. However, increasing the torsional stiffness of the roller shaft slightly decreases the effect of the dynamic responses. In order to provide improvement, simulations have been repeated for increased stiffness values. It has been found by simulations, the amplitude of the dynamic phenomenon has been decreased by increasing the torsional stiffness of the roller shaft (Section 4.5.1.7). Consequently, the shaft may be replaced a stiffer one. Nevertheless, the dynamic phenomenon can not be fully eliminated by only replacing the shaft.

Additionally, rolling disorders of the system have been investigated (See section 4.5.2). Initially, the out-of-roundness of the rolling parts investigated with a manual gauge and it has

been observed that wheel and roller have not a rolling disorder. However, a movement has been detected on the perpendicular plane to the cross-section of the roller shaft. A relation has been searched between this movement and the issues in the torque signal of the roller-rig. In order to investigate it, an experimental setup has been designed with laser displacement sensors such that more precise measurements can be conducted. Both data from roller-rig and laser displacement sensors compared with frequency analysis. The measured bundle of data from laser sensors is given in Figure 56-Figure 59. Frequency analyses of displacement results are also presented in Figure 60-Figure 63. Those related to the frequency analysis results of the torque signals are illustrated as well (see Figure 64-Figure 67). After a detailed analysis of the corresponding figures, it has been found that the dominant frequencies of the torque sensor located on the roller rig and laser displacement sensors placed independently from the roller rig do not overlap. The frequency of the displacement of the roller shaft quite lower than the torque signal of the roller-rig. Thus, in the author's opinion, there is no relationship between the stated issue and the rolling disorder of the shaft. Therefore, the hypothesis about the possibility of the wave motion mentioned in section 4.3.2 **falsified**.

With deeper analysis, it has been found that most of the noises on the torque signal are related to the AM control frequency which is connected to the electrical parts of the system (Voltage per frequency). Also, a constant frequency (1.33 Hz) for all speeds and conditions has been observed in the frequency analysis of the roller-rig. Due to being constant for all conditions, it has been concluded that, mentioned specific frequency does not occur due to mechanical reasons. The weight of the constant frequency has been changed relatively in the analysis results. Due to lower amplitudes of the signals at certain speeds, the constant frequency reveals itself more dominant in the frequency analysis results. This occurs due to the frequency analysis conducted exponentially. Because of this exponential method, high differences are also observed in the power value (e.g. 10^4-10^6) between the results of different cases. Thus, according to the author's opinion, the noises in the torque signal are related to AM control or electric/electronic components. Therefore, the hypothesis about the possibility of the wave motion in section 4.3.3 has been **verified**.

In order to eliminate or minimize these noises, a proper smoothing filter has been searched. Popular smoothing filters have been analyzed and a proper filtering method has been

found with performing several studies. Thus, the Svaitzky-Golay filter has been found as the most suitable filter which can perform well in different amplitudes and signal characteristics. An optimization study has been performed in order to find proper parameters for the Savitzky-Golay filter. Therefore, the Savitzky-Golay filter with specific parameters has been proposed in order to provide a solution to the signal noise for a wide range of speeds (Section 4.5.2.6).

For the CoA-Creep inconsistency, it has been concluded that no need to find a solution. The gap of the return curve occurs due to the second layer of filtering which is applied to the system already. Also, the decreasing rounded oscillation around zero Creep-CoA plot has been solved by the torsional stiffness and AM delay.

6 CONCLUSION

Roller rigs are widely used experimental types of equipment which are very crucial for railway engineering. Thus, they have been attracting many researchers since the early 19th century. The more robust designs have been pronounced by emerging technologies. However, the assessment of the actual response of the railway vehicles or related components still remains challenging due to certain issues during measurement. In this study, the main focus was first given on finding measurement issues on a full-scale vertical plane tram wheel roller-rig. Then, a solution for the stated issues is conceptually proposed so that the accuracy of the measurement results is going to be improved. This has been achieved by analyzing both the static and dynamic behavior of the system parts.

Current theoretical knowledge and experimental studies together with studies on roller rigs have been extensively reviewed. Also, general information about contact phenomenon and computation of wheel-rail forces has been presented. The technical specification of the roller-rig has been detailly given in the related section. The problem formulation and methodological solutions were also provided in an order. Particularly, it has been decided to investigate the whole mechanical system in two main parts. For the first part, which is stationary part of the roller rig, an FEA study has been performed. Several measurements taken from the roller rig showed that there is a close correlation with the experimentally verified FEA results. The gathered information from both FE analysis and experiments showed that the effect of the roller rig frame has insignificant or no impact on the global response.

Therefore, the second part, which is rolling parts has been investigated from two different points. The very first approach was generating a torsional model in MATLAB environment for simulating the dynamic behavior under different experimental conditions. The comparative results (i.e., between experimental and simulated) were provided by this approach. When the results are investigated in-depth, a very good match was found among the results. Those were also identified in the relevant section of the study. As a result of this part of the study, it has been found that the related issues occur mainly because of the behavior of the asynchronous motor and related components. Also, a mechanical issue has been found and

identified. A specific solution has been provided from the mechanical point of view and it has been verified with simulations.

The second approach for the rolling parts was investigating the rolling disorders. An experimental study had been conducted to observe rolling disorders of specific parts. The results showed that rolling disorders have not a direct impact on the measurement results of the roller-rig. Some specific frequencies had been observed in the frequency analysis of the roller rig measurement results. It is concluded that those are most likely related to the electrical frequencies of AM. A smoothing filter has been generated and optimized in order to provide a solution to this issue.

As a result of the whole study, three conceptual solutions are proposed, and proposed solutions have been simulated in order to provide an improvement in the measurement quality of the roller-rig.

7 FUTURE WORK

In this study, the mentioned full-scale tram wheel roller-rig has been investigated from the mechanical point of view. From this aspect, as a future work recommendation, the proposed mechanical changes may be applied and verified experimentally. From the other disciplines aspect, the electrical and electronic components of the system may be investigated by the researchers who are studying the electric/electronic field. As more specific recommendations, the data acquisition system may be investigated in order to find the noises and their causes in the gathered signals. A motor for the rotating rail may be designed, simulated and applied in order to provide a more precisely controlled behavior against load and speed changes. Additionally, for avoiding the influences of the dynamic response of the roller motor, torque measurement location may be changed, or estimation methods may be developed which are not using direct measurement techniques.

8 CONTRIBUTIONS OF THE DISSERTATION THESIS

- A comprehensive literature summary of the types, sizes, and purposes of the roller rigs have been provided.
- Specific issues related to adhesion measurement on a full-scale tram wheel roller rig have been identified.
- A FEM model of the roller-rig frame has been generated and the model has been verified with experiments. Also, the robustness of the frame of the roller-rig against the loads has been proven.
- A detailed torsional mathematical model has been generated. The behavior of the torsional system of the roller-rig has been obtained and verified with experiments. Thus, a validated model has been obtained that can simulate adhesion experiments. Also, this model can be used to simulate possible component changes in the system.
- The robustness of the mechanical system has been verified.
- It has been proven that the torque signal is not affected by bending in the shaft.
- The reasons for the specific issues have been found thus, the particular solutions have been provided and simulated.
- A smoothing filter has been designed and optimized in order to obtain better measurement results

9 APPENDICES

A. Measured Data from Torque Sensor

Torque signal for 5 km/h under 4.3 kN

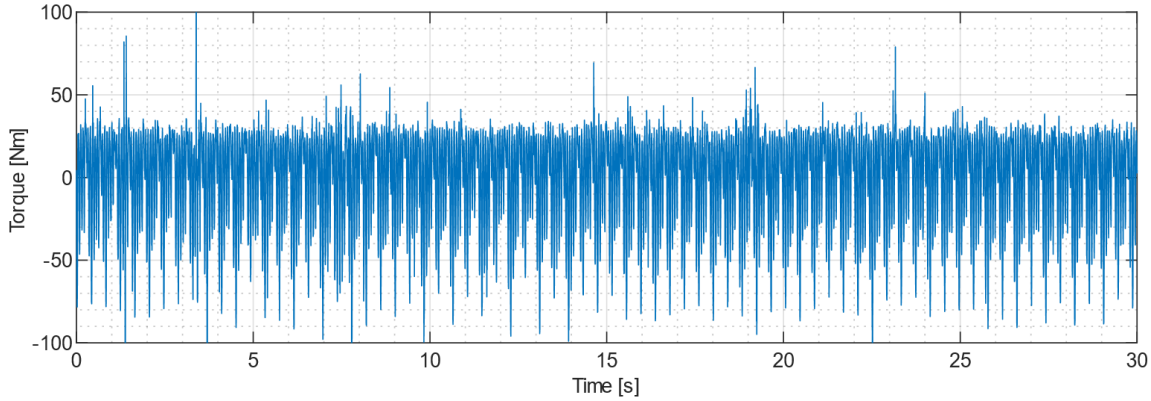

Torque signal for 5 km/h under 10 kN

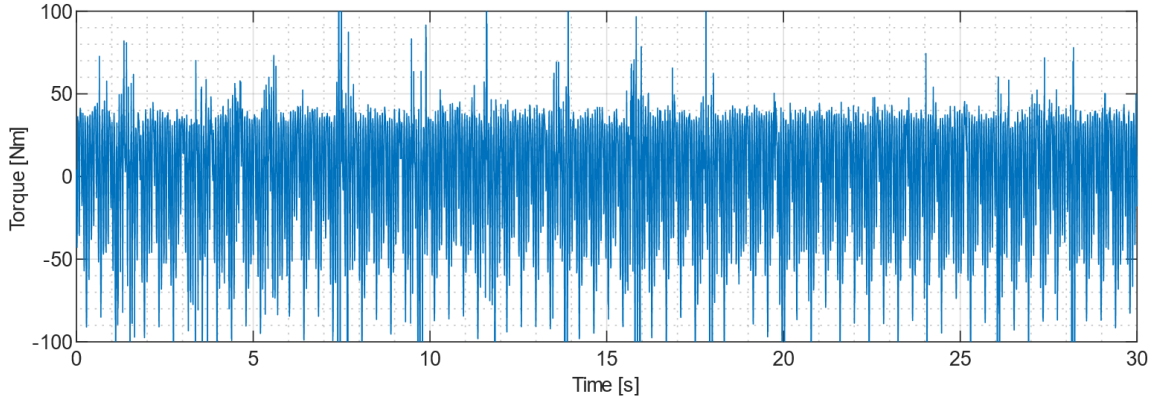

Torque signal for 5 km/h under 20 kN

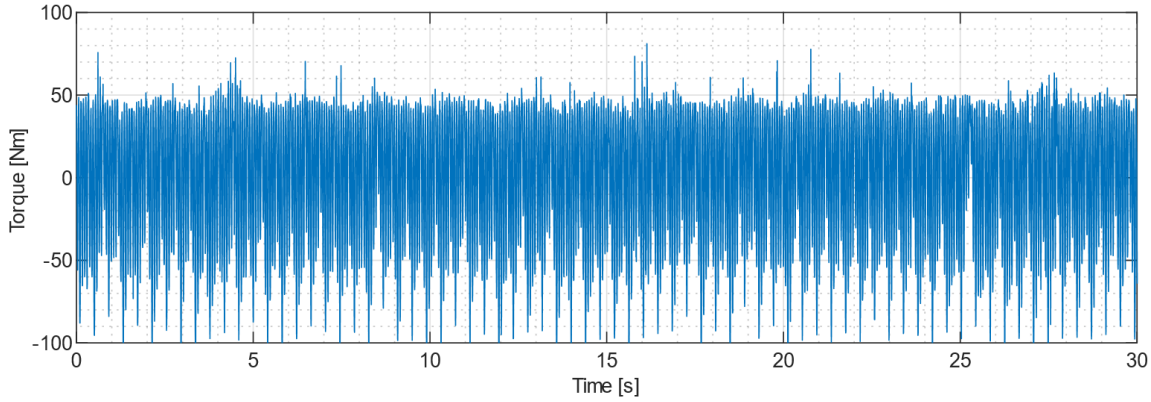

Torque signal for 10 km/h under 4.3 kN

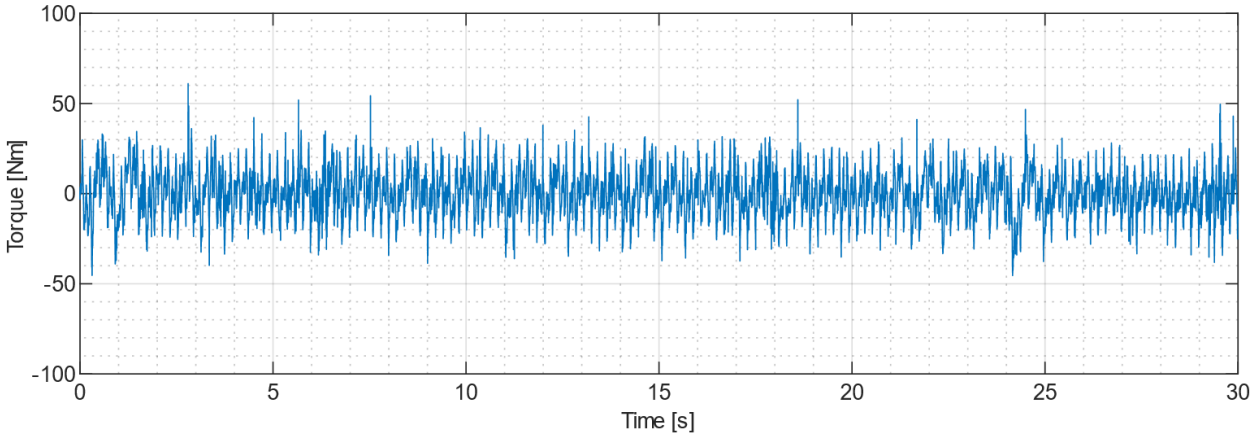

Torque signal for 10 km/h under 10 kN

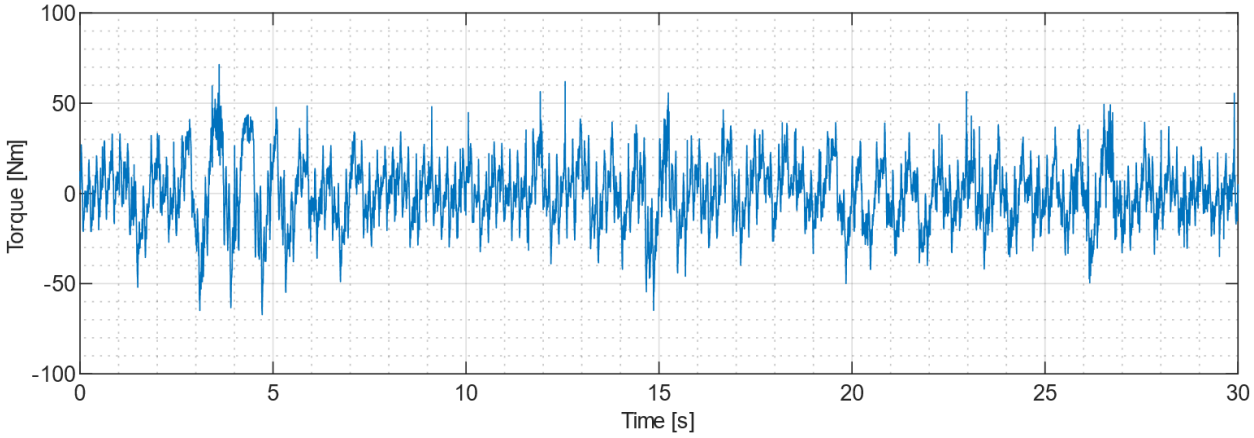

Torque signal for 10 km/h under 20 kN

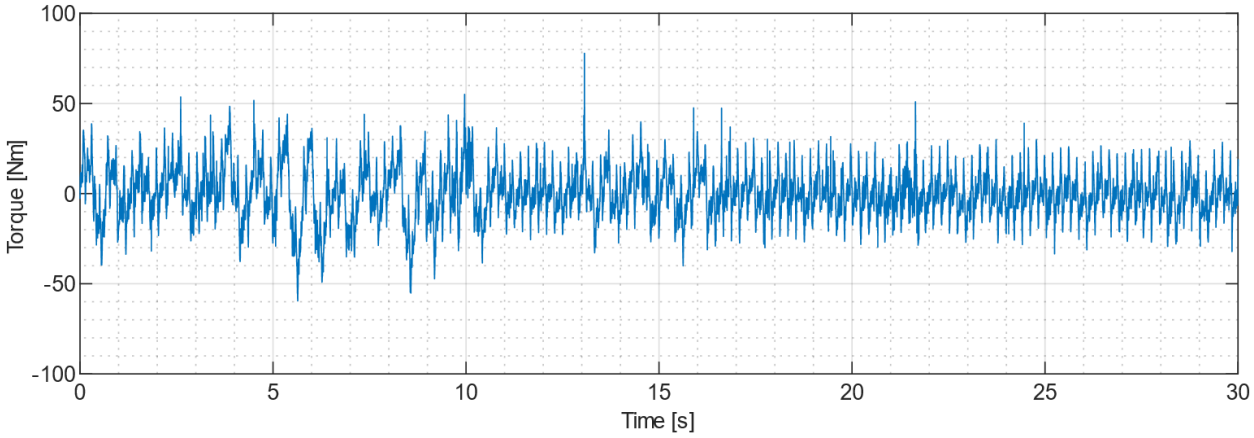

Torque signal for 20 km/h under 4.3 kN

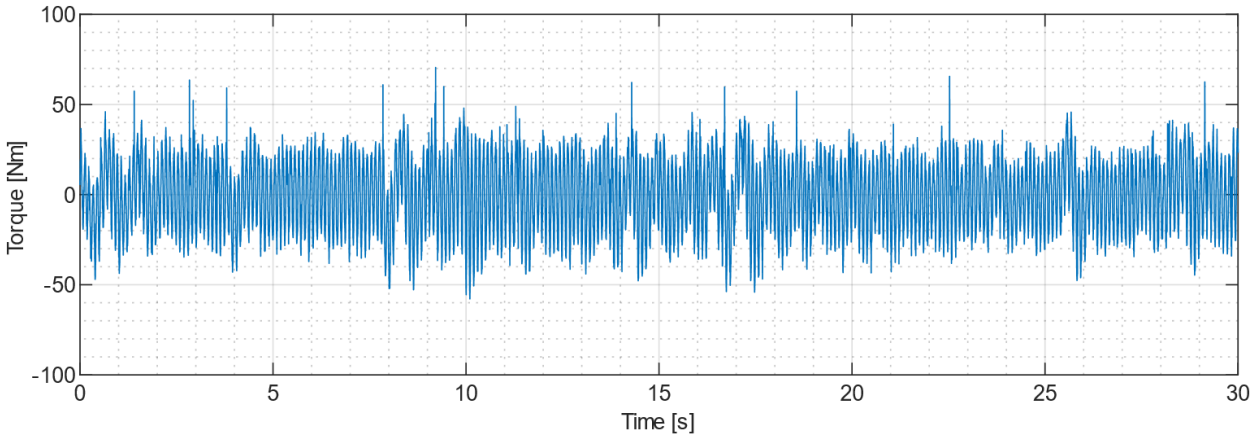

Torque signal for 20 km/h under 10 kN

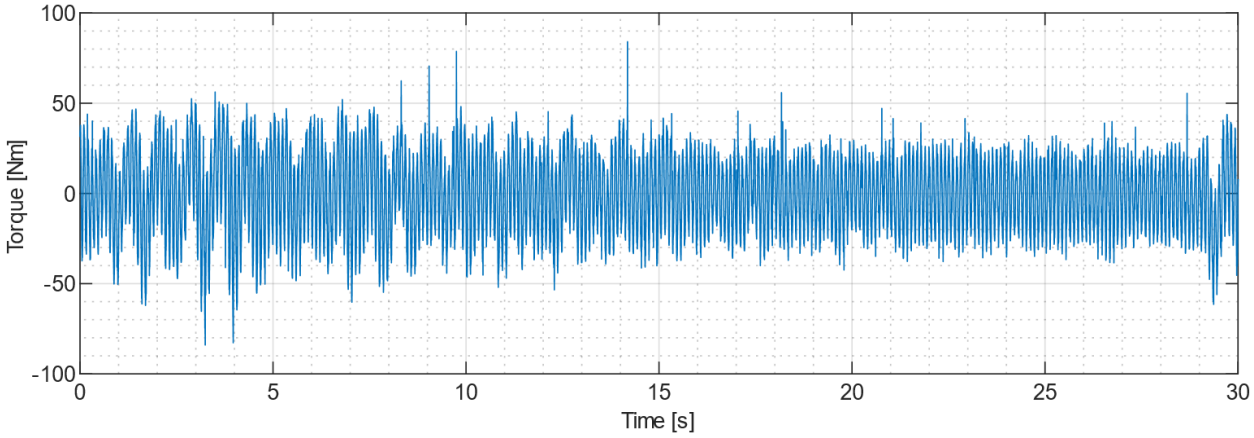

Torque signal for 20 km/h under 20 kN

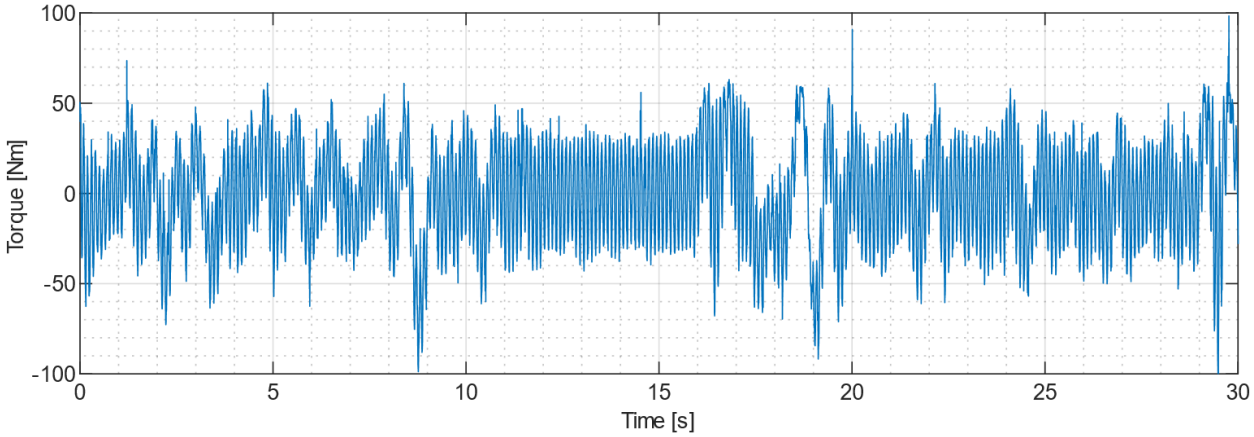

Torque signal for 30 km/h under 4.3 kN

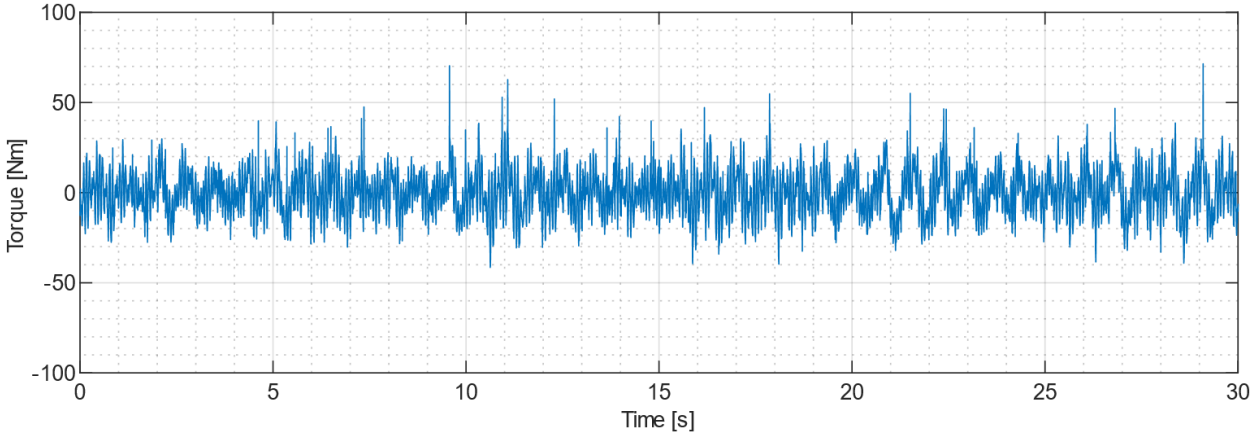

Torque signal for 30 km/h under 10 kN

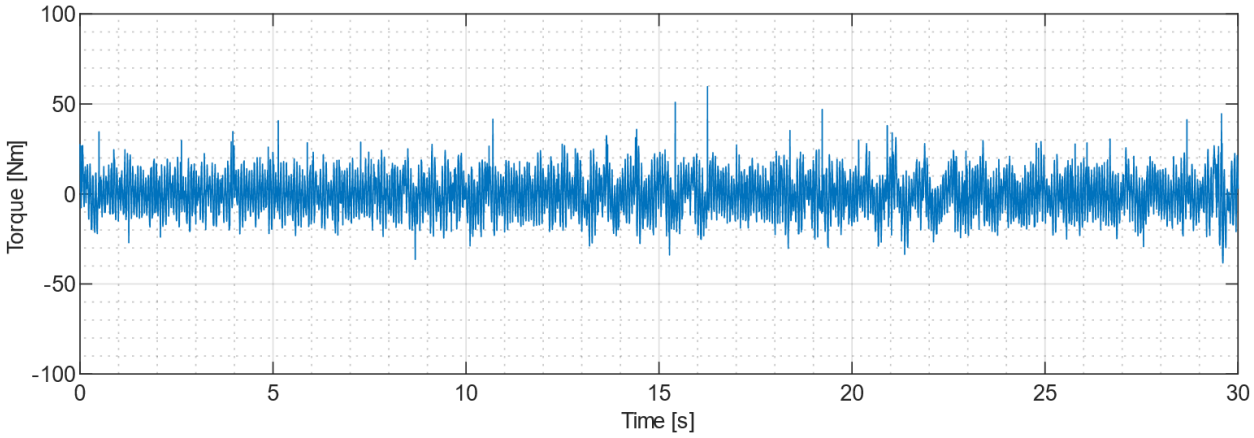

Torque signal for 30 km/h under 30 kN

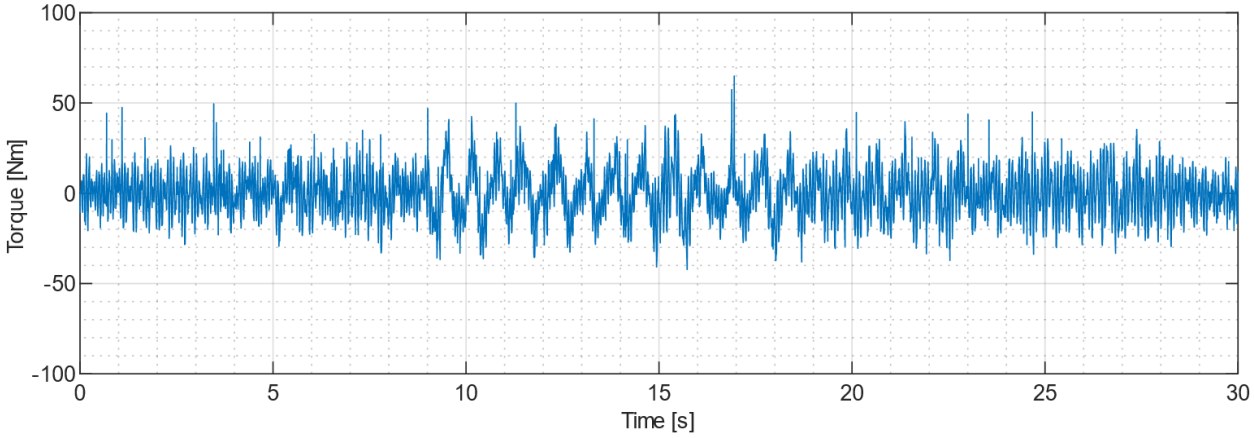

B. Measured Data from Displacement Sensors

Displacement measurement for 5 km/h under 10 kN

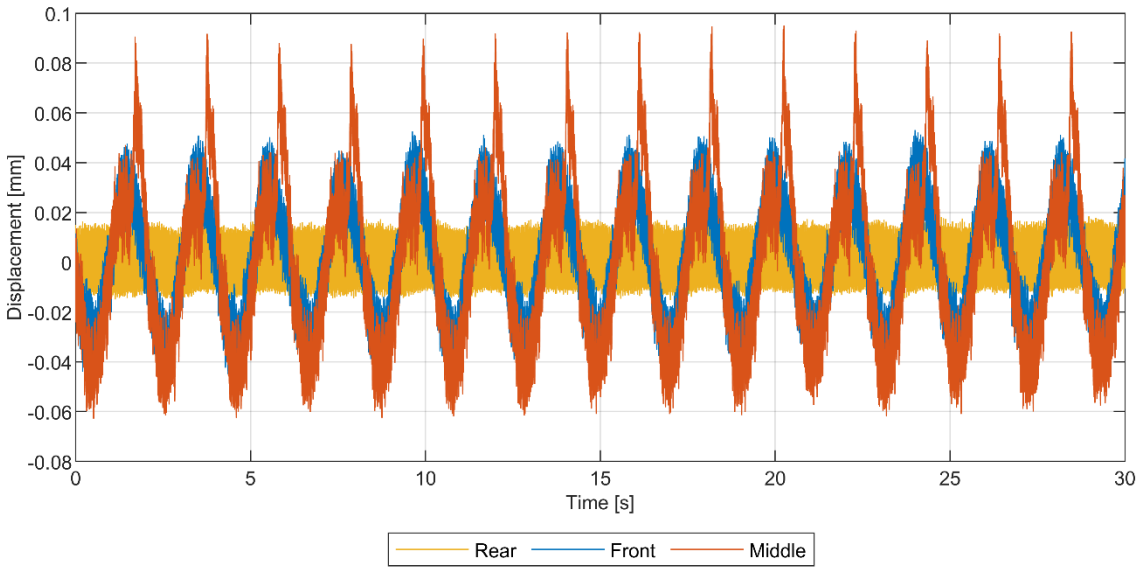

Displacement measurement for 5 km/h under 20 kN

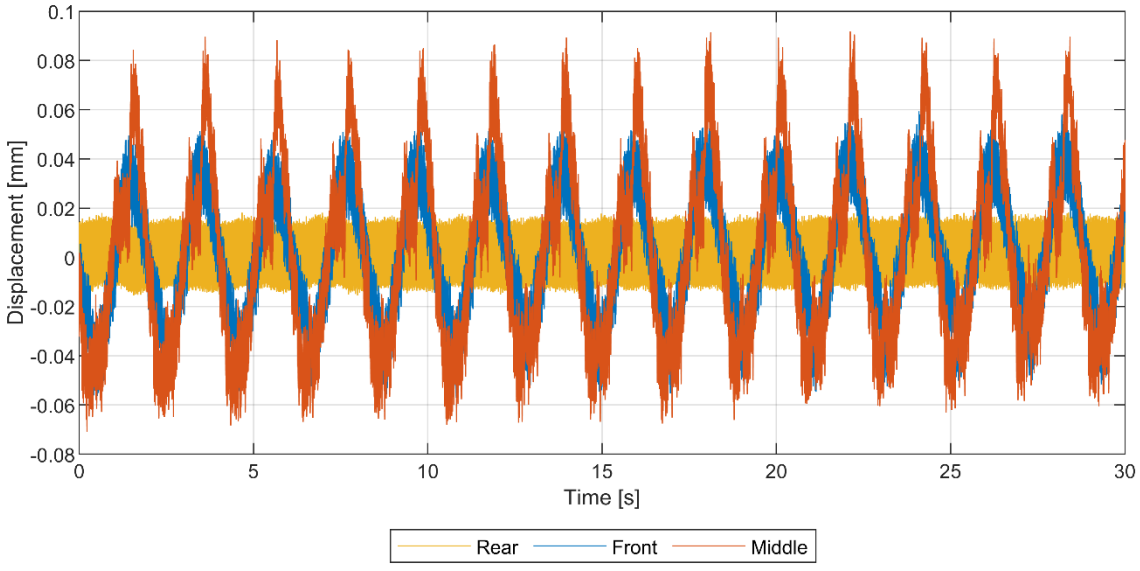

Displacement measurement for 10 km/h under 10 kN

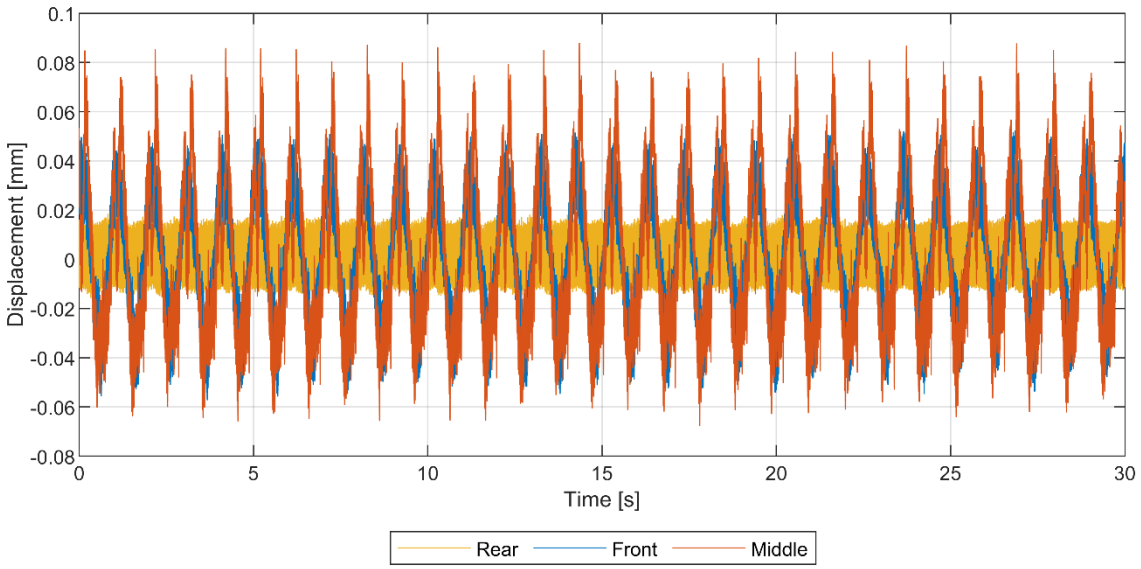

Displacement measurement for 10 km/h under 20 kN

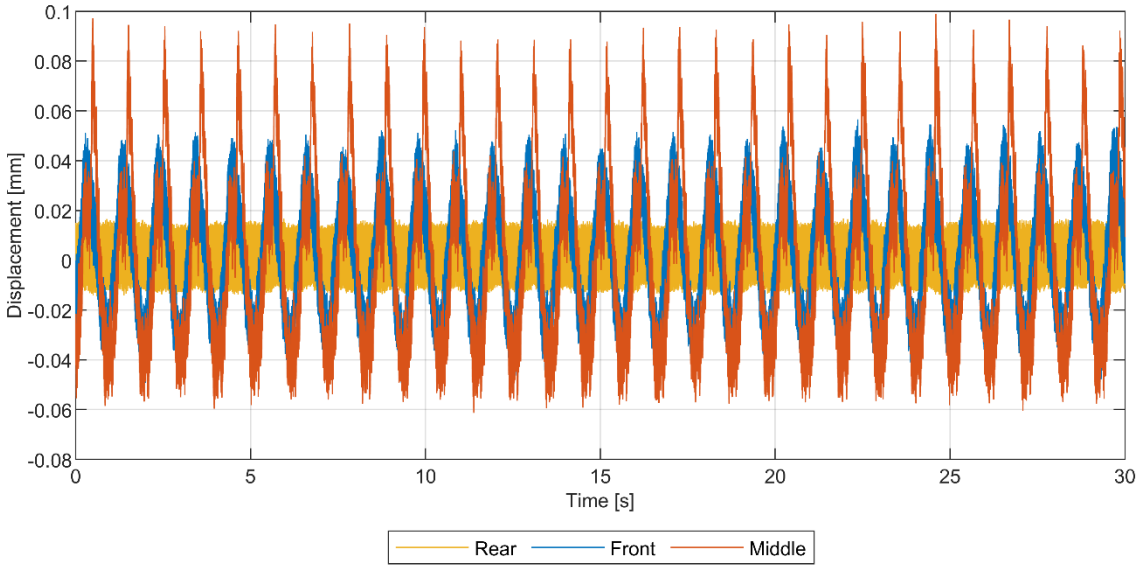

Displacement measurement for 20 km/h under 10 kN

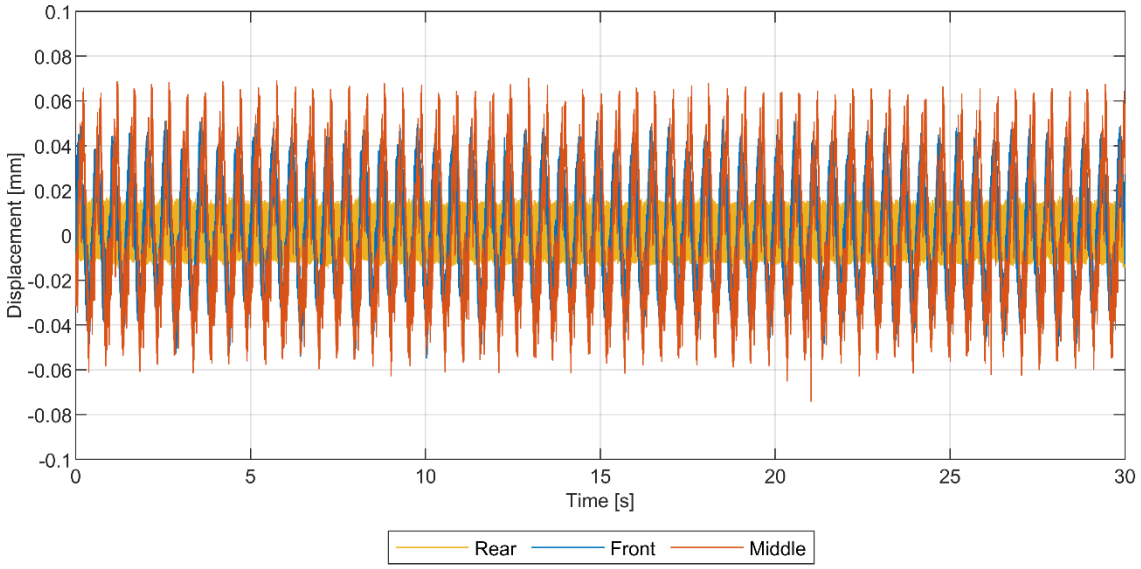

Displacement measurement for 20 km/h under 20 kN

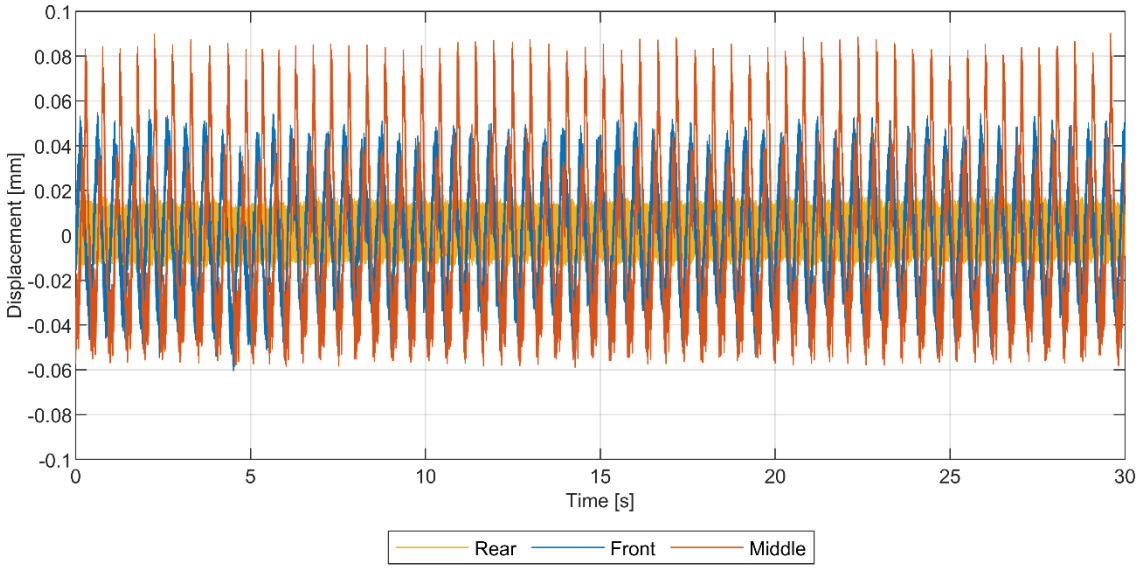

Displacement measurement for 30 km/h under 10 kN

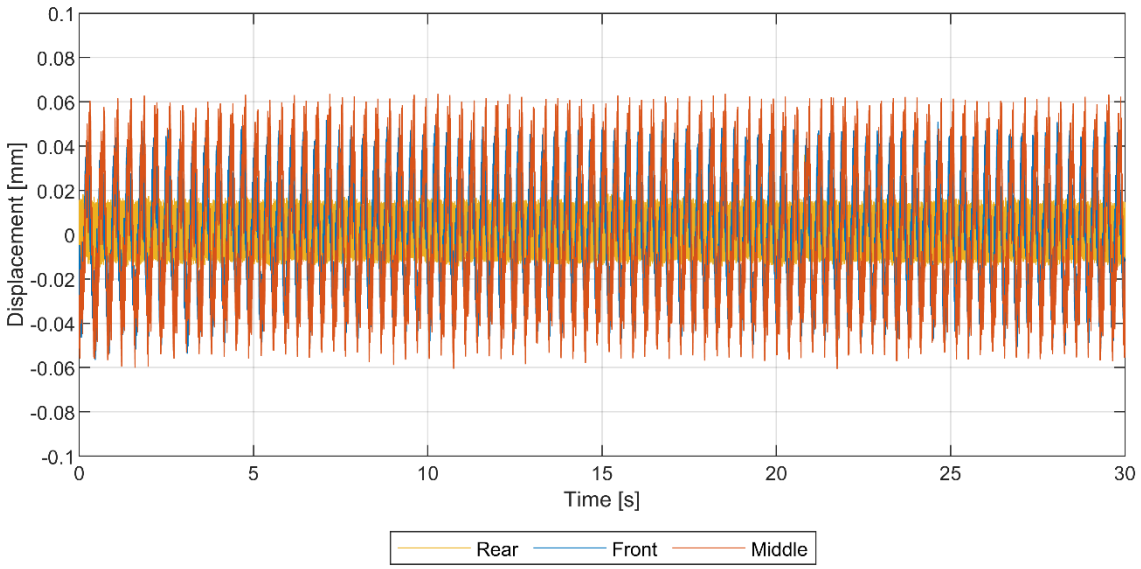

Displacement measurement for 30 km/h under 20 kN

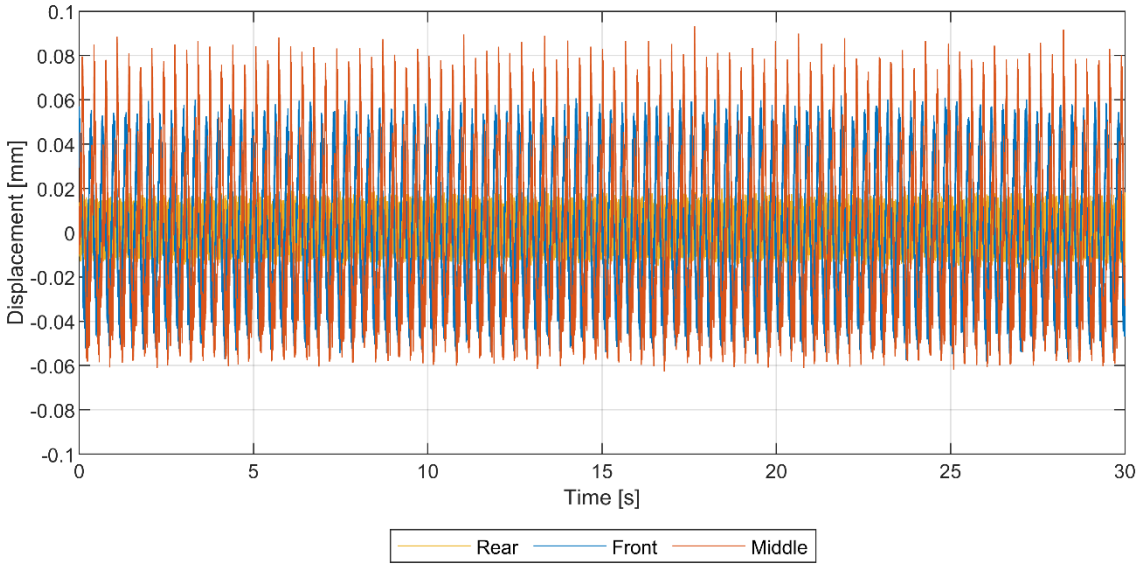

10 REFERENCES

[1] Iwnicki S, editor. Handbook of railway vehicle dynamics. Boca Raton: CRC/Taylor & Francis; 2006.
[2] Jaschinski A, Chollet H, Iwnicki S, Wickens A, Würzen J. The Application of Roller Rigs to Railway Vehicle Dynamics. Vehicle System Dynamics 1999;31:345–92. https://doi.org/10.1076/vesd.31.5.345.8360.
[3] Lata M, Voltr P. New practical results about adhesion limites obtained from experimental stand testing 2009:8.
[4] Carling DR. Locomotive Testing Stations (Part I). Transactions of the Newcomen Society 1972;45:105–44. https://doi.org/10.1179/tns.1972.008.
[5] Eadie DT, Elvidge D, Oldknow K, Stock R, Pointner P, Kalousek J, et al. The effects of top of rail friction modifier on wear and rolling contact fatigue: Full-scale rail–wheel test rig evaluation, analysis and modelling. Wear 2008;265:1222–30. https://doi.org/10.1016/j.wear.2008.02.029.
[6] Liu B. Study of Rail Vehicle Dynamics and Wheel-Rail Contact Using Full-Scale Roller Rigs. PhD. Thesis. Polytechnic University of Milan, 2016.
[7] Malvezzi M, Allotta B, Pugi L, Rindi A. Simulation of degraded adhesion conditions on a full scale locomotive roller rig 2007:6.
[8] Zhang W, Chen J, Wu X, Jin X. Wheel/rail adhesion and analysis by using full scale roller rig. Wear 2002;253:82–8. https://doi.org/10.1016/S0043-1648(02)00086-8.
[9] Matsumoto A, Sato Y, Nakata M, Tanimoto M, Qi K. Wheel-rail contact mechanics at full scale on the test stand. Wear 1996;191:101–6. https://doi.org/10.1016/0043-1648(95)06710-8.
[10] Jaschinski A. On The Application of Similarity Laws to a Scaled Railway Bogie Model. Master Thesis. Delft University of Technology, 1990.
[11] Collette C, Bastaits R, Horodinca M. Experimental Verification of Rail Corrugation Theories on a Scaled Roller Rig n.d.:6.
[12] Matsumoto A, Sato Y, Ono H, Wang Y, Yamamoto M, Tanimoto M, et al. Creep force characteristics between rail and wheel on scaled model. Wear 2002;253:199–203. https://doi.org/10.1016/S0043-1648(02)00100-X.
[13] Bosso N, Zampieri N. Real-time implementation of a traction control algorithm on a scaled roller rig. Vehicle System Dynamics 2013;51:517–41. https://doi.org/10.1080/00423114.2012.750001.
[14] Hernandez EAG. Wheel and Rail Contact Simulation Using a Twin Disc Tester n.d.:131.
[15] Savkoor AR, Ouwerkerk H. Tribological transitions due to heat dissipation during braking on contaminated rails 1995:6.
[16] Eom B-G, Kang B-B, Lee HS. A study on running stability assessment methods for 1/5 small scaled bogie of saemaul using small-scaled derailment simulator. International Journal of Precision Engineering and Manufacturing 2013;14:589–98. https://doi.org/10.1007/s12541-013-0079-x.
[17] Matsumoto A, Sato Y, Ohno H, Tomeoka M, Matsumoto K, Kurihara J, et al. A new measuring method of wheel–rail contact forces and related considerations. Wear 2008;265:1518–25. https://doi.org/10.1016/j.wear.2008.02.031.

[18] Meymand SZ. State of the Art Roller Rig for Precise Evaluation of Wheel-Rail Contact Mechanics and Dynamics. PhD. Thesis. Virginia Polytechnic Institute and State University, 2015.
[19] Keylin A. Analytical Evaluation of the Accuracy of Roller Rig Data for Studying Creepage in Rail Vehicles. Master Thesis. Virginia Polytechnic Institute and State University, 2012.
[20] Wang WJ, Zhang HF, Wang HY, Liu QY, Zhu MH. Study on the adhesion behavior of wheel/rail under oil, water and sanding conditions. Wear 2011;271:2693–8. https://doi.org/10.1016/j.wear.2010.12.019.
[21] Kumar S, Alzoubi MF, Allsayyed NA. Wheel/rail adhesion wear investigation using a quarter scale laboratory testing facility. Proceedings of the 1996 ASME/IEEE Joint Railroad Conference, Oakbrook, IL, USA: IEEE; 1996, p. 247–54. https://doi.org/10.1109/RRCON.1996.507984.
[22] Iwnicki SD, Wickens AH. Validation of a MATLAB Railway Vehicle Simulation Using a Scale Roller Rig. Vehicle System Dynamics 1998;30:257–70. https://doi.org/10.1080/00423119808969451.
[23] Bosso N, Zampieri N. Experimental and Numerical Simulation of Wheel-Rail Adhesion and Wear Using a Scaled Roller Rig and a Real-Time Contact Code. Shock and Vibration 2014;2014:1–14. https://doi.org/10.1155/2014/385018.
[24] Bosso N, Gugliotta A, Somà A. Dynamic identification of a 1:5 scaled railway bogie on roller rig. Computers in Railways X, vol. 1, Prague, Czech Republic: WIT Press; 2006, p. 829–38. https://doi.org/10.2495/CR060811.
[25] Meehan PA, Bellette P, Liu X, Milne C, Anderson D. Investigation of wheel squeal characteristics using a rolling contact two disk test rig. 9th World Conference on Railway Research, 2011.
[26] Rovira A, Roda A, Lewis R, Marshall MB. Application of Fastsim with variable coefficient of friction using twin disc experimental measurements. Wear 2012;274–275:109–26. https://doi.org/10.1016/j.wear.2011.08.019.
[27] Gallardo-Hernandez EA, Lewis R. Twin disc assessment of wheel/rail adhesion. Wear 2008;265:1309–16. https://doi.org/10.1016/j.wear.2008.03.020.
[28] Zhang W, Dai H, Shen Z, Zeng J. Roller Rigs. Handbook of railway vehicle dynamics, Boca Raton: CRC/Taylor & Francis; 2006.
[29] Myamlin S, Kalivoda J, Neduzha L. Testing of Railway Vehicles Using Roller Rigs. Procedia Engineering 2017;187:688–95. https://doi.org/10.1016/j.proeng.2017.04.439.
[30] Ahmadian M, Craft M. Evaluation Wheel-Rail Contact Mechanics : Concepts Report. Blacksburg, VA: Center for Vehicle Systems Safety; 2014.
[31] Savkoor AR, van der Schoor GH. Slip-time history influences on the interaction between friction and wear in contaminated rolling contacts of wheel-rail systems. Wear 1993;162–164:980–4. https://doi.org/10.1016/0043-1648(93)90107-W.
[32] ISVR Wheel/Rail Model Rig n.d. https://www.southampton.ac.uk/engineering/research/groups/dynamics/rail/wheel_rail_model_rig.page.
[33] Meymand SZ, Craft MJ, Ahmadian M. On the Application of Roller Rigs for Studying Rail Vehicle Systems. ASME 2013 Rail Transportation Division Fall Technical Conference, Altoona, Pennsylvania, USA: ASME; 2013, p. V001T01A015. https://doi.org/10.1115/RTDF2013-4724.

[34] Stock R, Eadie DT, Elvidge D, Oldknow K. The impact of rail grade selection and friction modifier application on rail degradation. n.d.:13.
[35] Paolo F, Fabio F. Instrumented Wheelsets for Two Type of Railway Vehicles (tilting and freight train). 2008.
[36] Ahn K, Park J, Ryew S. The construction of a full-scale wheel/rail roller rig in Korea. 2012 IEEE International Conference on Automation Science and Engineering (CASE), Seoul, Korea (South): IEEE; 2012, p. 802–3. https://doi.org/10.1109/CoASE.2012.6386485.
[37] Allen PD. Scale Testing. Handbook of railway vehicle dynamics, Boca Raton: CRC/Taylor & Francis; 2006.
[38] Jaschinski A. On the application of similarity laws to a scaled railway bogie model. 1991.
[39] Koch JR, Vincent N, Chollet H, Chiello O. Curve squeal of urban rolling stock—Part 2: Parametric study on a 1/4 scale test rig. Journal of Sound and Vibration 2006;293:701–9. https://doi.org/10.1016/j.jsv.2005.12.009.
[40] ILLINGWORTH R. Railway Wheelset Lateral Excitation by Track Irregularities. Vehicle System Dynamics 1977;6:144–7. https://doi.org/10.1080/00423117708968525.
[41] Schmidova E, Voltr P. Comperative Laboratory Tests of Solid Friction Modifiers. Pardubice,Czech Republic: 2014.
[42] Meymand SZ, Ahmadian M. Design, development, and calibration of a force-moment measurement system for wheel–rail contact mechanics in roller rigs. Measurement 2016;81:113–22. https://doi.org/10.1016/j.measurement.2015.12.012.
[43] Chen H, Tanimoto H. Experimental observation of temperature and surface roughness effects on wheel/rail adhesion in wet conditions. International Journal of Rail Transportation 2018;6:101–12. https://doi.org/10.1080/23248378.2017.1415772.
[44] Kim M-S. Study on the Adhesion Characteristic between Wheel and Rail using the Scaled Test-bench 2015;9:8.
[45] Polach O. Creep forces in simulations of traction vehicles running on adhesion limit. Wear 2005;258:992–1000. https://doi.org/10.1016/j.wear.2004.03.046.
[46] Voltr P, Zirek A, Kayaalp BT. New Experience and Results from Experimental Measurement of Adhesion on a Roller Rig, Česká Třebová, Czech Republic: University of Pardubice; 2017.
[47] Matsumoto K, Suda Y, Komine H, Nakai T, Tomeoka M, Shimizu K, et al. A proposal of wheel/rail contact model for friction control. Journal of Mechanical Science and Technology 2005;19:437–43. https://doi.org/10.1007/BF02916165.
[48] Naeimi M, Dollevoet R. Preliminary results on multi-body dynamic simulation of a new test rig for wheel-rail contact 2015:11.
[49] Wang WJ, Shen P, Song JH, Guo J, Liu QY, Jin XS. Experimental study on adhesion behavior of wheel/rail under dry and water conditions. Wear 2011;271:2699–705. https://doi.org/10.1016/j.wear.2011.01.070.
[50] Taheri M, Ahmadian M. Contact Patch Comparison Between a Roller Rig and Tangent Track for a Single Wheelset. 2012 Joint Rail Conference, Philadelphia, Pennsylvania, USA: ASME; 2012, p. 283. https://doi.org/10.1115/JRC2012-74148.
[51] Aymerich F, Pau M. Assessment of Nominal Contact Area Parameters by Means of Ultrasonic Waves. J Tribol 2004;126:639–45. https://doi.org/10.1115/1.1760764.
[52] Pau M. Estimation of real contact area in a wheel-rail system by means of ultrasonic waves. Tribology International 2003;36:687–90. https://doi.org/10.1016/S0301-679X(03)00014-8.

[53] Pau M, Aymerich F, Ginesu F. Ultrasonic measurements of nominal contact area and contact pressure in a wheel-rail system. Proceedings of the Institution of Mechanical Engineers, Part F: Journal of Rail and Rapid Transit 2000;214:231–43. https://doi.org/10.1243/0954409001531333.
[54] Ishida M, Abe N. Experimental study on rolling contact fatigue from the aspect of residual stress. Wear 1996;191:65–71. https://doi.org/10.1016/0043-1648(95)06712-4.
[55] Stock R, Pippan R. RCF and wear in theory and practice—The influence of rail grade on wear and RCF. Wear 2011;271:125–33. https://doi.org/10.1016/j.wear.2010.10.015.
[56] Clarke M. Wheel rolling contact fatigue (RCF) and rim defects investigation to further knowledge of the causes of RCF and to determine control measures. Rail Safety & Standards Board; n.d.
[57] Gretzschel M, Bose L. A New Concept for Integrated Guidance and Drive of Railway Running Gears. IFAC Proceedings Volumes 2000;33:259–64. https://doi.org/10.1016/S1474-6670(17)39154-1.
[58] Kurzeck B, Valente L. A novel mechatronic running gear: concept, simulation and scaled roller rig testing n.d.:10.
[59] G V, F. J. F, A K. New Rail Materials and Coatings. Sheffield: University of Sheffield; 2003.
[60] Onat A, Voltr P, Lata M. An unscented Kalman filter-based rolling radius estimation methodology for railway vehicles with traction. Proceedings of the Institution of Mechanical Engineers, Part F: Journal of Rail and Rapid Transit 2018;232:1686–702. https://doi.org/10.1177/0954409717745201.
[61] Zirek A, Kayaalp BT. The Performance Analysis of Bang-Bang Slip Control Method with Mathematical Model of a Tram-Wheel Test Stand Model, Pardubice,Czech Republic: Pardubice University; 2018.
[62] Braghin F, Bruni S, Diana G. Experimental and numerical investigation on the derailment of a railway wheelset with solid axle. Vehicle System Dynamics 2006;44:305–25. https://doi.org/10.1080/00423110500337494.
[63] Ishida H, Miyamoto T, Maebashi E, Doi H, Iida K, Furukawa A. Safety Assessment for Flange Climb Derailment of Trains Running at Low Speeds on Sharp Curves. QR of RTRI 2006;47:65–71. https://doi.org/10.2219/rtriqr.47.65.
[64] Nishimura K, Terumichi Y, Morimura T, Fukada J. Experimental Study on the Vehicle Safety by Earthquake Track Excitation with 1/10 Scale Vehicle and Roller Rig. JSDD 2010;4:226–38. https://doi.org/10.1299/jsdd.4.226.
[65] Dukkipati RV. Lateral stability analysis of a railway truck on roller rig. Mechanism and Machine Theory 2001:16.
[66] Allen PD, Iwnicki SD. The critical speed of a railway vehicle on a roller rig. Proceedings of the Institution of Mechanical Engineers, Part F: Journal of Rail and Rapid Transit 2001;215:55–64. https://doi.org/10.1243/0954409011531396.
[67] Kim N-P, Park T-W. A study on the dynamic performance of the 200km/h Korean tilting train by means of roller rig test. Journal of Mechanical Science and Technology 2009;23:910–3. https://doi.org/10.1007/s12206-009-0310-y.
[68] Redtenbacher F. Die Gesetze des Lokomotiv-Baues (English Title : The laws of the locomotive construction). Mannheim: Bassermann; 1855.
[69] Hertz H. Ueber die Berührung fester elastischer Körper. Journal Für Die Reine Und Angewandte Mathematik 1882;1882:156–71.

[70] Kalker JJ. Wheel—rail rolling contact theory. Wear 1991;144:243–61.
[71] Knothe K. History of wheel/rail contact mechanics: from Redtenbacher to Kalker. Vehicle System Dynamics 2008;46:9–26. https://doi.org/10.1080/00423110701586469.
[72] Piotrowski J, Chollet H. Wheel–rail contact models for vehicle system dynamics including multi-point contact. Vehicle System Dynamics 2005;43:455–83. https://doi.org/10.1080/00423110500141144.
[73] Piotrowski J, Kik W. A simplified model of wheel/rail contact mechanics for non-Hertzian problems and its application in rail vehicle dynamic simulations. Vehicle System Dynamics 2008;46:27–48. https://doi.org/10.1080/00423110701586444.
[74] Pombo J, Ambrósio J, Silva M. A new wheel–rail contact model for railway dynamics. Vehicle System Dynamics 2007;45:165–89. https://doi.org/10.1080/00423110600996017.
[75] Linder C. Verschleiss von Eisenbahnrädern mit Unrundheiten. PhD. Thesis. ETH Zurich, 1997. https://doi.org/10.3929/ethz-a-001845360.
[76] Sichani MSh, Enblom R, Berg M. Comparison of non-elliptic contact models: Towards fast and accurate modelling of wheel–rail contact. Wear 2014;314:111–7. https://doi.org/10.1016/j.wear.2013.11.047.
[77] Ayasse J-B, Chollet H. Wheel - Rail Contact. Handbook of Railway Vehicle Dynamics, 2006, p. 85–120.
[78] Zastrau BW, Knothe K, Wille R. Advanced Contact Mechanics: Road and Rail. Vehicle System Dynamics 2001;35:361–407. https://doi.org/10.1076/vesd.35.4.361.2043.
[79] Carter FW. On the Action of a Locomotive Driving Wheel. Proceedings of the Royal Society A: Mathematical, Physical and Engineering Sciences 1926;112:151–7. https://doi.org/10.1098/rspa.1926.0100.
[80] Johnson KL. The effect of spin upon the rolling motion of an elastic sphere on a plane. Journal of Applied Mechanics 1958;80:332–8.
[81] Vermeulen PJ, Johnson KL. Contact of Nonspherical Elastic Bodies Transmitting Tangential Forces. Journal of Applied Mechanics 1964;31:338. https://doi.org/10.1115/1.3629610.
[82] Kalker JJ. A Fast Algorithm for the Simplified Theory of Rolling Contact. Vehicle System Dynamics 1982;11:1–13. https://doi.org/10.1080/00423118208968684.
[83] Freibauer L. Adheze kola na vozidlové dráze ["En: Adhesion of wheel on track], Žilina: 1983.
[84] Onat A, Zirek A, Voltr P. Dynamic Modelling and Numerical Simulation of a Tram Wheel Test Stand. Third international symposium on electrical railway transportation systems, ERUSIS 2017, 2017, p. 7.
[85] Simanek J, Novak J, Cerny O, Dolecek R. FOC and flux weakening for traction drive with permanent magnet synchronous motor. Industrial Electronics, 2008. ISIE 2008. IEEE International Symposium on, IEEE; 2008, p. 753–8.
[86] Trummer G, Buckley-Johnstone LE, Voltr P, Meierhofer A, Lewis R, Six K. Wheel-rail creep force model for predicting water induced low adhesion phenomena. Tribology International 2017;109:409–15.
[87] Voltr P, Lata M. Transient wheel–rail adhesion characteristics under the cleaning effect of sliding. Vehicle System Dynamics 2015;53:605–18. https://doi.org/10.1080/00423114.2014.961488.
[88] Onat A, Voltr P. Swarm Intelligence Based Multiple Model Approach for Friction Estimation at Wheel-Rail Interface, Kyrenia, Cyprus: 2017.

[89] Onat A, Kayaalp BT. Normal Load Estimation by Using a Swarm Intelligence Based Multiple Models Approach. IV. International Symposium on Railway Engineering, Karabuk, TR: Karabuk University; 2018.
[90] Dolecek R, Novák J, Cerny O. Traction Permanent Magnet Synchronous Motor Torque Control with Flux Weakening. Radiengineering 2009;18:5.
[91] Mohamed YAI. Design and Implementation of a Robust Current-Control Scheme for a PMSM Vector Drive With a Simple Adaptive Disturbance Observer. IEEE Transactions on Industrial Electronics 2007;54:1981–8. https://doi.org/10.1109/TIE.2007.895074.
[92] Merzoug M salah, Naceri F. Comparison of Field-Oriented Control and Direct Torque Control for Permanent Magnet Synchronous Motor (PMSM), 2008.
[93] Sen PC. Principles of electric machines and power electronics. John Wiley & Sons; 2007.
[94] S˘tulrajter M, Hrabovcova V, Franko M. PERMANENT MAGNETS SYNCHRONOUS MOTOR CONTROL THEORY 2007;58:6.
[95] Shabana AA, Zaazaa KE, Sugiyama H. Railroad vehicle dynamics: a computational approach. Boca Raton: CRC Press; 2008.
[96] Onat A, Voltr P, Lata M. NONLINEAR WHEEL/RAIL CONTACT GEOMETRY CHARACTERISTICS & DETERMINATION OF HERTZIAN CONTACT. SCIENTIFIC PAPERS OF THE UNIVERSITY OF PARDUBICE 2014;Series B:9.
[97] Kalker JJ. On the rolling contact of two elastic bodies in the presence of dry friction. Delft University of Technology, 1967.
[98] Onat A. Estimation of States and Parameters from Dynamic Response of Wheelset. PhD. Thesis. University of Pardubice, 2017.
[99] Friction and Wear. Oxford ; New York: Elsevier; 1982. https://doi.org/10.1016/C2013-0-03333-6.
[100] GKN Automotive Limited. CV shaft catalog 2014.
[101] Allotta B, Pugi L, Malvezzi M, Bartolini F, Cangioli F. A scaled roller test rig for high-speed vehicles. Vehicle System Dynamics 2010;48:3–18. https://doi.org/10.1080/00423111003663576.
[102] Chen W, Xu D, Yang R, Yu Y, Xu Z. A novel stator voltage oriented V/F control method capable of high output torque at low speed. 2009 International Conference on Power Electronics and Drive Systems (PEDS), Taipei: IEEE; 2009, p. 228–33. https://doi.org/10.1109/PEDS.2009.5385840.
[103] Echavarria R, Horta S, Oliver M. A three phase motor drive using IGBTs and constant V/F speed control with slip regulation. IV IEEE International Power Electronics Congress. Technical Proceedings. CIEP 95, San Luis Potosi, Mexico: IEEE; 1995, p. 87–91. https://doi.org/10.1109/CIEP.1995.535939.
[104] Kohlrusz G, Fodor D. Comparison of Scalar and Vector Control Strategies of Induction Motors. Hungarian Journal of Industrial Chemistry n.d.;39:265–70.
[105] Molina JJM, Scarpetta JMR. Optimal u/f Control for Induction Motors. IFAC Proceedings Volumes 2002;35:329–33. https://doi.org/10.3182/20020721-6-ES-1901.01206.
[106] Patel HK. Steady State and Transient Performance Analysis of Three Phase Induction Machine using MATLAB Simulations 2009;1:5.
[107] Vlad I, Campeanu A, Enache S, Enache M-A. Study of direct-on-line starting of low power asynchronous motors. 2017 International Conference on Electromechanical and Power

Systems (SIELMEN), Iasi: IEEE; 2017, p. 137–42. https://doi.org/10.1109/SIELMEN.2017.8123313.
[108] Marra EG, Pomilio JA. Induction-generator-based system providing regulated voltage with constant frequency. IEEE Transactions on Industrial Electronics 2000;47:908–14.
[109] Bocker J, Mathapati S. State of the Art of Induction Motor Control. 2007 IEEE International Electric Machines & Drives Conference, Antalya, Turkey: IEEE; 2007, p. 1459–64. https://doi.org/10.1109/IEMDC.2007.383643.
[110] Mikhael H, Jalil H, Ibrahim I. Speed Control of Induction Motor using PI and V/F Scalar Vector Controllers. IJCA 2016;151:36–43. https://doi.org/10.5120/ijca2016911831.
[111] Spiryagin M, Wolfs P, Szanto F, Cole C. Simplified and advanced modelling of traction control systems of heavy-haul locomotives. Vehicle System Dynamics 2015;53:672–91. https://doi.org/10.1080/00423114.2015.1008016.
[112] Bosso N, Gugliotta A, Somà A, Spiryagin M. Model of Scaled Test Rig For Real Time Applications. vol. 5, 2012, p. 1288–98.
[113] Torque-Speed Characteristic of AM n.d.
[114] Keyence Corporation. Keyence Laser Displacement Sensors Catalogue.pdf 2018.
[115] QuantumX MX840A-P Data Sheet 2017.
[116] Keyence Corporation. LK-H055. Keyence Corporation 2019. https://www.keyence.com/products/measure/laser-1d/lk-g5000/models/lk-h055/index.jsp.
[117] Keyence Corporation. LK-H087. Keyence Corporation 2019. https://www.keyence.com/products/measure/laser-1d/lk-g5000/models/lk-h087/index.jsp.
[118] Jackson LB. Digital filters and signal processing with MATLAB exercises. New York; London: Springer; 2011.
[119] Candan Ç, Inan H. A unified framework for derivation and implementation of Savitzky–Golay filters. Signal Processing 2014;104:203–11. https://doi.org/10.1016/j.sigpro.2014.04.016.
[120] Schafer R. What Is a Savitzky-Golay Filter? [Lecture Notes]. IEEE Signal Processing Magazine 2011;28:111–7. https://doi.org/10.1109/MSP.2011.941097.
[121] Acharya D, Rani A, Agarwal S, Singh V. Application of adaptive Savitzky–Golay filter for EEG signal processing. Perspectives in Science 2016;8:677–9. https://doi.org/10.1016/j.pisc.2016.06.056.
[122] Press WH, Teukolsky SA. Savitzky-Golay Smoothing Filters. Computers in Physics 1990;4:669. https://doi.org/10.1063/1.4822961.
[123] Hosseinipour M. Electromechanical design and development of the Virginia Tech Roller Rig testing facility for wheel-rail contact mechanics and dynamics. PhD. Thesis. Virginia Polytechnic Institute and State University, 2016.
[124] Liu B. Speed control for permanent magnet synchronous motor based on an improved extended state observer. Advances in Mechanical Engineering 2018;10:1687814017747663. https://doi.org/10.1177/1687814017747663.

PUBLICATIONS OF THE PHD STUDENT

Voltr P, Zirek A, and Kayaalp B. T, 'New Experience and Results from Experimental Measurement of Adhesion on a Roller Rig', 23rd Conference: Current Problems in Rail Vehicles 2017, Ceska Trebova, September 2017. ISBN 978-80-7560-085-1

Zirek A and Kayaalp B T, 'The Performance Analysis of Bang-Bang Slip Control Method with Mathematical Model of a Tram-Wheel Test Stand Model', VII. International Scientific Conference of the Faculty of Transport Engineering, Pardubice, Czech Republic, September 2018. ISBN 978-80-7560-152-0

Onat A and Kayaalp B T, 'Normal Load Estimation by Using a Swarm Intelligence Based Multiple Models Approach', in IV. International Symposium on Railway Engineering, Karabuk, TR, October 2018. ISBN 978-605-9554-23-7

Kayaalp B T, Voltr P, and Lata M, 'A Mathematical Model for Torsional Simulation of a Tram Wheel Roller Rig', Interdisciplinary Scientific Conference QUAERE 2019, Hradec Kralove, CZ, June 2019, vol. IX. ISBN 978-80-87952-30-60

Onat A and Kayaalp B T, 'A Novel Methodology for Dynamic Weigh in Motion System for Railway Vehicles with Traction', IEEE Transactions on Vehicular Technology, 2019. ISSN 0018-9545

Kayaalp B T, 'Laboratory Equipment Used in Testing of Rail Transport Vehicles', Railway Engineering, Railway Engineers Association, 2020. ISSN 2149-1607. (Accepted – Under Publication Process)